“All endings are also beginnings. We just don't know it at the time.”

- Mitch Albom, *The Five People You Meet in Heaven*

Profiling Alkyl Phosphates in Petroleum Samples by Comprehensive Two-dimensional Gas Chromatography with Nitrogen-phosphorus Detection (GC×GC-NPD)

by

Katie Diana Nizio

A thesis submitted in partial fulfillment of the requirements for the degree of

Doctor of Philosophy

Department of Chemistry
University of Alberta

ABSTRACT

The profiling of alkyl phosphates in petroleum samples is of particular interest to refineries that process conventional crude oil derived from the Western Canadian Sedimentary Basin and other similar geologies. This is due to alkyl phosphate-based additives used during crude oil recovery processes and the subsequent contamination of the produced oil. Phosphate contamination causes numerous problems for refineries, including equipment fouling, the poisoning of catalysts, and potential impacts on downstream processes or consumers if these phosphates enter petroleum product streams. These issues have occurred at a number of facilities across Canada with the impacts measured in the tens of millions of dollars. In response, the Canadian Association of Petroleum Producers and the Canadian Crude Quality Technical Association have specified a limit of 0.5 μg mL^{-1} total distillable phosphorus in feedstock. This limit is monitored using inductively coupled plasma – optical emission spectroscopy (ICP-OES), a technique plagued with poor precision and a high limit of detection (0.5 ± 1 μg *phosphorus* mL^{-1}), thus making the current specification difficult to enforce. Furthermore, this method cannot provide speciation information, which is critical for developing an understanding of the challenge of alkyl phosphates at a molecular level.

This thesis approaches these challenges using comprehensive two-dimensional gas chromatography with post-column Deans switching to allow for effluent flow switching between a flame ionization detector and a

nitrogen-phosphorus detector (GC×GC-FID/NPD). Using trimethylsilyl derivatization, splitless injection, and concurrent backflushing, the GC×GC-FID/NPD method developed and optimized herein, represents the only analytical technique currently capable of: 1) separating the alkyl phosphates from each other and from the crude oil matrix; and 2) speciating and quantifying the phosphates reproducibly in petroleum samples at trace levels (levels two to three orders of magnitude below those achievable by ICP-OES). Overall, this work presents a significant step towards a routine, robust method for profiling trace alkyl phosphates in industrial petroleum and process samples in a production environment. In addition, this thesis presents preliminary results from the first-ever detailed study of alkyl phosphate contamination in a refining environment. The final results of this study will hopefully provide the chemical information needed to contemplate future mitigation strategies for handling the "phosphate problem". This will be important to refineries across Canada that struggle with issues of equipment fouling. A mitigation strategy would be, quite literally, a multimillion-dollar idea for the Canadian petroleum industry.

PREFACE

Portions of **CHAPTER 1** have been published as K.D. Nizio, T.M. McGinitie, J.J. Harynuk, Comprehensive Multidimensional Separations for the Analysis of Petroleum. J. Chromatogr. A 1255 (2012) 12. I was responsible for organizing the literature search and EndNote reference library for this invited review. Together, T.M. McGinitie and I read and summarized over 200 papers and were responsible for the initial manuscript composition and final edits. J.J. Harynuk was the supervisory author and was involved with concept formation and manuscript composition and edits.

Portions of **CHAPTER 1** and a version of **CHAPTER 3** have been published as K.D. Nizio, J.J. Harynuk, Analysis of Alkyl Phosphates using Comprehensive Two-dimensional Gas Chromatography with Nitrogen Phosphorus Detection (GC×GC-NPD) and Post-column Deans Switching. J. Chromatogr. A 1252 (2012) 171. I was responsible for the modification, operation and maintenance of instrumentation (GC×GC-FID/NPD), the data collection and analysis, as well as the manuscript composition/edits. J.J. Harynuk was the supervisory author and was involved with concept formation and manuscript composition and edits.

Portions of **CHAPTER 1** and a version of **CHAPTER 4** have been published as K.D. Nizio, J.J. Harynuk, Profiling Alkyl Phosphates in Industrial Petroleum Samples by Comprehensive Two-dimensional Gas Chromatography with Nitrogen Phosphorus Detection (GC×GC-NPD), Post-column Deans Switching and Concurrent Backflushing. Energy Fuels 28 (2014) 1709. I was responsible for the operation and maintenance of instrumentation (GC×GC-FID/NPD), the data collection and analysis, as well as the manuscript composition/edits. J.J. Harynuk was the supervisory author and was involved with concept formation and manuscript composition and edits.

DEDICATION

To my Uncle Stephen…

"You are my sunshine, my only sunshine.
You make me happy when skies are grey.
You'll never know dear, how much I love you.
So please don't take my sunshine away."

- Jimmy Davis & Charles Mitchell

ACKNOWLEDGEMENTS

First and foremost, I would like to thank my supervisor Dr. James Harynuk for giving me the opportunity to be a part of his research group and for all his support and guidance over the past five years. I am extremely grateful for all of the conference and travel opportunities he has granted me, including CSC in Montreal, the AITF Summit in Banff, the GC×GC Symposium in Italy (twice!), Petrophase in Paris, and the MDC Workshop in Toronto.

Secondly, I would like to thank my fellow group members (most notably Brandon, Brianne, Teague, Nikolai, Paulina, Lawrence, and Chantel) with whom I have had the pleasure of working with and who have made each day of grad school pass by with plenty of laughter. To Brandon, thanks for the endless conversation and banter that only a best friend can provide and to Teague, thanks for being by my side throughout the torture of the lit review.

Thirdly, thank you to my committee members (Dr. Serpe, Dr. Hall, Dr. McDermott, and Dr. Reiner) for their time and feedback.

I would also like to thank my family: especially Mom, Dad, and Adam for their unconditional love and support. I also appreciate Mom, Dad, Adam, Sharon, Becky, and Katrina for taking the time to come out to Edmonton and visit, giving me plenty of excuses to explore Alberta. Thanks of course to all of my friends both here in Edmonton, out east in Halifax, and back home in Oshawa. A special shout out to Meagan, for providing me a shoulder on which to lean day in and day out, to Christine, for helping me with all things organic, and to CC, for helping get me through the long days and nights.

Without sports as a release from the stresses of grad student life, I would not have made it through. So thank you to my teammates on the Inter and AC Milan soccer teams, the Chemistry Brothers' hockey team, the Killer Frogs slo-pitch team and the Razorbacks/APEX women's field lacrosse teams.

Ken Schmidt (Wilson Analytical), Bryce McGarvey (ESSO Imperial Oil), and a Western Canadian Refinery are all gratefully acknowledged for supplying the fracture fluid and industrial petroleum/refinery samples used herein as well as for sharing with me their knowledge regarding alkyl phosphate contamination. I also wish to thank Olivier Niquette and KC Walbank (LECO) for helping me time and time again with the gremlins inhabiting my GC×GC instrumentation and Paul Patterson (DET) for answering all of my questions regarding the nitrogen-phosphorus detector.

Finally, this research would not have been possible without the financial support provided by NSERC, AITF, the Imperial Oil University Research Awards program, and the University of Alberta. In addition, I sincerely appreciate AITF, CASSS, and the University of Alberta's Graduate Students' Association and Faculty of Graduate Studies and Research for providing me with financial support in the form of conference travel grants.

TABLE OF CONTENTS

List of Tables

List of Figures

List of Schemes

List of Abbreviations

1°	–	Primary
1D	–	One-dimensional
2°	–	Secondary
^{2}D	–	Secondary dimension
AED	–	Atomic emission detector
ANN	–	Artificial neural network
bpd	–	Barrels per day
BSTFA	–	*N,O*-bis(trimethylsilyl)trifluoroacetamide
CAPP	–	Canadian Association of Petroleum Producers
CCQTA	–	Canadian Crude Quality Technical Association
CFT	–	Capillary Flow Technology
dB2EHP	–	Derivatized bis(2-ethylhexyl) phosphate
dDBP	–	Derivatized dibutyl phosphate
dMBP	–	Derivatized monobutyl phosphate
ECD	–	Electron capture detector
EPC	–	Electronic pressure control
FAME	–	Fatty acid methyl ester
FID	–	Flame ionization detector
FPD	–	Flame photometric detector
GC	–	Gas chromatography
GC×GC	–	Comprehensive two-dimensional gas chromatography
GC-MS	–	Gas chromatography – mass spectrometry

HDS	–	Hydrodesulfurization
HGO	–	Heavy gas oil
ICP-OES	–	Inductively coupled plasma – optical emission spectroscopy
IUPAC	–	International Union of Pure and Applied Chemistry
LOD	–	Limit of detection
LOQ	–	Limit of quantification
mFPD	–	Multiple flame photometric detector
MS	–	Mass spectrometry
MS/MS	–	Tandem mass spectrometry
$n\mathrm{C}_{19}$	–	Nonadecane
NCD	–	Nitrogen chemiluminescence detector
NPD	–	Nitrogen-phosphorus detector
PAH	–	Polycyclic aromatic hydrocarbon
pFPD	–	Pulsed flame photometric detector
PIONA	–	Paraffins, isoparaffins, olefins, naphthenes, and aromatics
ppm	–	Parts per million
PTFE	–	Polytetrafluoroethylene
qMS	–	Quadrupole mass spectrometry
R&D	–	Research and development
SCD	–	Sulfur chemiluminescence detector
SEP×SEP	–	Comprehensive multidimensional separations
S/N	–	Signal-to-noise ratio

T5P	–	Tripentyl phosphate
TBP	–	Tributyl phosphate
TCD	–	Thermal conductivity detector
TEP	–	Triethyl phosphate
THP	–	Trihexyl phosphate
TID	–	Thermionic ionization detector
TiPP	–	Triisopropyl phosphate
TMCS	–	Trimethylchlorosilane
TOFMS	–	Time-of-flight mass spectrometry
TOP	–	Trioctyl phosphate
TPhP	–	Triphenyl phosphate
TPP	–	Tripropyl phosphate
μECD	–	Micro-electron capture detector
VGO	–	Vacuum gas oil
VOC	–	Volatile organic compound
WCOT	–	Wall-coated open tubular
WCSB	–	Western Canadian sedimentary basin

List of Symbols

${}^1I^T$	–	Temperature-programmed retention indices in the first dimension
${}^1n_c$	–	Peak capacity of column in the first dimension
${}^2n_c$	–	Peak capacity of column in the second dimension
${}^1t_r$	–	Primary retention time
${}^1t'_{r,n}$	–	Adjusted retention time in the first dimension of the *n*-alkane eluting just before the phosphate of interest
${}^1t'_{r,N}$	–	Adjusted retention time in the first dimension of the *n*-alkane eluting just after the phosphate of interest
${}^1t'_{r,phosphate}$	–	Adjusted retention time of the phosphate of interest in the first dimension
${}^2t_r$	–	Secondary retention time
α	–	Selectivity factor
$[A]_M$	–	Concentration of the analyte in the mobile phase
$[A]_S$	–	Concentration of the analyte in the stationary phase
A_S	–	Peak area of the internal standard signal
A_X	–	Peak area of the analyte signal
β	–	Column phase ratio
d_f	–	Stationary phase film thickness
F	–	Response factor
H	–	Height equivalent to a theoretical plate
k	–	Retention factor; number of replicates of the sample that were measured
K	–	Distribution or partition coefficient

k_2	–	Retention factor of the later eluting analyte
L	–	Length of the column
m	–	Calibration slope
$MW_{phosphate}$	–	Molecular weight of the alkyl phosphate
m/z	–	Mass-to-charge ratio
n	–	Number of *xy* pairs in the calibration curve; number of carbon atoms of the *n*-alkane eluting just before the phosphate of interest
N	–	Theoretical number of plates; number of carbon atoms of the *n*-alkane eluting just after the phosphate of interest
n_c	–	Peak capacity of a column
P_M	–	Modulation period
R^2	–	Coefficient of determination
r_c	–	Internal radius of the column
R_s	–	Resolution
$[S]$	–	Concentration of the internal standard
s_x	–	Estimated standard deviation in concentration based on the calibration curve
s_y	–	Standard deviation in *y* of the calibration curve
t_m	–	Retention time of an unretained species (i.e. dead time)
t_r	–	Retention time of an analyte
$t_{r,1}$	–	Retention time of the early eluting analyte
$t_{r,2}$	–	Retention time of the later eluting analyte
$t_{r,max}$	–	Maximum retention time of your system
V_M	–	Volume of the mobile phase

V_S	–	Volume of the stationary phase
w_1	–	Peak width of the early eluting analyte at half height
w_2	–	Peak width of the later eluting analyte at half height
w_b	–	Peak width at the base
$[X]$	–	Concentration of the analyte
x_i	–	x values from the calibration curve
x_u	–	Average predicted concentration for the unknown based on k measurements

CHAPTER ONE: Introduction[1]

1.1 Motivation and Thesis Overview

Alkyl phosphates are used in a variety of ways in the petroleum industry. From additives used in well fracture processes to corrosion inhibitors, there are many routes by which traces of phosphorus-containing compounds can enter into petroleum processing facilities. When traces of phosphorus appear in crude oils they cause problems such as catalyst poisoning and distillation tower fouling [1,2]. These issues have occurred at a number of facilities across Canada with impacts measured in the tens of millions of dollars. Early research suggested that volatile phosphorus-containing compound(s) distilling at or below ~205 °C (400 F) are to blame, as evidenced by the fouling of the jet draw area [3].

This issue is particularly important for Canada because a significant fraction of Canada's conventional oil reserves are situated within geologies that require the use of phosphorus-containing additives during oil extraction. The Canadian Association of Petroleum Producers (CAPP) and the Canadian Crude Quality Technical Association (CCQTA) have specified a limit of 0.5 μg mL^{-1} total distillable phosphorus in feedstock [2,4]. This limit is monitored using inductively coupled plasma – optical emission spectroscopy (ICP-OES) [5,6], a technique that is plagued with poor precision and a high

[1] Portions of this chapter have been published in: a) K.D. Nizio, J.J. Harynuk, J. Chromatogr. A 1252 (2012) 171; b) K.D. Nizio, T.M. McGinitie, J.J. Harynuk, J. Chromatogr. A 1255 (2012) 12; c) K.D. Nizio, J.J. Harynuk, Energy Fuels 28 (2014) 1709.

limit of detection (0.5 ± 1 µg *phosphorus* mL^{-1}). Furthermore, this method is only capable of measuring total volatile phosphorus and cannot be used to identify or quantify individual phosphorus-containing compounds in petroleum samples. Without information about the species of phosphorus in the sample, it is impossible to truly study the chemistry surrounding phosphorus in refineries.

The Harynuk Group has approached this challenge using comprehensive two-dimensional gas chromatography (GC×GC) [7] to develop an innovative analytical technique that can be used to profile (i.e. speciate and quantify) alkyl phosphates in petroleum samples with improved precision and a lower limit of detection and quantification. In turn this will provide new information about alkyl phosphates in refineries, ultimately allowing for opportunities to develop and study mitigation strategies that cannot currently be contemplated due to a lack of understanding of the underlying chemistry.

GC×GC is a separations technique with numerous applications in many fields, especially petroleum [8,9,10]. GC×GC employs two gas chromatographic columns of different selectivity that separate compounds based on different retention mechanisms. As a result, mixtures with hundreds or even thousands of compounds may be separated. In using this technique, structurally similar compounds elute with distinct patterns on the retention plane aiding in compound identification [11,12,13]. In addition, GC×GC allows for improved resolution and separation power due to

increased peak capacity. Furthermore, this two-dimensional technique has enhanced sensitivity over one-dimensional gas chromatography (1D GC) because the chromatographic peaks are compressed into highly focused pulses. This is due to zone compression occurring at the modulator coupled with a chromatographic separation from chemical noise in the second dimension [14,15]. Overall, this technique is particularly valuable for separating complex samples such as petroleum, in addition to allowing for sample characterization and lower limits of detection and quantification.

For the speciation of di- and tri-alkyl phosphates in petroleum samples, the Harynuk Group first introduced a method based on trimethylsilylation derivatization followed by GC×GC separation using a flame ionization detector (FID) [16]. Although this analytical approach yielded quantification limits and a level of precision that exceeded the capabilities of the currently-accepted ICP-OES methodology, the research demonstrated the necessity for selective detection in this application, which was later achieved through the use of time-of-flight mass spectrometry (TOFMS) [17]. Overall, the TOFMS method was capable of both speciating and quantifying individual alkyl phosphates in petroleum samples with better precision and lower limits of quantification when compared to ICP-OES. However, GC×GC-TOFMS instrumentation is very expensive and is not suitable for use in on-line or at-line monitoring in a refinery environment.

This thesis presents the use of nitrogen-phosphorus detection in conjunction with comprehensive two-dimensional gas chromatography for

the speciation of trace alkyl phosphates in petroleum samples. The nitrogen-phosphorus detector (NPD) is a much more affordable and rugged detector (due to a larger dynamic range and the need for less frequent calibration) compared to a TOFMS detector, making this approach more attractive for implementation in an industrial setting.

The remainder of **CHAPTER 1** introduces the challenges of petroleum analysis and the relationship between alkyl phosphates and the oil industry. A brief discussion outlining the essential aspects of one-dimensional gas chromatography, nitrogen-phosphorus detection, and comprehensive two-dimensional gas chromatography is also presented. **CHAPTER 2** explores the development and optimization of a technique for the derivatization of mono- and di-alkyl phosphates, which are not volatile enough for analysis by gas chromatography. The use of a Deans switch for detector selection is also investigated. **CHAPTER 3** presents a method using GC×GC-FID/NPD and post-column Deans switching that provides qualitative and quantitative profiles of alkyl phosphates in industrial petroleum samples with increased precision and at levels less than or comparable to those achievable by ICP-OES [18]. A refinement to this method is presented in **CHAPTER 4** where the addition of splitless injection and concurrent backflushing resulted in limits of quantification two to three orders of magnitude lower than that capable by ICP-OES while still maintaining an increased precision [19]. **CHAPTER 5** applies this method to a study profiling alkyl phosphate contamination in a Western Canadian Refinery. Preliminary results are presented in which both

crude oil entering the refinery as well as petroleum product streams exiting the refinery are inspected. The final chapter of this work, **CHAPTER 6**, summarizes the conclusions made throughout this thesis and proposes future research for this project.

1.2 The Petroleum Analytical Challenge

Separation of the overwhelming number of compounds present in petroleum samples is one of the most complex analytical challenges a chemist can face. This complexity stems from the enormous number of individual components present in each class, rather than the number of chemical classes present in the sample, which are relatively limited for petroleum [20]. For example, middle distillates (boiling point range of 150 – 370 °C), are estimated to contain over one million components which are typically considered analytes of potential interest and not matrix constituents [11]. Furthermore, the number of components in a petroleum fraction increases exponentially with boiling point [12], adding to the analytical challenge. The sheer number of compounds in a petroleum sample quickly exceeds the available peak capacity of single-column techniques and even multidimensional separations are often limited to group-type analyses. It is well established that a separation of more than a few hundred components will almost invariably require comprehensive multidimensional separation (SEP×SEP) techniques [21,22,23].

Moreover, in order to satisfy the ever increasing demand for petroleum-based fuels and related products, industry is turning more and more frequently to the upgrading of heavier cuts of crude oil, such as extra heavy gas oils (HGOs) and vacuum gas oils (VGOs). These samples are inherently more complex than those from lighter oil sources, posing new challenges for the analysts involved in petroleum research and production. Additionally, these heavier fractions tend to include a higher proportion of nitrogen-, oxygen-, and sulfur-containing species than the lighter fractions; compounds that cause problems both with refinery operations and in finished products, making for interesting analytical targets. Comprehensive multidimensional separations are ideally suited to addressing the analytical challenges associated with measuring these compounds in petroleum samples.

SEP×SEP can also bring specific benefits to the entire spectrum of petroleum analyses, from the profiling of potential oilfields during exploration, to monitoring product streams during refinery operations, to assessing the presence of petroleum and its combustion products in the environment. Broadly speaking, petroleum analyses can be classified as follows: group-type analyses (including fingerprinting techniques) and the analysis of one or more target compounds in a petroleum sample.

1.2.1 Group-type Separations of Petroleum Samples

Group-type separations remain crucial for petroleum analyses. As the name implies, in these separations, the goal is to isolate specific groups of compounds in the samples. These group-type separations are useful for monitoring compositional changes of a petroleum sample over various time scales, ranging from over a period of minutes or hours (i.e. conversion of feeds in a refinery) to a period of years (i.e. changes of a petroleum product released into and weathered by the environment).

A classic example of a petroleum group-type analysis is the PIONA analysis used to profile the hydrocarbon content of a sample according to the concentrations of paraffins, isoparaffins, olefins, naphthenes, and aromatics to give an overview of its composition [24,25]. This analysis was initially improved through the use of multidimensional gas chromatography [26,27,28,29,30] and then further improved by the implementation of comprehensive two-dimensional gas chromatography [31], due to improved separation between families of hydrocarbons.

Considering the analysis of species containing heteroatoms, profiles of oxygen-, sulfur-, and nitrogen-containing compounds are all important. Oxygenates are a group of compounds that can cause rapid catalyst deactivation during hydroprocessing [32], and are often present at the $\mu g\ g^{-1}$ level [33]. In addition, some oxygen-containing compounds can polymerize, causing fuel instability and/or poor performance during combustion [32]. Profiling of oxygenates is thus required for monitoring product quality and

evaluating processes aimed at decreasing the oxygen content of petroleum products.

Likewise, sulfurous compounds in petroleum must be limited as organic sulfur can poison catalysts used during hydrocracking of heavy oils to generate lighter products [33]. Additionally, the sulfur content of fuels is now regulated in many jurisdictions since combustion oxidizes the sulfur into SO_2 and SO_3, which are significant atmospheric pollutants [34]. Methods to assess the distribution of sulfur across several chemical classes are essential, as the behaviour of the species with respect to catalyst poisoning, equipment corrosion, and sulfur-removal processes like hydrodesulfurization is dependent upon the class of sulfurous species present [34].

To remove sulfur from petroleum products, hydrodesulfurization (HDS) catalysts are used. These catalysts are easily poisoned by basic nitrogen-containing compounds (e.g. anilines) [35]. Nitrogenous species are also known to have adverse effects on the stability of fuels during storage [36]. This has driven the demand for methods capable of quantifying groups of nitrogenous compounds in petroleum samples with as much speciation as possible to provide insight into which specific compounds significantly impact these parameters. 1D GC coupled with nitrogen-specific detectors (e.g. AED, NCD, NPD, MS) only delivers limited information due to the numerous coelutions among the nitrogenous compounds in the samples [37,38].

Heavier crude fractions are but one unconventional petroleum fuel source being explored; processes such as Fischer-Tropsch reactions are being used to generate liquid fuels from coal and shale [39]. In these reactions, accurate monitoring of group-type composition is required to optimize the process for the synthesis of "greener" fuels with low sulfur and aromatic content [40]. However, coelutions of oxygenates (generated as by-products during Fischer-Tropsch reactions) with hydrocarbons result in inconsistent results when analyzed by conventional 1D separation techniques [41].

Other alternative sources of fuel include biodiesels and bio-oils, which are gaining some popularity in both the European Union and North America as possible routes to more sustainable transportation fuels [42]. Biodiesels are produced from the trans-esterification of vegetable oils (soybean, rapeseed, palm, etc.) or animal fats, resulting in a mixture of fatty acid methyl esters (FAMEs). Newer generations of biofuels may rely on waste biomass or algae as the feedstock. The FAME profiles of biodiesels vary depending on the feedstock and processing conditions, resulting in differences in product performance. Thus, profiling the FAME content of biodiesels (before and after blending with conventional petroleum fuels) is important to ensure product quality. However, the limited peak capacity of 1D separations is quickly exceeded by these samples [43,44].

1.2.2 Target Molecule Analysis in Petroleum Samples

The task of quantifying specific molecules within petroleum samples is challenging, but important. For example, biomarkers and their distributions can be used to characterize the source or level of maturity of crude oil [45], and can also be used to track spilled, weathered, and biodegraded petroleum pollution in the environment [46]. The identification of biomarkers in crude oils is a difficult undertaking using conventional 1D separations due to the sheer complexity of the samples and the generally low concentrations of biomarker compounds [47].

Techniques for the analysis of specific targets are also very important for environmental research. Numerous compounds are emitted as combustion products when fuels are consumed. These include volatile organic compounds (VOCs) and semi-volatiles such as the polycyclic aromatic hydrocarbons (PAHs), which are generated from incomplete combustion of petroleum products [12]. Some VOCs and PAHs represent significant health risks due to suspected carcinogenicity, mutagenicity, and teratogenicity. These compounds are also transformed during numerous atmospheric reactions, producing secondary products that are a potential health concern [48]. Separation and quantification of VOCs and PAHs in atmospheric particulate samples using conventional analytical techniques is difficult since they are at trace concentrations and of a complex nature [12,49].

The speciation of alkyl phosphate contaminants in petroleum samples is also an important target molecule analysis [7,16,17,18,19], and is the motivation of this thesis. These compounds enter certain crude oil supplies through their use as additives in some hydraulic well fracturing procedures and as a result, damage distillation towers, poison catalysts, and potentially contaminate products, affecting consumers.

1.3 Alkyl Phosphates and the Oil Industry

1.3.1 Oil Production and Fracture Fluids

Oil production involves the extraction of crude oil from underground reservoirs, as well as the processing of raw crude within refineries in order to produce petroleum products. The choice of oil extraction technique relies heavily on the features of the well being processed [50]. Hydraulic fracturing is one of the most common, particularly in partially-depleted reservoirs. This process uses the repetitive pumping of a fracture fluid into the well at pressures on the order of 15,000 psi [51]. These high pressures create a network of fractures within the rock that provide channels through which the oil can flow to the wellhead. A propping agent (proppant) such as advanced ceramics [52], sand grains, walnut shell fragments, tempered glass beads, aluminum pellets, nylon pellets or a mixture thereof [53] is introduced with the fracture fluid. The proppant serves to prevent a collapse of the

fracture network once the pressure is removed, ensuring clear passages to the wellhead.

During the fracturing process the fracture fluid must be viscous in order to both maintain the proppant particles in suspension and effectively transmit the fracturing pressure into the rock. Gellants are added to the fracture fluids as viscosity builders. Once the fracturing process is complete, the viscosity of the fracture fluid must be reduced so that it can be easily withdrawn from the well while leaving the proppant in place. This is achieved through the addition of a breaker that disrupts the self-assembly properties of the gel, greatly decreasing the gel's viscosity [51].

As previously mentioned, the choice of fracture fluid and gellant are influenced by the geology of the well being processed. Water-sensitive geologies (i.e. those containing clays that may swell or dislodge and migrate with the use of water-based fracture fluids, effectively closing off the fractures and restricting flow), like those found in the Western Canadian Sedimentary Basin (WCSB) (**Figure 1-1**), require oil-based fracture fluids. These oil-based fracture fluids typically contain a dialkyl phosphate ester gellant [54]. Hexacoordinate metal cations (e.g. Fe^{3+} from ferric sulfate; Al^{3+} from aluminum chloride, aluminum acetate, or aluminum isopropoxide) are added along with the dialkyl phosphates in order to establish a viscous, cross-linked gel. The mechanism of self-assembly is not entirely understood, although a few mechanisms have been proposed including the formation of double-bridged polymers between the phosphorus containing compound and

metal cations [55], as well as the formation of highly ordered cylindrical aggregates [56,57,58]. Nevertheless, the formation of these flexible gel networks is vital to the fracture fluid's function. Finally, this self-assembled gel can be disrupted by the addition of water, alcohols, surfactants, or by adjusting the pH [51]. The process of gel disruption can take several hours to complete; therefore the gel breaker can be added during the formation of the fracture fluid without compromising the fracture fluid's performance during the well fracturing procedure.

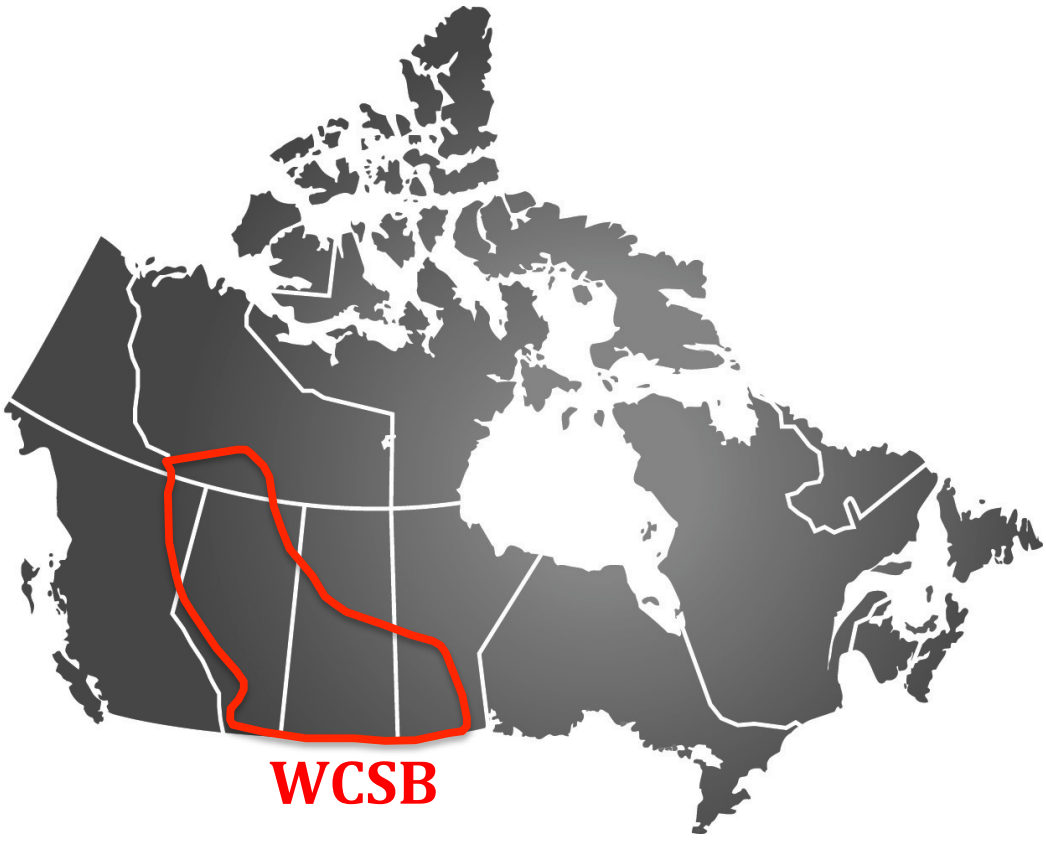

Figure 1-1. Map depicting the location of the Western Canadian Sedimentary Basin (WCSB).
Figure adapted from reference [59].

1.3.2 Chemical Properties of Alkyl Phosphates

An alkyl phosphate (**Figure 1-2**) is composed of a phosphoric acid (H_3PO_4) core, where at least one or more of the hydroxyl protons is replaced by an alkyl chain. The alkyl phosphates containing three alkyl chains are called trialkyl phosphates, while those only containing one or two alkyl groups are referred to as mono- and di-alkyl phosphates, respectively. The gellants added to oil-based fracture fluids are typically dialkyl phosphates with alkyl chains 2 – 30 carbons in length [60,61]. However, these gellants are manufactured as a technical mixture formed from the reaction of phosphorus pentoxide, phosphorus pentachloride, or phosphorus oxychloride with selected alcohols, resulting in a mixture containing dialkyl phosphates as the major components, with small amounts of mono- and tri-alkyl phosphates [51,54]. Depending on the alcohol(s) added, the alkyl chains may be of the same (i.e. pure phosphate) or differing lengths (i.e. mixed phosphate). Alkyl phosphate volatility increases with the degree of alkylation (i.e. monoalkyl < dialkyl < trialkyl; due to less intermolecular hydrogen bonding) and decreases with increasing chain length (due to increasing molecular weight).

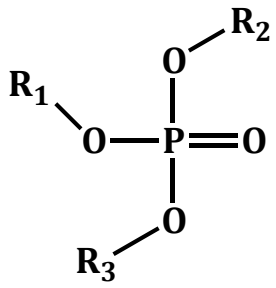

Figure 1-2. Chemical structure of an alkyl phosphate, where R_1, R_2, and R_3 are either a hydrogen atom or an alkyl chain, and at least one of R_1, R_2, or R_3 must be an alkyl chain.

1.3.3 Alkyl Phosphates and Refinery Fouling

Once oil has been recovered, it is sent to a refinery where it is processed in a distillation tower to produce various petroleum products such as gasoline, kerosene, diesel fuel, jet fuel, lubrication oils etc. In 1995, three Canadian refineries experienced throughput restrictions in their distillation towers due to plugging of distillation tower trays in the jet fuel draw area. Inspection of the towers revealed a polymerized, glue-type foulant that impeded tray operation [62]. All three refineries experienced fouling again in 1998. Since 1998, additional fouling in heat exchanger equipment, steam strippers, hydrotreaters, and distillation towers has occurred at refineries processing Canadian light sweet crude in both Canada and the United States. In addition, a catalyst bed with a projected lifetime of two years was poisoned and deactivated after only four months.

The photo in **Figure 1-3A** shows a typical, clean distillation tower tray while **Figure 1-3B** shows a plugged/fouled distillation tower tray containing a solid, grit-like deposit. Elemental analysis of these deposits confirmed the

presence of a number of expected elements (i.e. 30 to 40% carbon, 3 to 4% hydrogen, 3 to 7% nitrogen, and 1 to 2% copper/nickel by weight) along with surprisingly high levels of phosphorus, about 8 to 12% by weight [62].

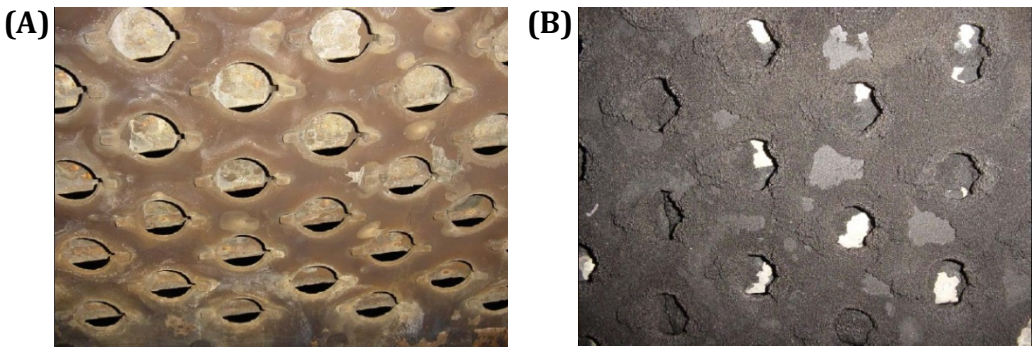

Figure 1-3. Photographs of (A) a typical clean, operational distillation tower tray and (B) a fouled distillation tower tray containing a grit-like deposit [3].

These traces of phosphorus are the suspected source of refinery equipment damage. The potential also exists for the phosphorus-containing compounds to deactivate hydrodesulfurization catalysts [63,64], as well as contaminate final products, affecting consumers. Overall, this contamination has resulted in decreased and unpredictable lifespans of refinery equipment, in addition to more recurrent maintenance shutdowns. Outages for unplanned maintenance shutdowns can last for 7 days in order to steam out, purge and blank the distillation tower, perform vessel entry and inspection, complete any repairs that are required (e.g. grit blasting of deposits on trays) and then purge and restart the tower [3]. During this time, tanks containing unprocessed crude begin to fill up and product output is severely decreased.

To put this into perspective, a typical distillation tower processes about 70,000 – 120,000 barrels of crude per day (bpd), which is approximately 8.3 – 14.3 million litres (1 standard US barrel = 119.24 L). As a result, deals must be made with other refiners to cover the product shortfall and help take care of the unprocessed crude that has been purchased, but cannot be accommodated. Overall, these unanticipated outages can cost North American refineries tens of millions of dollars.

The Canadian Crude Quality Technical Association (CCQTA) formed a Phosphorus Project Group [65] to study and manage the phosphorus problem. The group was formed in 1996 and is still meeting today, bringing together representatives from refineries, pipeline companies, service companies, chemical producers, and testing laboratories. Initial studies by the Phosphorus Project Group determined that the phosphorus most likely originated from a pre-refinery additive or contaminant entering the refinery with the unprocessed crude.

Phosphorus-containing compounds are used in a variety of ways in the petroleum industry. From additives used in well fracture processes to corrosion inhibitors, there are many ways in which traces of phosphorus-containing compounds could potentially enter into petroleum processing facilities. However, the use of phosphonate ester compounds ($R\text{-}PO(OR)_2$) as corrosion inhibitors was quickly ruled out as the source of the fouling, as the corrosion inhibitors did not produce any volatile phosphorus when tested [66].

After fracturing, spent fracture fluid mixed with crude oil (flowback) is ideally diverted prior to the well going into production. However, it is a challenge to identify when the majority of the fracture fluid has been removed, and traces of gellant will inevitably contaminate the oil. Therefore, the phosphorus-based gellants (i.e. alkyl phosphates) used in well fracturing became the suspected source of the refinery-fouling incidents. When the crude oil containing traces of phosphorus-based gellant is heated to 340 °C during distillation, some of the phosphates may be of low enough molecular weight to vaporize and distill up the tower. This includes both tri- and di-alkyl phosphates [1]. Studies have also shown that alkyl phosphates begin to decompose at approximately 240 °C, undergoing hydrolysis of the ester linkages (provided there is a source of water), forming more volatile, lower molecular weight species [2,66,67]. It is also possible that these compounds form more volatile species through other unknown chemical reactions (e.g. transesterification) during distillation. Overall, the volatile species appear to be distilling at or below ~205 °C (400 F) as suggested by the fouling of the jet fuel draw area [3]. As the phosphorus-containing compounds condense out of the gas phase, they may undergo further reaction to form grit-like deposits, ultimately plugging the holes in the distillation tower trays. In addition, it is possible that the phosphorus-containing compounds may be present in the distillate stream of the jet fuel draw, affecting consumers [66].

In 1995, no phosphorus removal processes were available to prevent the phosphorus-containing material from entering the refinery. Furthermore,

no alternative phosphate-free gellant chemistry was commercially available. As a result, in 2007, the CCQTA and the Canadian Association of Petroleum Producers (CAPP) set a limit/specification of 0.5 μg mL^{-1} as the maximum concentration of total volatile phosphorus permissible in the distillate fraction of feedstock, which is monitored using inductively coupled plasma – optical emission spectroscopy (ICP-OES) [5,6]. If this limit is not met, the producers must discontinue deliveries until the specification is achieved or provide a remediation plan for meeting the specification within a defined timeframe. Unfortunately, the impact of phosphorus on refineries appears to be a result of chronic exposure to trace levels of phosphorus rather than acute exposure at elevated levels [67]. Consequently, the specification set forth by the CCQTA and CAPP has not completely eliminated maintenance shutdowns but has lessened their frequency.

As a result of the ever-increasing demand for oil production, more wells are put into production each year in the Western Canadian Sedimentary Basin, further increasing refinery operations. This demand puts pressure on the well fracturing companies to begin rushing oil into the pipelines as soon as possible, which is likely to lead to flowback fluid contamination of the crude. Potential solutions to limit volatile phosphorus (150 – 300 μg *phosphorus* mL^{-1} in current dialkyl phosphate technology) contamination of crude oil have been proposed [3]. Proposals include the formulation of new, less volatile phosphonate ester oil gellants (3 – 6 μg *phosphorus* mL^{-1}) [2,66,68,69], as well as the use of phosphate-based

gellants with longer alkyl chain moieties (15 – 30 μg *phosphorus* mL^{-1}) [1]. However, increasing the molecular weight of the alkyl phosphates does not prevent these compounds from undergoing hydrolysis, producing more volatile, lower molecular-weight species within the distillation tower. On the other hand, the new phosphonate gellant systems are too expensive to commercialize and register for use in Canada [2]. Therefore, the ICP-OES method is currently the only accepted way to prevent or predict refinery shutdowns as a result of fouling through routine monitoring of volatile phosphorus levels in crude.

1.3.4 Identification and Quantification of Alkyl Phosphates in Crude

The fouling of refinery equipment is thought to be the result of chronic exposure to trace quantities of volatile phosphorus [67]. Unfortunately, the ICP-OES based method for the analysis of total volatile phosphorus in distillate fractions of crude oil [5,6] is plagued with poor precision and a high limit of detection (0.5 ± 1 μg *phosphorus* mL^{-1}). As a result of these limitations, the total volatile phosphorus specification set forth by the CCQTA and CAPP is actually enforced at 1.5 μg mL^{-1} as opposed to 0.5 μg mL^{-1}. The poor precision and high limit of detection is likely a consequence of poor mass transfer efficiency in the ICP nebulizer as a result of irreproducible viscosity due to the varying composition of distillate fractions (i.e. higher viscosity results in bigger droplets and less mass transfer to the flame). Additionally, the ICP-OES method cannot speciate the

phosphates, leaving industry incapable of studying this chemistry at a molecular level. Consequently, a method that is effectively capable of pinpointing phosphate sources and enforcing the 0.5 μg mL^{-1} specification of total volatile phosphorus is currently unavailable. The Harynuk Group has approached this challenge using comprehensive two-dimensional gas chromatography (GC×GC), a separations technique with many applications in several fields [7].

Petroleum analysis presents many unique challenges as a result of the large number of compounds present in petroleum samples. Consequently, the use of multidimensional separation techniques will almost invariably be required in order to overcome these challenges. GC×GC in particular, has established itself as an indispensable tool for the analysis of petroleum samples. Many petroleum analyses are focused on group-type separations; however, the separation power afforded by GC×GC is being exploited more and more for the targeted analysis of specific analytes in these complex matrices. The application of GC×GC to the petroleum field has been reviewed recently [10] and several other reviews cover broader aspects of the technique [9,70,71,72,73,74,75,76,77,78].

The Harynuk Group first introduced a method based on trimethylsilylation derivatization followed by GC×GC separation using a flame ionization detector (FID) for the speciation of di- and tri-alkyl phosphates in petroleum samples [16]. Although this analytical approach yielded quantification limits and a level of precision that exceeded the

capabilities of the currently-accepted ICP-OES methodology, the research demonstrated the necessity for selective detection in this application, which was achieved through the use of time-of-flight mass spectrometry (TOFMS) [17]. Overall, this method was capable of both speciating and quantifying alkyl phosphates in petroleum samples with better precision and lower limits of detection when compared to ICP-OES. However, TOFMS instrumentation is very expensive and is therefore not suitable for use in on-line or at-line monitoring in a refinery environment.

As a result of this work, the Harynuk Group began testing a nitrogen-phosphorus detector (NPD) as a cheaper and more rugged alternative (due to a larger dynamic range and the need for less frequent calibration) for selective detection. Derivatization is required for mono- and di-alkyl phosphates in order to render them volatile enough for analysis by gas chromatography. Unfortunately, the excess silylation reagents from the trimethylsilylation derivatization mixture were found to coat the NPD bead in a layer of SiO_2 (**Figure 1-4**), deactivating the surface chemistry responsible for the analytical signal and fully quenching the signal after fewer than 10 chromatographic runs. A silicon-free derivatization technique using 1-chloro-3-iodopropane [79] was investigated (see **CHAPTER 2**; **Section 2.2**), however, the derivatization reaction yields were low in hydrocarbon solvents, which were used to simulate a petroleum sample matrix.

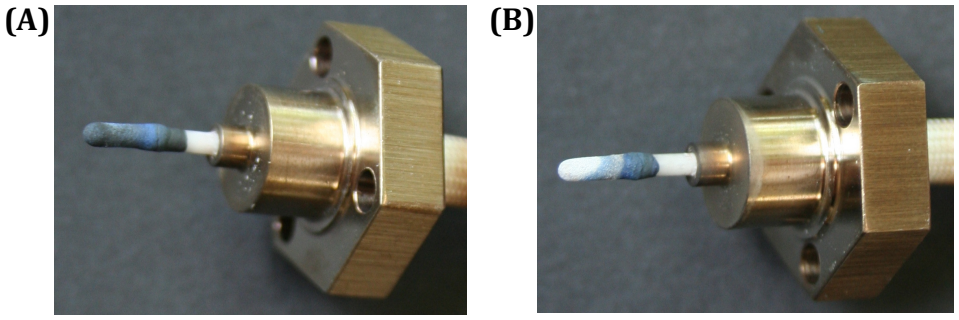

Figure 1-4. Photographs of (A) a typical clean, operational NPD bead and (B) a severely fouled, defective NPD bead containing a deposit of SiO_2.

The flame photometric detector (FPD), another robust and affordable phosphorus-selective detector, was considered next due to its recent success at selectively detecting organophosphorus pesticide compounds when coupled to GC×GC [80,81]. However, the analyte chemiluminescence in conventional continuous-mode FPDs is known to have severe complications with quenching in the presence of even modest quantities of co-eluting hydrocarbons [82,83,84]. On the other hand, the pulsed-FPD (pFPD) has minimal quenching but is limited by the rate at which the flame can be pulsed. As a result, the pFPD is only capable of collecting data at a rate of 3 – 5 Hz, which is too slow for GC×GC. Finally, the more recently-developed multiple flame photometric detector (mFPD), produced by Hayward and Thurbide [85,86], is resistant to quenching and only limited by the electrometer chosen (i.e. data collection rates of 50 – 200 Hz are possible). Therefore, the mFPD would be ideal for this application; however, it is not yet commercially available.

Consequently, the purpose of this research was to develop an approach that would allow for the profiling of alkyl phosphates in industrial petroleum samples using the combination of trimethylsilyl derivatization, GC×GC, and an NPD, while also maintaining a low limit of detection and quantification and increased precision when compared with ICP-OES. This combination was accomplished with the aid of Agilent's Capillary Flow Technology (i.e. Deans switch), which was used to divert the excess silylation reagents away from the NPD to an FID (see **CHAPTER 2**; **Section 2.3**). With the addition of the Deans switch, the lifetime of the NPD bead was increased from approximately 5 chromatographic runs to over 1,000. **CHAPTER 3** and **CHAPTER 4** then use this technology to develop and optimize a method for profiling alkyl phosphates in real industrial petroleum samples, while **CHAPTER 5** implements this method for profiling alkyl phosphate contamination within a refinery.

1.4 Chromatography

1.4.1 One-dimensional Gas Chromatography

Gas chromatography, introduced in 1952 [87], is a technique used for the separation and analysis of compounds that can be vaporized without decomposition. This includes compounds with appreciable vapour pressures within the range of temperatures accessible by gas chromatography (i.e. ambient up to ~350 °C). In addition some semi-volatile compounds and

compounds containing functional groups with active/labile protons, such as –SH, –OH, –NH, and –COOH (that can result in intermolecular hydrogen bonding), require derivatization (i.e. a chemical reaction to produce a product of similar structure) in order to render these compounds volatile enough for analysis by GC. The essential components of a gas chromatograph, (**Figure 1-5**) include the sample inlet (i.e. injection port), column, oven, and detector. In addition, a computer is used to control the instrument and to record and display the detectors output.

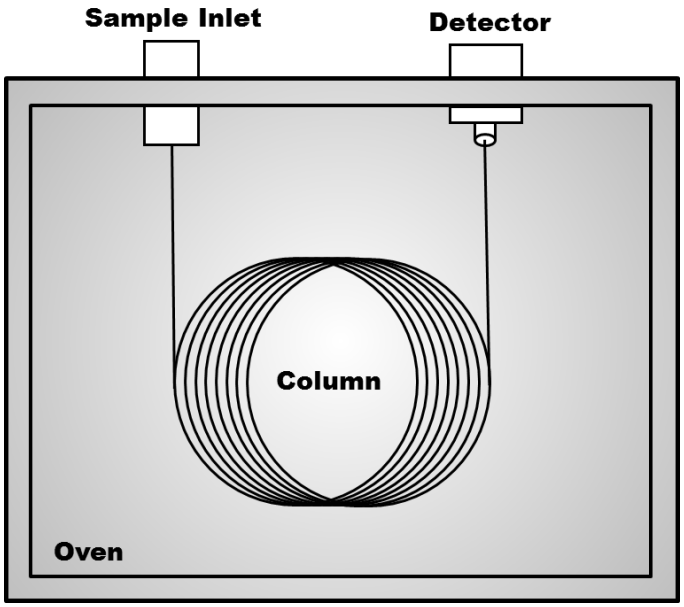

Figure 1-5. Schematic of a one-dimensional GC system.

In gas chromatography the sample is introduced into the heated injection port (typically 250 °C) using a microsyringe, where it undergoes vaporization. The vaporized sample is then swept onto the chromatographic

column by an inert gaseous mobile phase, such as helium, hydrogen, or nitrogen, which is controlled by a flow or pressure regulator. The mobile phase (also known as the carrier gas) carries the sample through the column, which is housed within an oven that can be heated isothermally or with a temperature-programmed ramp. The column is composed of a fused silica capillary that is coated on the inside with a thin layer of polymer or viscous liquid known as the stationary phase. The chemistry of the stationary phase can vary greatly (e.g. apolar phases such as polydimethyl siloxane versus polar phases like cyanopropyl) and is chosen based on the chemistry/structure/characteristics (i.e. possible intermolecular forces) of the analytes being separated (based on the general chemical principle that "like dissolves like"). Column dimensions for these wall-coated open tubular (WCOT) columns are typically 10 – 30 m in length and 0.18 – 0.25 mm in internal diameter with a stationary phase film thickness of 0.1 – 5.0 μm. As the analyte molecules travel down the chromatographic column, they partition/equilibrate between the mobile phase and the stationary phase to cause separation.

The distribution or partition coefficient, *K*, is used to describe the ratio of the equilibrium concentration of an analyte in the stationary phase ($[A]_S$) to the equilibrium concentration of analyte in the mobile phase ($[A]_M$) as expressed in Equation (1-1):

$$K = \frac{[A]_S}{[A]_M} = k\beta \qquad (1\text{-}1)$$

where the distribution coefficient can be calculated using the retention factor (k) and the phase ratio (β). Analytes with a larger distribution coefficient have a higher affinity for the stationary phase and are consequently more retained by the stationary phase resulting in longer retention times (i.e. the time required for the analyte to elute from the column). Therefore separation occurs if the components of the sample have different affinities for the stationary phase (i.e. different distribution coefficients leading to different retention times). Since the distribution coefficient is temperature-dependent, increasing the temperature in temperature-programmed separations causes the distribution coefficient to decrease, and analytes are less retained (i.e. shorter retention times). Consequently, temperature-programming is often used to decrease the overall analysis time.

As mentioned previously, the distribution coefficient is determined from the retention factor of the analyte and the phase ratio of the column. The retention factor, k, often used to describe the migration rate of an analyte on a column, can be determined from the retention time of the analyte (t_r) and the dead time (i.e. the retention time of an unretained species, t_m) as indicated in Equation (1-2):

$$k = \frac{t_r - t_m}{t_m} \qquad (1\text{-}2)$$

where the dead time can be obtained from the injection of unretained species, such as methane or air. The phase ratio, β, is described as the ratio of the volume of the mobile phase to the volume of the stationary phase as shown in Equation (1-3):

$$\beta = \frac{V_M}{V_S} = \frac{r_C}{2d_f} \quad (1\text{-}3)$$

where the phase ratio can be calculated using the internal radius of the column (r_c) and the stationary phase film thickness (d_f), which are provided by the column manufacturer.

Once the analytes reach the end of the column, they are analyzed by a detector. The purpose of the detector is to convert a chemical species (through a chemical or physical process) into a measurable electronic signal that can be registered by a computer, thus allowing the chromatographic separation to be "visualized". This visual output is known as a chromatogram, which plots signal intensity versus retention time. Several different detectors are available for gas chromatography. These detectors can be classified as universal (i.e. registers a response for all analytes) or selective (i.e. only registers a response for analytes containing a specific element for example). Universal detectors include the thermal conductivity detector (TCD) and the mass spectrometer (MS). In addition, the flame ionization detector (FID) responds to most carbon-containing compounds and is therefore considered almost universal. Selective detectors include: the atomic emission detector (AED), which is a multielement detector that can be used to measure up to 23 different elements (the carbon and hydrogen modes can be considered universal); the flame photometric detector (FPD), which is selective for sulfur and phosphorus; the electron capture detector (ECD), which is selective for halogenated compounds (as well as phosphorus- and nitrogen-containing compounds in some cases); the nitrogen-phosphorus detector (NPD), which

is selective for nitrogen and phosphorus; the nitrogen chemiluminescence detector (NCD), which is selective for nitrogen; and the sulfur chemiluminescence detector (SCD), which is selective for sulfur.

The detector employed throughout this project was an element-selective thermionic ionization detector (TID) operated in the specific mode of detecting nitrogen- and phosphorus-containing compounds. In this mode, the TID is more commonly referred to as a nitrogen-phosphorus detector or NPD. **Figure 1-6** displays a schematic of the thermionic ionization detector. Overall, the TID is very similar in design to the FID, except for the addition of an electrically-heated thermionic bead (see **Figure 1-4**) composed of an alkali salt in an inorganic ceramic cement matrix [88]. The element selectivity of the TID depends on the bead composition, bead surface temperature, and the gaseous environment composition, which ultimately determines the gaseous products formed from the decomposition of the sample components [89,90].

The thermionic ionization detector is named for the nature of the ionization process, where the sample molecules are converted to negative ions through the extraction of electrons emitted from the electrically-heated thermionic bead [88]. The overall operating principles of the NPD are not yet completely understood and a detailed mechanism for the specificity of the ionization process remains elusive [88,90,91]. Nevertheless, an acceptable theory involves surface catalytic ionization in which the alkali atoms (e.g. rubidium or cesium [88]) incorporated in the ceramic bead do not leave

the bead surface, but rather catalyze electron transfer taking place on the bead surface [89,92].

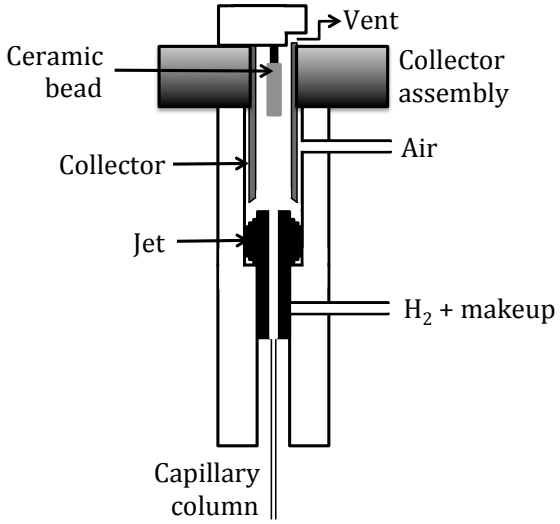

Figure 1-6. Schematic of a thermionic ionization detector.
Figure adapted from Figure 7.7 in reference [141].

The carrier gas (containing the sample analytes) is mixed with hydrogen gas at the base of the detector. The hydrogen flow rate is set low (10 – 15× lower than that used for an FID), between 2 – 6 mL min^{-1}, in order to prevent a self-sustaining flame from being established like that used in an FID [88]. The carrier gas/hydrogen mix then flows through a jet into the detector where it is mixed with air. Inside the detector, the gaseous mixture interacts with the electrically-heated ceramic bead, which is situated above the jet, generating a plasma. The plasma particles are thought to collide with the alkali metal atoms causing ionization on the surface of the bead [91]. Nitrogen- and phosphorus-containing compounds enter the plasma where

they decompose, generating negative ions through an ionization process that remains unclear [93]. A voltage is set between the collector electrode and the jet tip allowing for the collection of negative ions by the positive collector electrode; the resulting ion current is measured by an electrometer and the overall detector output current is then proportional to the number of ions collected [90].

It is well known that thermionic ionization detectors exhibit decreasing sensitivity with increasing operating time due to the depletion of the thermionic bead activity [90]. It is believed that as the bead ages the surface of the bead changes, resulting in decreased sensitivity; some claim this is a result of depletion of the alkali metal [94] while others claim that it is due to the deposition of contaminants [93]. In addition, the use of high bead voltages and/or temperatures reduces the lifetime of the bead. As a result, the thermionic bead needs to be replaced periodically. Herein the NPD bead was replaced when a background output of 10 pA could no longer be achieved by increasing the bead voltage. Finally, detector gas flows have been shown to have a significant impact on peak magnitude and peak asymmetry [91]. Therefore, the detector gas flows must be properly optimized in order to obtain optimal results.

In chromatography, resolution (R_S) is a measurement of the separation between two adjacent peaks, relative to their peak widths, as described in Equation (1-4):

$$R_S = \frac{2(t_{r,2} - t_{r,1})}{1.699(w_1 + w_2)} \quad (1\text{-}4)$$

where $t_{r,2}$ is the retention time of the later eluting analyte, $t_{r,1}$ is the retention time of the early eluting analyte, w_1 is the peak width of the early eluting analyte at half height, and w_2 is the peak width of the later eluting analyte at half height. Baseline resolution is achieved between two analytes when the resolution between them equals 1.5. Resolution can be improved by maximizing the three terms in Equation (1-5):

$$R_s = \left(\frac{\sqrt{N}}{4}\right)\left(\frac{k_2}{k_2+1}\right)\left(\frac{\alpha-1}{\alpha}\right) \quad (1\text{-}5)$$

where N is a measure of column efficiency known as the theoretical number of plates, k_2 is the retention factor of the later eluting analyte, and α is the selectivity factor. The theoretical number of plates, which originates from distillation, can be calculated from the retention time of the analyte (t_r) and the peak width at the baseline (w_b) as shown in Equation (1-6).

$$N = 16\left(\frac{t_r}{w_b}\right)^2 = \frac{L}{H} \quad (1\text{-}6)$$

The theoretical number of plates can also be described as the length of the column (L) divided by the height equivalent to a theoretical plate (H). Therefore, column efficiency, and thus resolution, can be improved by increasing the column length. However, this leads to an increase in overall analysis time, which is often undesirable. Furthermore, efficiency has a square-root dependence; therefore a four-fold increase in efficiency is required to give a two-fold improvement in resolution. Such an increase in efficiency is often difficult to achieve without making the column, and therefore the separation, unreasonably long. Increasing the retention factor

by lowering the temperature of the column can also lead to an improved resolution, however this too results in an increase in retention time. Finally, the resolution between two analytes can be improved through a change in selectivity by changing the chemistry of the stationary phase and thus changing the interactions between the analytes and the stationary phase.

A final measure of column efficiency and overall system performance is peak capacity, the maximum theoretical number of resolvable peaks that can fit within a given separation space at a specified resolution. The peak capacity of a column (n_c) can be calculated using Equation (1-7):

$$n_c = \frac{t_{r,max} - t_m}{w_b R_s} \quad (1\text{-}7)$$

where $t_{r,max}$ is the maximum retention time of your system, t_m is the dead time, w_b is the peak width at the base, and R_S is the resolution. Unfortunately, the maximum theoretical peak capacity is rarely achieved as a result of the random distribution of peaks, which can lead to peaks occupying the same space (i.e. overlapping), as well as the presence of unused or unoccupied separation space [22]. The sheer number of compounds in a complex sample like petroleum quickly exceeds the available peak capacity of single-column techniques. Therefore, as postulated by Giddings, a multidimensional separation (i.e. multi-column technique) is likely to be required when the number of independent variables that must be specified to separate the components of a sample (i.e. sample dimensionality) exceeds the number of different separation mechanisms to which the sample is subjected (i.e. system/instrument dimensionality) [23].

1.4.2 Multidimensional Chromatography

Multidimensional separations have been developed in response to the challenges presented by petroleum and other complex samples (e.g. biological or environmental). Early examples of multidimensional separations for petroleum samples emerged in the late 1950s, when researchers were analyzing various Platformer streams for the key components involved in C6 conversion using a two-stage, gas–liquid chromatographic unit [95]. The theory pertaining to comprehensive multidimensional separations was developed largely by Giddings and co-workers in the 1980s and 1990s [23,96,97] and is still a matter of discussion in recent literature [98,99,100].

In roughly the last 20 years, significant technological advances in areas such as column and column-coupling technology, mobile phase flow control, and detector design have been combined with improvements in electronics and computers resulting in a proliferation of multidimensional separation techniques. These techniques have been applied to numerous samples in all areas where conventional separations are used, such as food and flavour [101,102], biological samples [103,104], environmental studies [44,105,106], forensics [107,108,109], and petroleum products [8,9]. My recently published review [10] highlights technology that has been (or could be) used for multidimensional separations of petroleum and fuels.

In order for a separation to be considered multidimensional, it must meet two criteria: 1) sample components must be displaced by two or more

separation techniques, where each technique provides different selectivity and demonstrates a distinct retention profile (i.e. there is some degree of orthogonality between dimensions); 2) components separated by any single separation must not be recombined in any further separation dimension (i.e. the sampling/fractionation rate of material entering a separation dimension is sufficiently high to maintain the profiles of compounds eluting from the separation that immediately precedes it).

Multidimensional separations can be categorized as either heart-cut or comprehensive. In heart-cutting multidimensional separations, only a subset of the sample components are passed on to further separation dimensions. In contrast, comprehensive multidimensional separations require that the entire sample, or a representative portion thereof, be submitted to each separation dimension such that the resulting chromatogram is representative of the entire sample [110]. Therefore, heart-cutting is best suited for the analysis of a few target constituents while comprehensive multidimensional separations are best suited for more complete compositional analyses. This thesis will focus on the use of comprehensive multidimensional separations, specifically comprehensive two-dimensional gas chromatography; however, additional information on the evolution, applications, and future prospects of heart-cutting multidimensional gas chromatography can be found in a recent review by Tranchida *et al*. [111].

1.4.3 Comprehensive Two-dimensional Gas Chromatography

Comprehensive two-dimensional gas chromatography (GC×GC) was first demonstrated by Liu and Phillips in 1991 [112]. The petroleum community has played a very active role in supporting and promoting the technique. Compared to one-dimensional gas chromatography, GC×GC allows for improved resolution and separation power due to increased peak capacity. The peak capacity in 1D GC is equal to the peak capacity of a single column (n_c), while in GC×GC the peak capacity is equal to the product of the individual peak capacities of the columns in both the primary and secondary dimensions ($^1n_c \times ^2n_c$). Unfortunately, like with 1D GC, this increased maximum theoretical peak capacity is rarely achieved as a result of the random distribution of peaks [22].

In addition to increased peak capacity, GC×GC provides enhanced sensitivity and detectability of peaks over one-dimensional GC. Secondary separation removes interfering chemical signals (decreases noise) to improve sensitivity. Increased detectability is achieved due to the chromatographic peaks being compressed into highly focused pulses as a result of zone compression occurring at the modulator (this effect is lessened in pneumatic modulators) [14,15]. Furthermore, structurally-related compounds elute with distinct patterns on the retention plane to result in ordered chromatograms, which can assist in sample characterization and compound identification [11,12,13].

As shown in **Figure 1-7**, GC×GC instrumentation is very similar to that used for 1D GC, the only differences being the addition of a secondary (2°) column and a modulator. Some systems also have a separate second dimension oven. The two GC columns employed in GC×GC are of different selectivity, where the primary (1°) column is typically coated with an apolar stationary phase such as dimethylpolysiloxane, while the secondary column usually has a more selective, polar stationary phase like 50%-diphenyldimethylpolysiloxane or polyethylene glycol. Although the apolar×polar column configuration is most commonly used, operators are not confined to this arrangement and in some cases a polar×apolar column configuration [113,114,115,116,117,118] is more favourable.

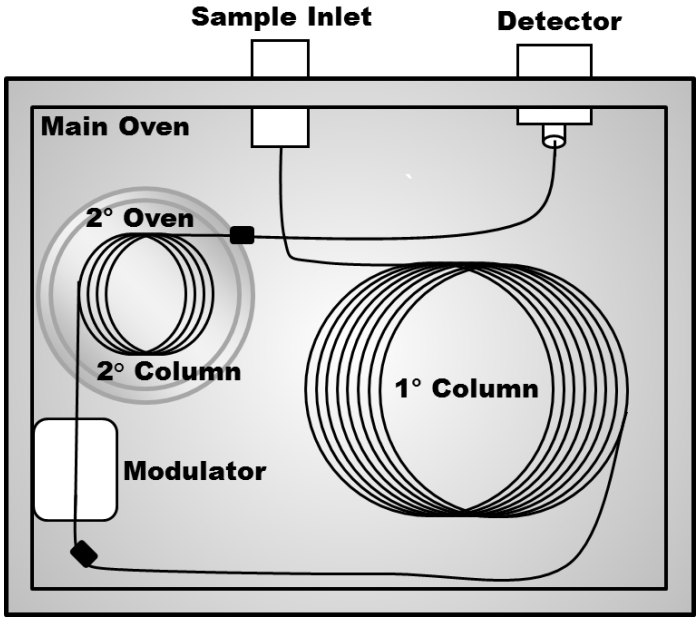

Figure 1-7. Schematic of a GC×GC system.

The first dimension column is typically of similar dimensions to that used in a conventional one-dimensional separation (10 – 30 m × 0.18 – 0.25 mm), while the second dimension column is typically shorter and narrower (0.5 – 2 m × 0.1 – 0.18 mm). This is the general setup for column sets with the more common thermal modulators. With differential flow pneumatic modulators, it is often advantageous to use a narrow-bore column in the first dimension (0.1 mm) and a wider diameter in the second dimension (0.25 mm) [119]. This is because the primary dimension in flow-modulated systems is typically operated at a very low flow rate (typically <1 mL min^{-1}) and the second dimension is operated at a much higher flow rate (15 – 20 mL min^{-1}).

The primary and secondary columns are coupled at an interface known as a modulator. The purpose of the modulator is to trap/collect effluent from the primary column and then periodically introduce the collected fraction onto the secondary column as a narrow pulse. Ideally, the modulator will collect three or four fractions for each first-dimension peak in order to preserve the separation achieved in the first dimension [120]. The secondary separation is performed quickly (e.g. 2 – 3 s); preferably, each pulse introduced onto the secondary column is separated before the following pulse is introduced in order to prevent wrap-around [121], which occurs when the second dimension retention time exceeds the modulation period.

The modulator is often referred to as the 'heart' of a GC×GC system. Many different modulator designs exist. The various designs can be categorized as either pneumatic modulators (valve- or flow-based) [122,123,124,125,126,127,128,129] or thermal modulators (heater-based or cryogenic) [112,130,131,132,133,134,135,136]. The valve- or flow-based modulators utilize valves and pressure differentials (i.e. pneumatic means) to physically compress (in some cases) and divert gas phase analytes from the primary column onto the secondary column. Alternatively, thermal modulators use temperature differentials to focus and inject analytes onto the secondary column. Heater-based modulators apply an increase in temperature, while cryogenic modulators apply a decrease in temperature. Overall, thermal modulation is more commonly applied than pneumatic modulation. More information concerning individual modulator development, design, and function may be found in the following reviews [75,76].

Pneumatic modulators are applicable to a wide range of analytes, including even the most volatile, being able to modulate analytes ranging from helium to C_{40}. Thermal modulators, on the other hand, do not trap highly volatile analytes very well. Systems using liquid nitrogen can modulate C_4 to C_{40}, while those using liquid carbon dioxide or chilled air can modulate C_7/C_8 and above. Thermal modulators, however, are much more flexible in operation compared to pneumatic modulators. Thermal modulators can have a wide range of modulation periods from 1.5 s up to 10 s, or higher if

necessary. Unfortunately, the range of useable modulation periods for pneumatic modulators is defined by column geometries and channel volumes and is usually restricted to less than 2 s. Finally, the pneumatic modulators do not require a cryogen, which makes these instruments cheaper to run and potentially capable of being field portable, unlike instruments using a thermal modulator.

The modulator used to collect the data presented in this thesis is a dual-stage, quad-jet thermal modulator (LECO), which is depicted in **Figure 1-8**. This particular design is considered to be "consumable-free" as it uses purified air (i.e. free of water and carbon dioxide) chilled to -70 °C, as opposed to expensive coolants like liquid nitrogen or liquid carbon dioxide. The disadvantage here is that the chilled air is not cold enough to trap and modulate highly volatile analytes.

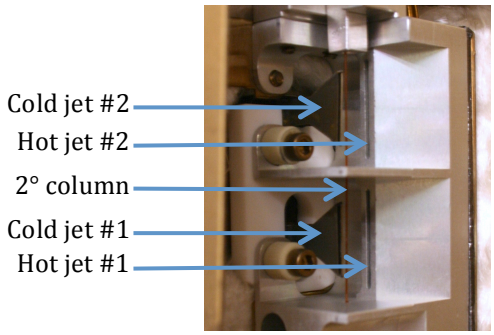

Figure 1-8. Consumable-free LECO GC×GC system dual-stage, quad-jet thermal modulator (LECO Instruments, St. Joseph, MI, United States).

A column connecter made of fused silica joins the primary and secondary columns. The secondary column is then threaded through the

modulator passing in front of the hot and cold jets (**Figure 1-8**) before entering the secondary oven. The analytes are modulated on the secondary column in order to maintain the focusing effect gained by the modulator. In addition, the column connecter would be difficult to fit between the modulator and second dimension oven in this setup (**Figure 1-7**).

Figure 1-9 shows a schematic of the dual-stage, quad-jet thermal modulator system. When material enters the modulator (**Figure 1-9A**) it is first trapped and focused (**Figure 1-9B**) by cold jet #1 in the first stage of the modulator. Cold jet #1 then turns off while hot jet #1 turns on (**Figure 1-9C**), causing the trapped material to begin moving down the column towards the second stage of the modulator where cold jet #2 is turned on to further focus the material (**Figure 1-9D**). The purpose of dual stage modulation is to prevent the breakthrough of unfocused material onto the secondary column. Next, hot jet #1 is turned off while cold jet #1 is turned back on to continue trapping and focusing another round of material. Subsequently, hot jet #2 is turned on to inject the first set of trapped material onto the secondary column in the secondary oven (**Figure 1-9E**). Cold jet #1 remains on at this point in order to prevent breakthrough. This process then repeats throughout the entire run. The frequency of this process depends on the modulation period, which is defined in the GC method within the LECO ChromaTOF software. The hot pulse time and cooling time between stages can also be modified within the method.

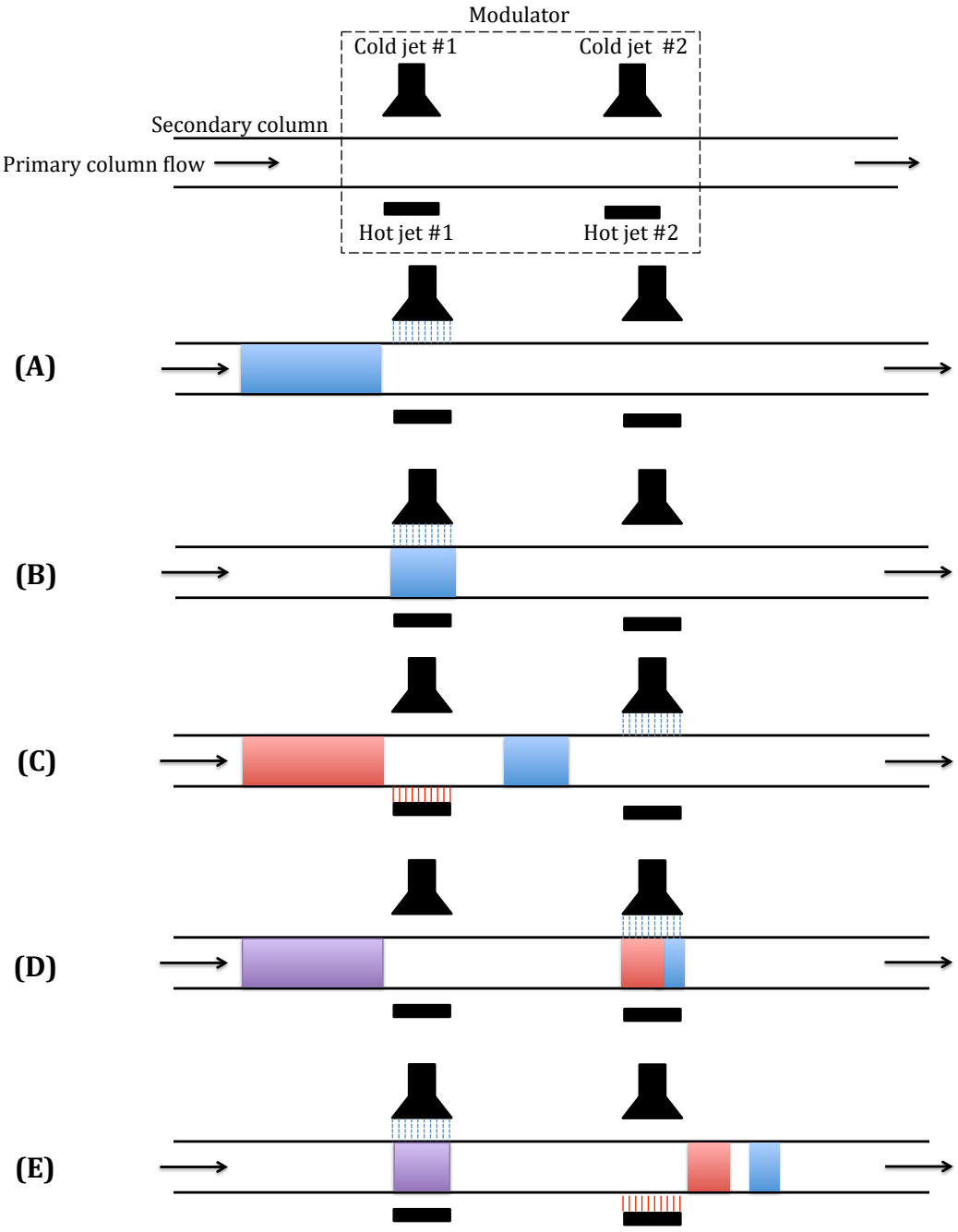

Figure 1-9. Schematic depicting the operation of LECO's dual-stage, quad-jet thermal modulator system. As material enters the modulator (A) it is focused into a narrow band by cold jet #1 (B). Cold jet #1 then turns off while hot jet #1 turns on releasing the material and cold jet #2 turns on to prevent breakthrough (C) and further focus the material (D). Finally, cold jet #2 turns off while hot jet #2 turns on launching an injection pulse onto the second dimension (E) and cold jet #1 turns back on to prevent breakthrough. This process then repeats itself.

As a result of the short columns used in the second dimension, the separation in this dimension occurs quickly (and usually isothermally) to result in chromatographic peaks typically 100 – 400 ms wide at the base. Therefore, the detector must be capable of collecting data at a minimum rate of 50 – 100 Hz in order to ascertain the minimum ten detection data points across a peak width required for acceptable quantification.

Many of the detectors that can be used for conventional 1D GC can also be used for GC×GC; this list includes the flame ionization detector, atomic emission detector, flame photometric detector, micro-electron capture detector (μECD), nitrogen-phosphorus detector, nitrogen chemiluminescence detector, sulfur chemiluminescence detector, and time-of-flight mass spectrometer. Nevertheless, due to the narrow peaks that result from GC×GC, some detectors suitable for conventional 1D GC are not capable of fast enough acquisition rates for GC×GC. An example of such a detector is the quadrupole mass spectrometer. However, despite the slower scan rate of the quadrupole mass spectrometer, some GC×GC users have evaluated the applicability of quadrupole mass spectrometry (qMS) for use with GC×GC through a reduced mass scan range, which results in an increase in the scan speed [137,138]. In addition, B.J.G Silva *et al*. [139] demonstrated the potential use of rapid-scanning qMS (20 Hz scanning frequency and scan speeds of 10,000 amu s^{-1}) as a detector for GC×GC for both qualitative and quantitative analyses yielding satisfactory results. Other detectors not suitable for GC×GC include the pulsed FPD, the thermal conductivity detector,

and the conventional or macro-ECD. Further information involving detector technologies for comprehensive two-dimensional gas chromatography can be found in the following review [140] and book [141].

Data analysis in GC×GC involves the transformation of a linear one-dimensional raw chromatogram (**Figure 1-10A**) into a two-dimensional contour plot (**Figure 1-10D**) characteristic of this technique. Regardless of the type of detector used, the detector records a continuous series of short second dimension chromatograms that are strung together into a linear one-dimensional raw chromatogram as portrayed in **Figure 1-10A**. Here, t_1, t_2, and t_3 signify the times at which an injection onto the secondary column occurred. A computer software program (e.g. LECO's ChromaTOF software) then slices the raw chromatogram into numerous individual chromatograms at the indicated injection times (**Figure 1-10B**). Next, the software aligns the individual chromatograms side-by-side with the primary (${}^1t_r$) and secondary (${}^2t_r$) retention times on the x- and y-axes, respectively, and the signal intensity on the z-axis (**Figure 1-10C**). Three-dimensional GC×GC data is more commonly viewed from the *xy*-plane (like a topographical map) where the peaks appear as colour coded spots (**Figure 1-10D**). This representation of the data, referred to as a contour plot, allows for much easier interpretation of the data, as demonstrated in **Figure 1-11**, which displays both a three-dimensional chromatogram and a contour plot of a real industrial petroleum sample.

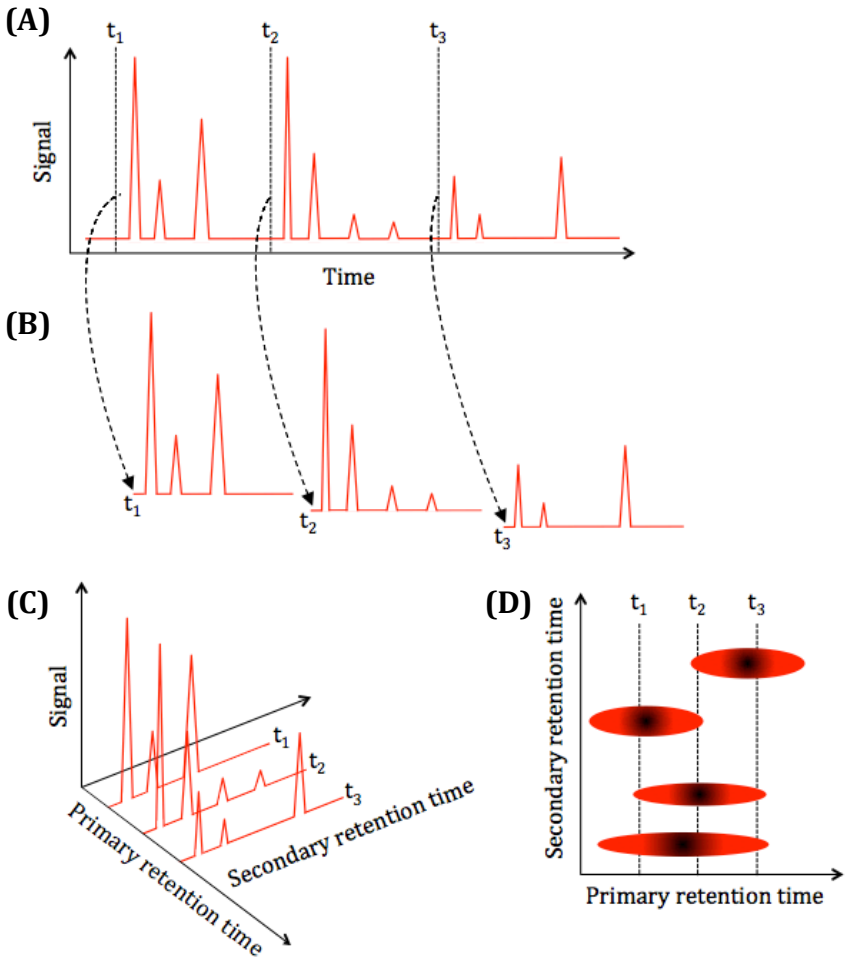

Figure 1-10: GC×GC data representation. The detector records a continuous series of short second dimension chromatograms strung together in a raw chromatogram (A), where t_1, t_2, and t_3 signify the times at which an injection onto the secondary column transpired. The computer then slices the raw chromatogram (A) at the indicated injection times resulting in numerous individual chromatograms (B). The individual chromatograms (B) are then aligned with the primary and secondary retention times on the x- and y-axes respectively and the signal intensity on the z-axis (C). However, GC×GC data is conventionally viewed from above where the peaks appear as colour coded spots (D). This representation of the data is referred to as a contour plot.
Figure adapted from Figure 7 in reference [70].

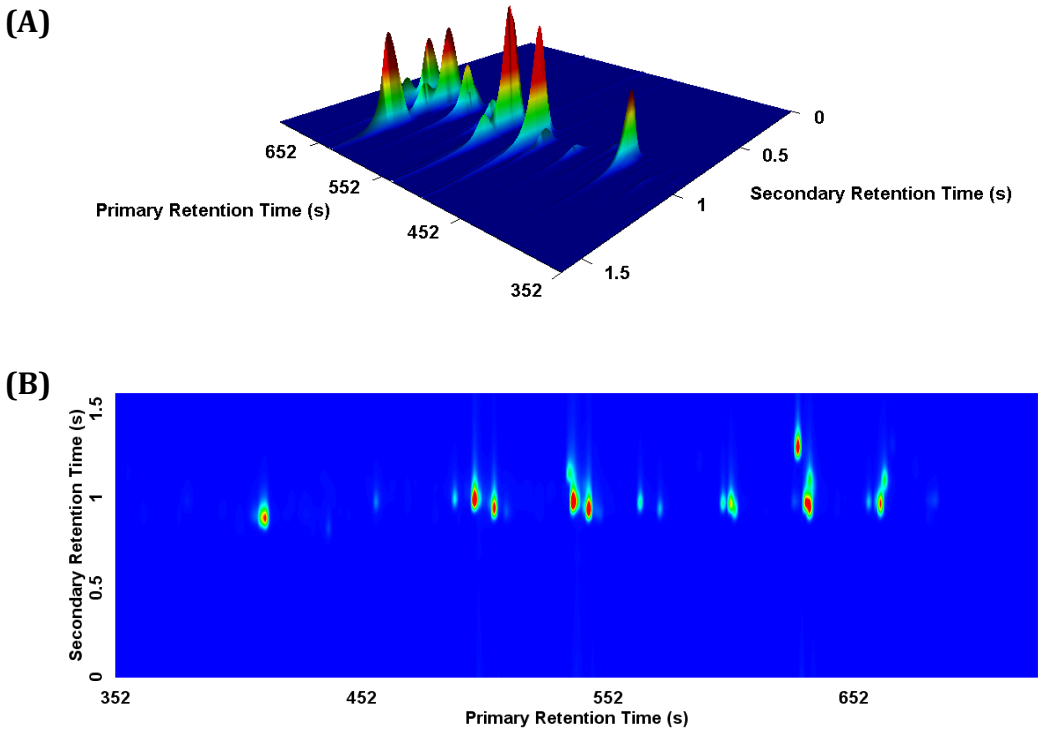

Figure 1-11. A three-dimensional chromatogram (A) and a contour plot (B) of a real industrial petroleum sample (crude mixed with fracture fluid, Imperial Oil, Sarnia, ON, Canada) analyzed using GC×GC-NPD.

Since the analyte peaks are fractionated into a number of slices during the modulation process (i.e. a base peak and multiple sub-peaks), the total signal for an analyte is calculated using the cumulative area that results from the integration of the base peak and each sub-peak deemed to originate from the same compound on the basis of retention coordinates and, if available, mass spectral matching criteria. Unfortunately, the modulation process produces two potential sources of error in GC×GC that do not exist in conventional 1D GC [98]. These errors can arise as a result of: 1) the summation of multiple sub-peaks, which each contains their own integration

error; or 2) phase shifting, which affects the proportion of analyte in each sub-peak. The calculations defined in the literature for determining an analyte's limit of detection (LOD) and limit of quantification (LOQ) [142,143] do not account for these errors and are therefore specific to one-dimensional techniques. The International Union of Pure and Applied Chemistry (IUPAC) defines the LOD as "the minimum single result which, with a stated probability, can be distinguished from a suitable blank value", while the LOQ is defined as "the minimum quantifiable value" [144]. Without LOD and LOQ calculations specific to comprehensive multidimensional separations, some studies have used the classical approach of 3σ of the noise for the LOD and 10σ for the LOQ [145,146,147,148], while other studies have proposed their own definitions/approaches [149,150,151,152,153]. Consequently, a theoretical study of these terms is ongoing in the Harynuk Group [154].

One of the biggest challenges for comprehensive multidimensional separations is handling the complex data that are generated by these systems. Though the basics of transforming the raw chromatographic data into the three-dimensional representation (^1t_r, ^2t_r, signal intensity) and the need for unique data processing tools have been long-since established [70,122,149,155], new tools for data interpretation are continually under development [156,157,158,159,160,161,162]. My review [10] presents some recent developments in the area of data interpretation and analysis, focusing on approaches that have been or could be particularly useful in the analysis of petroleum and fuels. Readers wishing a more thorough discussion are

directed to reviews of the application of chemometrics to the analysis of multidimensional separations data [163,164,165,166,167].

Finally, GC×GC method optimization can be very difficult and time consuming compared to conventional 1D GC optimization [168]. This is due to the increased number of parameters associated with GC×GC, many of which are interconnected and therefore a small change to any one parameter can have a large affect on another. Mostafa *et al.* review the optimization of main operational parameters in GC×GC, including stationary phase chemistries, column dimensions, carrier gas flow, temperature programs, and modulation and detector settings [169].

1.5 Summary

The analysis of alkyl phosphates in petroleum samples is of particular interest to refineries that process conventional crude oil derived from the Western Canada Sedimentary Basin and other similar geologies. This is due to the use of alkyl phosphate-based additives that are used during crude oil recovery processes, and the subsequent contamination of the produced oil. Phosphate contamination causes numerous problems including refinery equipment fouling, the poisoning of catalysts, and potential impacts on downstream processes or consumers if these phosphates enter various product streams. As a result, the Canadian Association of Petroleum Producers has specified a level of 0.5 μg mL^{-1} total volatile phosphorus as the maximum concentration acceptable in feedstock. However, at present, no

analytical methodology exists to facilitate the identification or quantification of the individual phosphorus-containing compounds in petroleum samples at such trace levels; thus making the current specification of 0.5 μg mL^{-1} difficult to enforce. Consequently, this thesis explores the use of comprehensive two-dimensional gas chromatography combined with nitrogen-phosphorus detection for the speciation and quantification of trace alkyl phosphates in real industrial petroleum samples.

CHAPTER TWO: Development and Optimization of a Derivatization Method for Mono- and Di-alkyl Phosphates

2.1 Introduction

Alkyl phosphate volatility increases with degree of alkylation (i.e. monoalkyl < dialkyl < trialkyl; due to less intermolecular hydrogen bonding) and decreases with increasing chain length (due to increasing molecular weight). As a result, the mono- and di-alkyl phosphates - those containing only one or two alkyl groups, respectively - require derivatization in order to render these compounds volatile enough for analysis by gas chromatography (GC). Previous research in the Harynuk Group [16] examined the derivatization of dialkyl phosphates by trimethylsilylation [170,171]. In the course of this reaction (illustrated in **Scheme 2-1**) trimethylsilyl groups ($-Si(CH_3)_3$), from either trimethylchlorosilane (TMCS) or *N,O*-bis(trimethylsilyl)trifluoroacetamide (BSTFA), replace the labile protons on the mono- and di-alkyl phosphates. TMCS is typically added to BSTFA in small quantities (1% volume per volume is usually sufficient) as a silylation catalyst, ensuring effective derivatization of hindered hydroxyl groups [172,173,174]. The overall reaction occurs in two steps. In the first step, pyridine acts as a base deprotonating the acidic proton on the phosphate in order to create the more nucleophilic anionic species. The second step is viewed as a nucleophilic attack upon the silicon atom of the silyl donor, producing a bimolecular transition state (i.e. an S_N2-like

mechanism) [171,172,173,174,175]. The leaving group (X), in the case of both BSTFA and TMCS, is readily lost from the transition state as a result of the leaving group's low basicity and ability to stabilize a negative charge. The resulting silylated phosphate is more volatile than the parent phosphate due to the replacement of the labile hydrogen atom with a trimethylsilyl group, effectively eliminating the possibility of intermolecular hydrogen bonding between the phosphate molecules [172]. The by-products from this reaction (i.e. trimethylsilyltrifluoroacetamide and trifluoroacetamide) are highly volatile and, as a result, usually elute early in GC analyses along with the solvent therefore rarely interfering with analyte peaks in the resulting chromatogram [174].

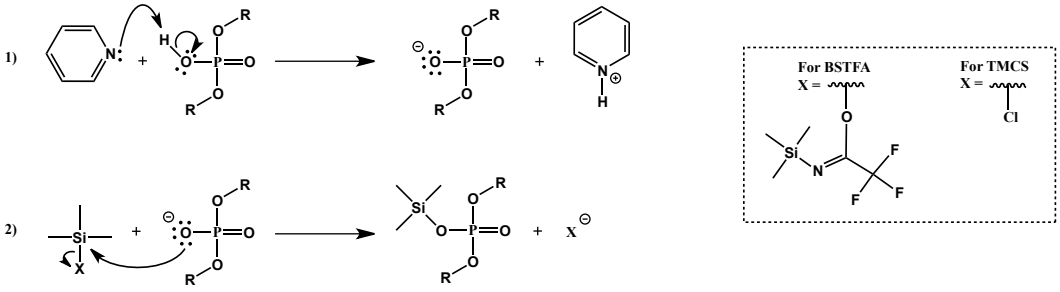

Scheme 2-1. Reaction scheme for mono- and di-alkyl phosphate derivatization by trimethylsilylation using BSTFA, TMCS, and pyridine.

Further research in the Harynuk Group [7,16] revealed the need for comprehensive multidimensional separations (i.e. comprehensive two-dimensional gas chromatography, GC×GC) coupled with selective detection for the speciation of alkyl phosphates in petroleum samples, which are

comprised of complex and highly variable matrices. Together, GC×GC and selective detection reduce the chance of coelutions between matrix compounds and the analytes of interest. Thus reducing chemical noise and subsequently increasing the overall signal-to-noise ratio, resulting in lower limits of detection and quantification. In addition, GC×GC separations provide ordered chromatograms that group structurally-related compounds together [11,12,13], thus facilitating sample characterization (i.e. speciation), which is further aided by the use of a selective detector.

The first selective detector investigated was a nitrogen-phosphorus detector (NPD); however, this detector was quickly discovered to be incompatible with the trimethylsilylation reaction required for derivatization of the mono- and di-alkyl phosphates. The excess silicon from the silylation reagents was found to coat the NPD bead in a layer of SiO_2, deactivating the surface chemistry responsible for the analytical response and fully quenching the signal after fewer than 10 chromatographic runs. Consequently, this chapter explores possible solutions for the problem of excess silicon which include: 1) the use of a different selective detector that would not be deactivated by excess silicon; 2) the use of a silicon-free derivatization method; and finally, 3) the use of a Deans switch to allow for post-column flow switching to protect the NPD from excess silylation reagents.

The flame photometric detector (FPD), selective for sulfur and phosphorus, has demonstrated recent success at selectively detecting organophosphorus pesticides in food matrices when coupled to

GC×GC [80,81]. However, despite this success, conventional continuous-mode FPDs are known to have severe complications with quenching in the presence of even modest quantities of co-eluting hydrocarbons [82,83,84] and are therefore not ideal for this work, which involves the analysis of petroleum samples. Furthermore, pulsed-mode FPD detectors, which are expected to have negligible quenching, have data collection rates on the order of 3 – 5 Hz, which is too slow for GC×GC. Nevertheless, a multiple flame photometric detector (mFPD), recently developed by Thurbide *et al.* [85,86], is resistant to quenching and has data collection rates of greater than 50 Hz. In addition, this detector would allow for the use of a single calibration curve for all alkyl phosphates as a result of a uniform alkyl phosphate response factor, permitting the quantification of both known and suspected alkyl phosphates. Overall, this detector would be ideal for the speciation of alkyl phosphates in petroleum samples; however, this detector is not yet commercially available.

The only other feasible option for the selective detection of alkyl phosphates in combination with GC×GC is time-of-flight mass spectrometry (TOFMS). When applied to the analysis of alkyl phosphates in petroleum samples, GC×GC-TOFMS was capable of both speciating and quantifying individual alkyl phosphates in petroleum samples with good precision and low limits of quantification [17]. However, the NPD and FPD are much more rugged (due to a larger dynamic range and the need for less frequent calibration) and affordable detectors compared to a TOFMS detector and,

therefore, would be greatly preferred for routine use in a refinery process laboratory. Consequently, this chapter investigates both the use of a derivatization reaction that does not involve the use of silicon, as well as the use of a Deans switch in order to find a way to utilize both GC×GC and nitrogen-phosphorus detection for the selective detection and speciation of alkyl phosphates in petroleum samples without deactivating the NPD bead.

2.2 Silicon-free Derivatization Method: 1-Chloro-3-iodopropane

2.2.1 Overview

Herein, a silicon-free derivatization reaction from the literature [176] utilizing 1-chloro-3-iodopropane and potassium carbonate is investigated (**Scheme 2-2**). The overall reaction occurs in two steps resulting in the labile protons on the mono- and di-alkyl phosphates being replaced with chloropropyl groups. In the first step, the base, potassium carbonate, deprotonates the acidic proton on the phosphate in order to create the more nucleophilic anionic species as described previously for the trimethylsilylation reaction (**Scheme 2-1**). The second and final step is a bimolecular nucleophilic substitution (i.e. S_N2 reaction) resulting in the loss of an iodide anion due to the iodide ion's low basicity and ability to stabilize a negative charge.

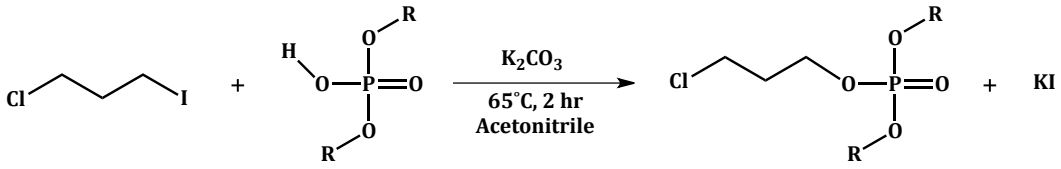

Scheme 2-2. Reaction scheme for mono- and di-alkyl phosphate derivatization using 1-chloro-3-iodopropane and potassium carbonate [176].

2.2.2 Experimental

2.2.2.1 Materials and Reagents

All reagents were used as received unless otherwise stated. Derivatization was performed according to a method reported by De Alwis *et al*. [176] using 1-chloro-3-iodopropane (Sigma–Aldrich, Oakville, ON, Canada), anhydrous potassium carbonate (Caledon, Georgetown, ON, Canada), and acetonitrile (BDH Chemicals, VWR, Edmonton, AB, Canada). The derivatization reaction was also performed in heptane (Caledon), as well as both with and without the addition of pyridine (Caledon). The alkyl phosphate standards used for the examination of the derivatization reaction consisted of a mixture of mono- and di-butyl phosphates (Alfa Aesar, Ward Hill, MA, United States). Tributyl phosphate (Sigma–Aldrich) was used as an internal standard diluted in both acetonitrile (BDH Chemicals, VWR) and hexane (Sigma–Aldrich) to give 1,076 and 1,026 μg mL^{-1} stock solutions respectively.

All derivatization reactions were carried out in 1.8 mL glass GC vials with polytetrafluoroethylene (PTFE)-lined silicone septa (Chromatographic Specialties, Brockville, ON, Canada). Derivatization was performed by adding

20 mg of potassium carbonate and 30 µL of 1-chloro-3-iodopropane to 500 µL of a monobutyl and dibutyl phosphate solution prepared in either acetonitrile (55 µg mL^{-1}) or heptane (61 µg mL^{-1}). In some cases, 30 µL of pyridine was also added. The reaction was left to proceed for two hours at either room temperature (~26 °C) or in an oven at 67 °C. The vials were shaken every 30 min. After the two hours were complete, the vials were left to cool to room temperature if necessary and centrifuged for 5 min. The supernatant was pipetted to a new vial and 10 µL of internal standard solution (tributyl phosphate) was added before analysis by gas chromatography. The tributyl phosphate solution prepared in acetonitrile was added to the reactions performed in acetonitrile and the tributyl phosphate solution prepared in hexane was added to the reactions performed in heptane.

2.2.2.2 Instrumentation and Experimental Conditions

Analysis was conducted using a Varian CP-3800 GC (Varian, Saint-Laurent, Quebec, Canada) equipped with a flame ionization detector (FID) and a Varian 1079 split/splitless injector. The column configuration consisted of a 30 m × 0.25 mm, 0.25 µm SLB-5ms column (Supelco, Oakville, ON, Canada). All injections were performed manually using 1 µL of sample and a split ratio of 20:1. The inlet temperature was 250 °C. The oven temperature program was 150 – 260 °C at 8 °C min^{-1}. Ultra-high purity helium (Praxair, Edmonton, AB, Canada) was used as the carrier gas with a

linear velocity of 30 cm s^{-1}. The FID was kept at 280 °C. Data were acquired at a rate of 40 Hz and processed using Galaxie software (Varian).

Gas chromatography – mass spectrometry (GC-MS) was used to confirm if the peaks were indeed derivatized dibutyl and monobutyl phosphate. GC-MS analysis was carried out using a 7890A GC with a 5975 quadrupole MS (Agilent Technologies, Mississauga, ON, Canada) equipped with a 30 m × 0.25 mm, 0.25 μm HP-5 column (Agilent Technologies). A volume of 2 μL was injected with an Agilent 7683B Series autosampler and a split ratio of 20:1. The inlet temperature was 250 °C. The oven temperature program was 150 – 260 °C at 8 °C min^{-1}. Ultra-high purity helium (Praxair) was used as a carrier gas at a constant flow rate of 1.0 mL min^{-1}. The initial solvent delay was 3 min and mass spectra were collected from *m/z* 45 to *m/z* 300 at a rate of 10 spectra s^{-1}. Data were processed using Galaxie (Varian) and Chemstation™ (Agilent Technologies) software.

2.2.3 Results and Discussion

In the literature, the derivatization of dialkyl phosphates using 1-chloro-3-iodopropane was performed in acetonitrile [176]. Herein, the reaction was also tested in heptane (i.e. a hydrocarbon solvent) in order to mimic the matrix of future crude oil and petroleum samples. The addition of pyridine to the reaction mix was also evaluated in an attempt to speed up the reaction. Finally, the reaction was carried out at both room temperature and 67 °C as executed in the literature [176]. Reaction success and failure was

established using gas chromatography and the presence or absence, respectively, of peaks representing the derivatized mono- and di-butyl phosphates. Peak identities were confirmed using mass spectrometric fragmentation patterns collected using GC-MS.

Overall, the derivatization reaction was found to proceed at room temperature in acetonitrile in both the absence and presence of pyridine as displayed in **Figure 2-1A** and **B**. The peak appearing at 6.1 min represents tributyl phosphate (TBP), which was used as an internal standard. The peaks for derivatized mono- (dMBP) and di-butyl (dDBP) phosphate appear at 10.1 and 7.8 min respectively. Unfortunately, when the derivatization reaction was repeated in heptane at room temperature, the reaction failed in both the absence (**Figure 2-1C**) and presence (**Figure 2-1D**) of pyridine, as suggested by the absence of peaks at 7.8 and 10.1 min.

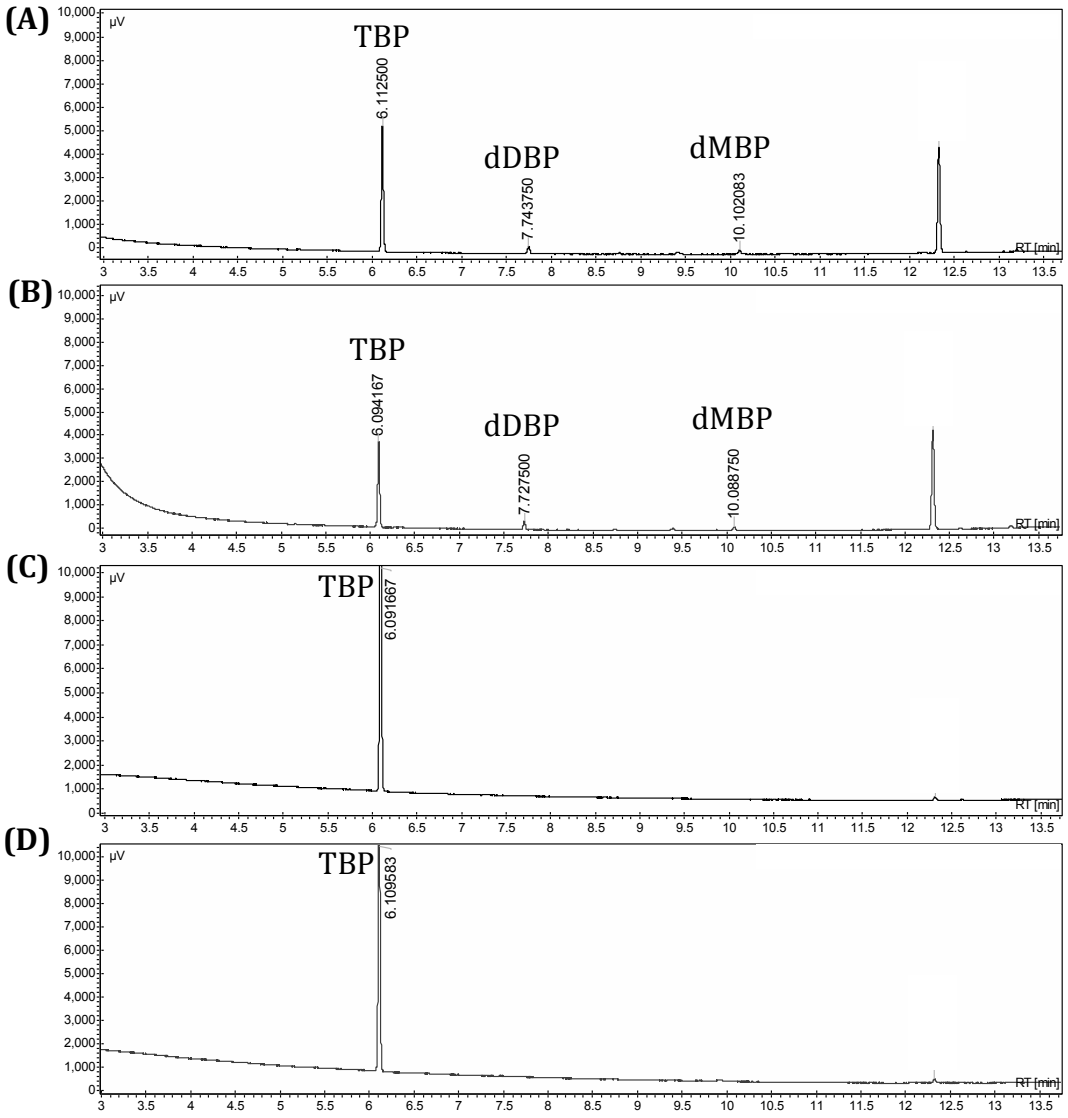

Figure 2-1. Derivatization reaction performed using 1-chloro-3-iodopropane and potassium carbonate at room temperature for 2 hours in: (A) acetonitrile without pyridine, (B) acetonitrile with pyridine, (C) heptane without pyridine, and (D) heptane with pyridine (TBP = tributyl phosphate; dDBP = derivatized dibutyl phosphate; dMBP = derivatized monotbutyl phosphate).

When the reaction temperature was increased to 67 °C for two hours, the reaction was found to work extremely well in acetonitrile in the absence of pyridine (**Figure 2-2A**). However, in the presence of pyridine, the reaction failed, and the internal standard, tributyl phosphate, disappeared (**Figure 2-2B**). This is likely a result of pyridine's nucleophilicity initiating further reaction. On the other hand, at the increased reaction temperature, the derivatization reaction was found to proceed in heptane, but only in the presence of pyridine (**Figure 2-2D**); unfortunately, the reaction did not work well or consistently.

The identities of the peaks at 6.1 min (tributyl phosphate), 7.8 min (derivatized dibutyl phosphate), and 10.1 min (derivatized monobutyl phosphate) were confirmed using GC-MS fragmentation patterns (**Figure 2-3**). The peak at 12.3 min was not identified but assumed to be a by-product of the derivatization reaction.

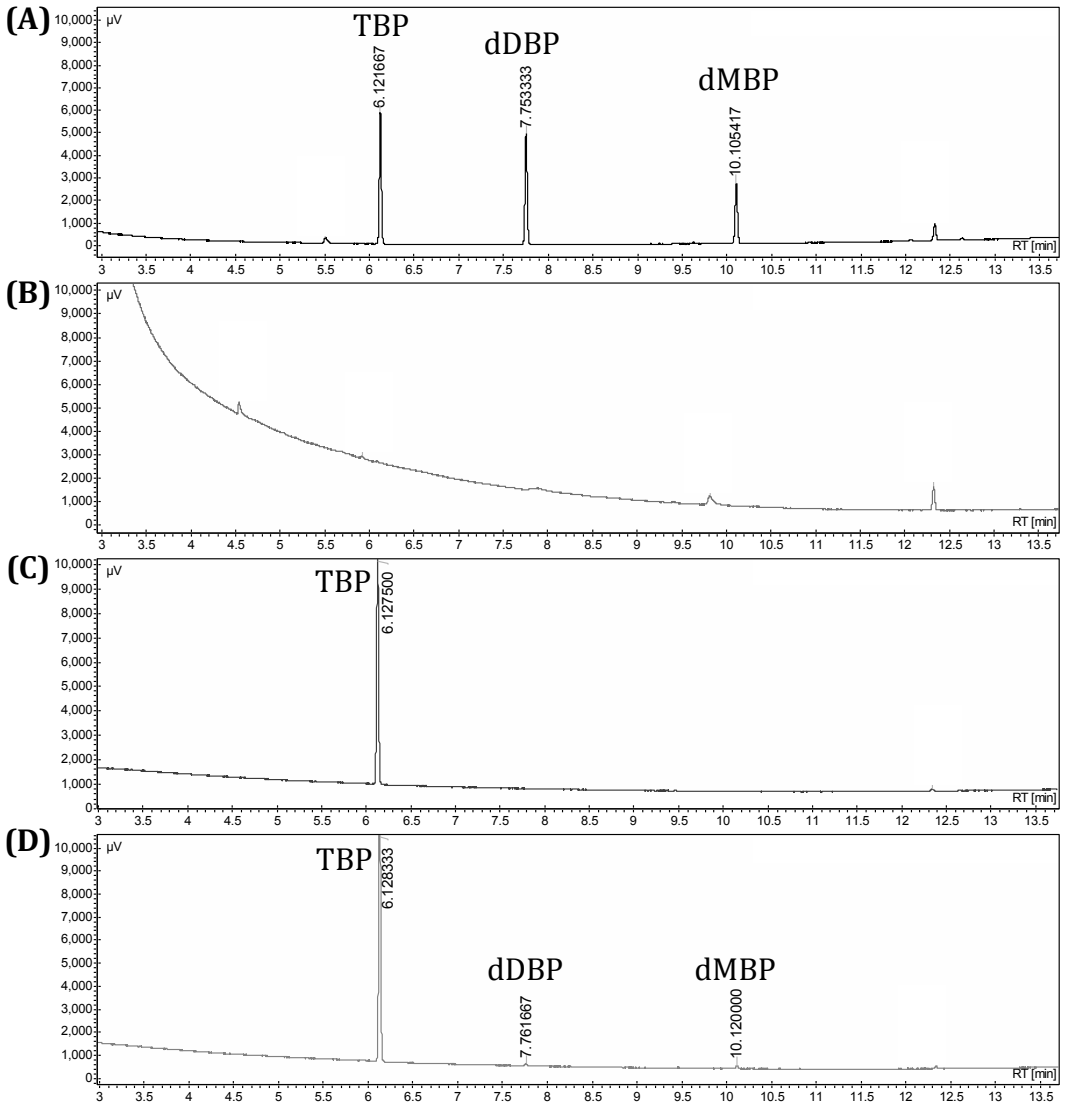

Figure 2-2. Derivatization reaction performed using 1-chloro-3-iodopropane and potassium carbonate at 67 °C for 2 hours in: (A) acetonitrile without pyridine, (B) acetonitrile with pyridine, (C) heptane without pyridine, and (D) heptane with pyridine (TBP = tributyl phosphate; dDBP = derivatized dibutyl phosphate; dMBP = derivatized monotbutyl phosphate).

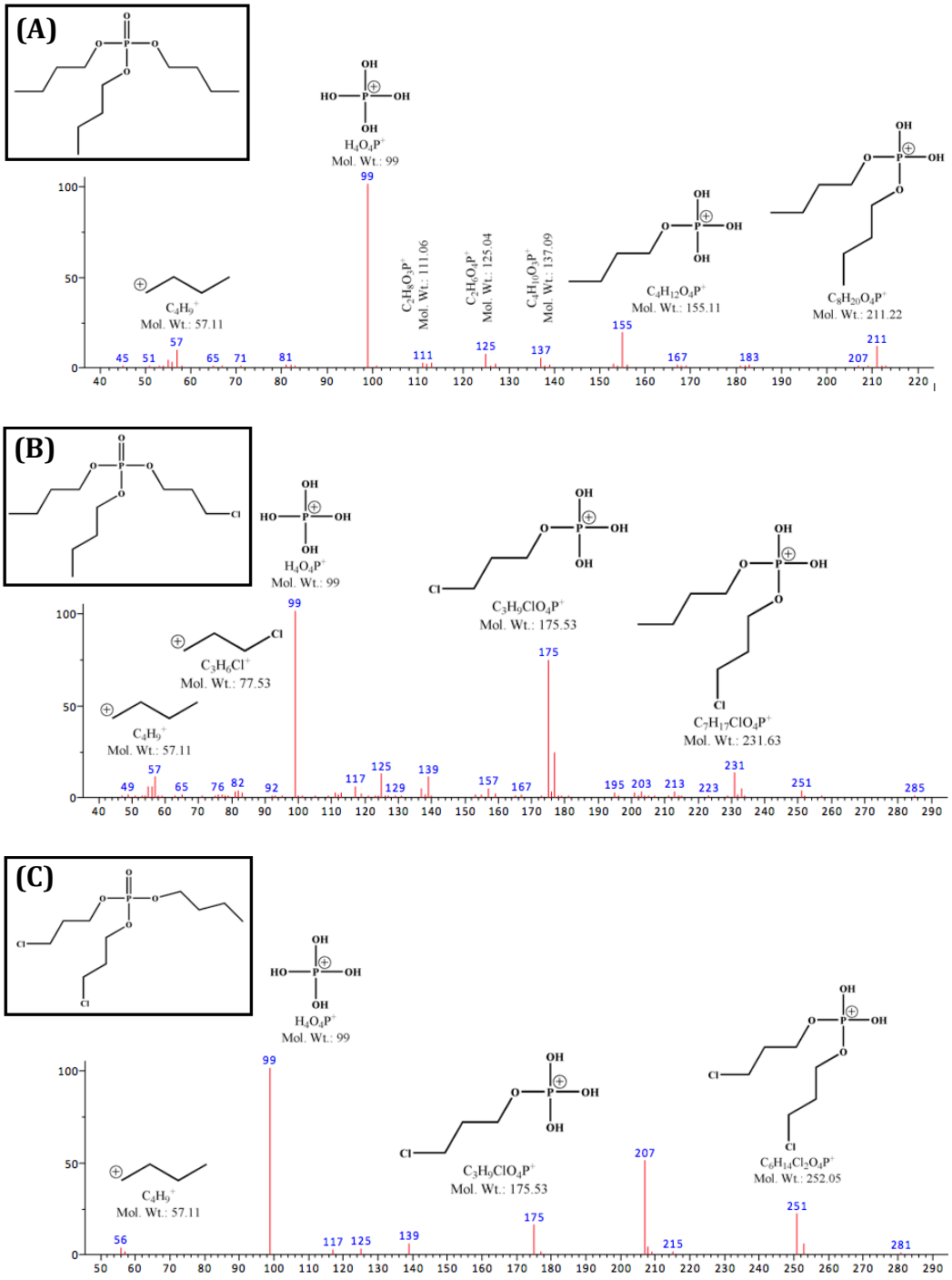

Figure 2-3. Mass spectra collected from the derivatization reaction performed using 1-chloro-3-iodopropane and potassium carbonate at 67 °C for 2 hours in acetonitrile without pyridine for: (A) tributyl phosphate (peak at 6.1 min), (B) derivatized dibutyl phosphate (peak at 7.8 min), and (C) derivatized monobutyl phosphate (peak at 10.1 min).

2.3 Diversion of Excess Silicon Away From the NPD: Deans Switch

2.3.1 Overview

When the reaction using 1-chloro-3-iodopropane failed to consistently derivatize mono- and di-alkyl phosphates in heptane, the pursuit of silicon-free derivatization was abandoned and the use of a Deans switch was investigated. The Deans switch mechanism, first described in 1965 by D.R. Deans [177], is a pneumatic-based effluent-switching technique that enables the control of carrier gas flow direction. The objective of Deans' approach was to eliminate the need for mechanical valves within the GC oven and sample flow path, which can suffer from mechanical failure, temperature limitations (maximum temperatures of 200 – 300 °C), leakages, material degradation (i.e. can off-gas material), insufficient inertness (i.e. can sorb material resulting in loss of analytes), and can have large dead volumes (resulting in extra-column band broadening). The flow-switching technique pioneered by Deans achieves control of gas flow direction within a network of flow paths through the use of pressure/flow differentials, which can be controlled by valves external to both thermal zones and sample flow path.

Despite Deans' enhancements in flow-switching methodology, Deans switching did not become a practical technique until precise pressure settings could be applied using automated electronic pressure/flow control systems, which were introduced to GC in ~1995 and improved column-coupling and gas phase microfluidic chips were introduced in the early

2000s. Contemporary flow-switching devices include both in-house constructed designs [126, 178, 179, 180, 181], as well as commercially available systems from Agilent (Capillary Flow Technology) [182], SGE (SilFlow™ micro-fluidic platform) [183], Shimadzu (Advanced Flow Technology Series) [184], PerkinElmer (Swafer™ Micro-Channel Wafer Technology) [185], and Gerstel (Multicolumn Switching MCS) [186].

To provide flow-switching capabilities, the in-house constructed designs often use a series of interconnected tee unions, crosses, or Y-type press-fit connections, and deactivated fused silica tubing. The commercially available systems, on the other hand, combine all necessary flow-switching components into a single deactivated microfluidic platform with very small internal flow channels. A simple on/off, three-port solenoid valve, located outside the GC oven and sample flow path, can control the gas flows in both cases. Although the microfluidic platforms are mounted within the GC oven and sample flow path, these devices have eliminated the chromatographic problems observed with the use of mechanical valves by having: 1) no moving parts; 2) no practical temperature limit; 3) a low thermal mass to allow the device to track the GC oven ramp closely; 4) chemically inert surfaces to prevent peak tailing and loss of analytes; 5) low, well-swept dead volumes to reduce extra-column band broadening; and 6) leak-free capillary connections (e.g. SGE's SilTite™ metal ferrules [187]). In addition, many of the commercial systems come with software applications to help calculate system flows and switching pressures (e.g. Agilent's Deans Switch

Calculator). For more detailed information on individual contemporary flow-switching devices the reader is referred to the following references [77, 188].

Although Deans initially designed his effluent-switching system for the backflushing of gas chromatographic columns [177], he later modified the technique to facilitate heart-cutting in gas chromatography [189]. Today, both in-house constructed designs and manufacturers offer a wide variety of flow-switching configurations that allow the Deans switching technique to be used not only for backflushing [19, 190 , 191] and heart-cutting [179,190,191,192,193], but also for multiple detector [18,19,178] or column selection [180], and modulation in GC×GC [126,127,128].

Herein, a commercially available Deans switch plate from Agilent (**Figure 2-4**) [194] was installed to allow the user to control the direction of column effluent to one of two detectors, in this case either an FID or an NPD. The overall objective of this system is to divert the effluent containing the excess silicon-containing trimethylsilyl derivatization reagents to the FID (i.e. away from the NPD), while still being able to selectively detect and analyze the derivatized alkyl phosphates with the NPD. To achieve this goal, the Deans switch plate was connected post-column, as illustrated in **Figure 2-5** for a one-dimensional GC system (i.e. GC-FID/NPD). As a result, the direction of the effluent exiting the GC column is controlled by a solenoid valve and can be directed to either an FID when the solenoid valve is closed (“off” position), or an NPD when the valve is opened (“on” position).

Figure 2-4. Agilent's commercially available Deans switch plate.

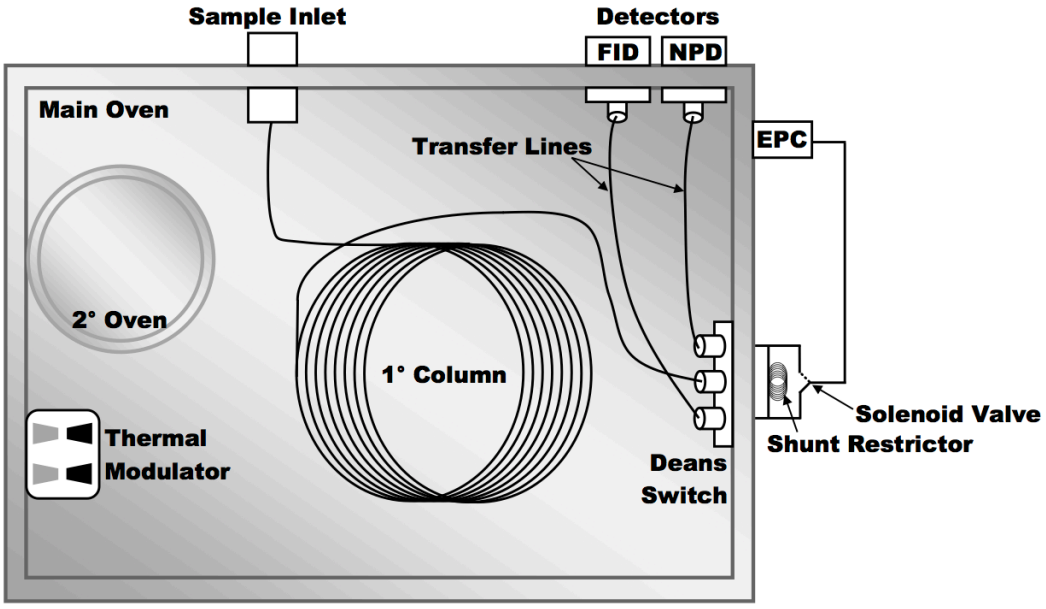

Figure 2-5. Schematic of the GC-FID/NPD system with post-column Deans switch.

Figure 2-6 takes a closer look at how this Deans switch setup works. When the solenoid valve is closed, an external pressure control (EPC) system sends pure carrier gas (i.e. helium) through the Deans switch plate to the NPD, as well as along the Deans switch plate, collecting the effluent exiting

the secondary column and carrying it on to the FID (**Figure 2-6A**). When the valve is opened, the carrier gas flow in the Deans switch plate reverses direction, with the EPC system now sending pure carrier gas to the FID and the secondary column effluent to the NPD (**Figure 2-6B**).

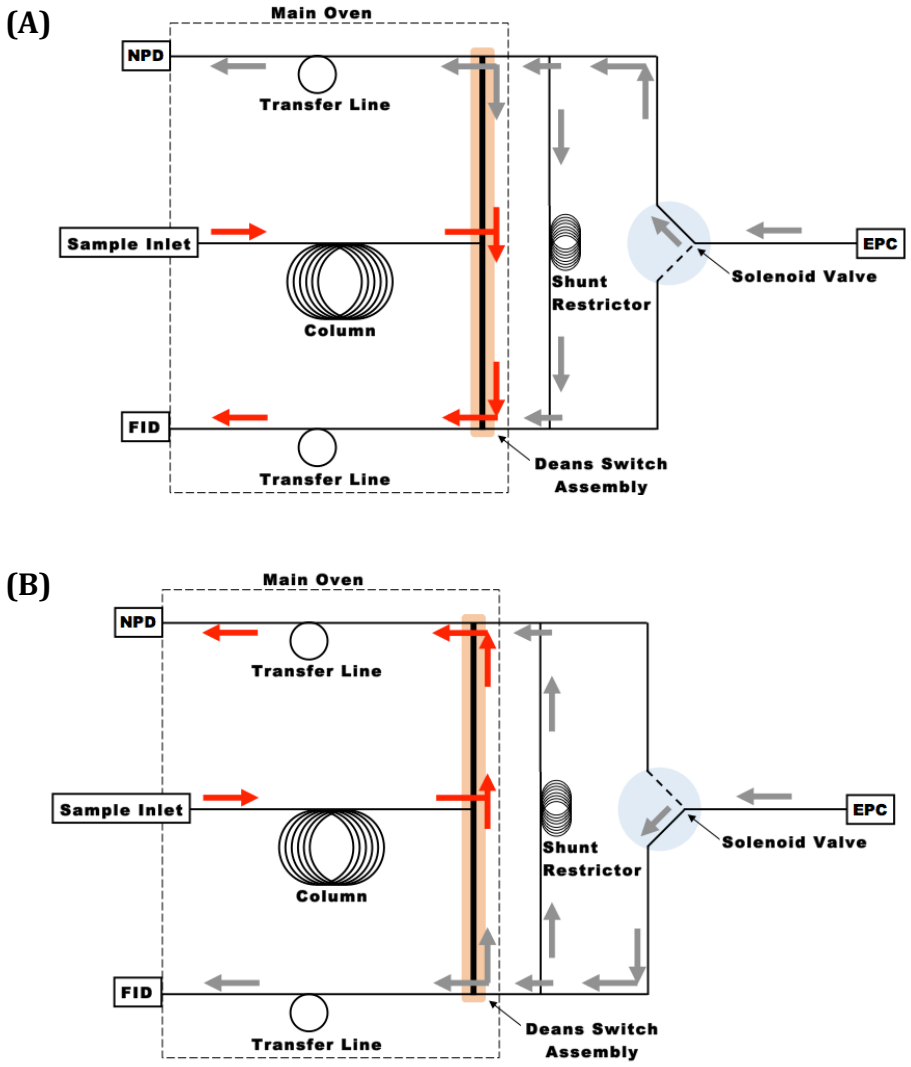

Figure 2-6. Deans switch schematic for the GC-FID/NPD system: (A) effluent directed to FID (solenoid valve closed) and (B) effluent directed to NPD (solenoid valve open).

2.3.2 Experimental

2.3.2.1 Materials and Reagents

All reagents were used as received unless otherwise stated. Standards used to test the Deans switch included a mixture of mono- and di-butyl phosphates (Alfa Aesar), bis(2-ethylhexyl) phosphate (Alfa Aesar), triphenyl phosphate (Sigma–Aldrich), and nonadecane (Sigma–Aldrich). CHROMASOLV® grade hexane (Sigma–Aldrich) was used as a solvent.

Derivatization was performed according to a previously established protocol [16] using a mixture of BSTFA (Sigma–Aldrich), pyridine (Caledon), and TMCS (Sigma–Aldrich) in a 10:5:2 ratio by volume. A total of 50 µL of the derivatization reagent mixture was added to 500 µL of sample. All derivatization reactions were carried out in 1.8 mL glass GC vials with PTFE-lined silicone septa (Chromatographic Specialties).

2.3.2.2 Instrumentation and Experimental Conditions

Analysis was conducted using a consumable-free LECO GC×GC system (LECO Instruments, St. Joseph, MI, United States) set-up in one-dimensional GC mode (**Figure 2-5**). The instrument was equipped with a CFT (Capillary Flow Technology) Deans switch (Agilent Technologies) and both FID and NPD detectors. The column configuration consisted of a 10 m × 0.18 mm, 0.2 µm Rtx-5 (Restek, Bellefonte, PA, United States) column. The transfer lines consisted of 0.18 mm inner diameter deactivated fused silica (Agilent Technologies), where 0.23 m connected the secondary column to the Deans switch and 0.30 m sections connected the Deans switch with the detectors.

All injections were performed using 1 µL of sample with an Agilent 7683B Series autosampler and a split ratio of 50:1. The inlet temperature was 250 °C. The oven temperature program was 50 (0.2 min) – 300 °C at 10 °C min^{-1}. Ultra-high purity helium (Praxair) was used as the carrier gas with a ramped pressure program of 150.3 (0.2 min) – 285.9 kPa at 5.4 kPa min^{-1} for the inlet and 85.9 (0.2 min) – 169.3 kPa at 3.3 kPa min^{-1} for the Deans switch plate. The pressure programs were calculated using the Agilent Deans Switch Calculator and HP Flow Calculator. The timing for switching the solenoid valve to the open and closed positions to actuate the Deans switch and send the effluent back and forth between the FID and NPD was determined experimentally (**Table 2-1**).

Table 2-1. Deans switch solenoid valve switching events.

Time (s)	Valve
Initial	Closed
500	Open
620	Closed
930	Open
960	Closed
1090	Open
1120	Closed

Both detectors were kept at 325 °C. The NPD used a modified capillary-optimized jet (DETector Engineering & Technology, Inc., Walnut Creek, CA, United States) and a TID-2 black ceramic bead (DETector Engineering & Technology, Inc.). This NPD jet has a large enough bore to permit the capillary column to pass through the jet and be positioned a few

millimetres from the detector bead, improving the response characteristics of the detector over the conventional design [195].

Data were acquired at a rate of 100 Hz and processed using ChromaTOF software (version 4.32; LECO). The data processing method used a baseline offset of 1, auto smoothing, expected peak width of 4 s, and a minimum signal-to-noise ratio (S/N) of 500 for peak detection.

2.3.3 Results and Discussion

The Deans switch solenoid valve can be opened and closed multiple times throughout a run, at any time specified in the GC method. This is demonstrated in **Figure 2-7**, where the valve was opened and closed six different times. The silylation reagents (i.e. the source of excess silicon) are known to be highly volatile and are expected to elute early along with the solvent. The chromatogram displayed in **Figure 2-7** confirms this expectation. Furthermore, the earliest eluting phosphate (i.e. triethyl phosphate) was found to elute late enough after the elution of the excess derivatization reagents to allow enough time for the solenoid valve to switch the effluent flow from one detector to the other. Thus, at the beginning of a run with the valve closed, the effluent containing the solvent and excess derivatization reagents can be directed to the FID. The valve can then be opened mid-run, switching the effluent stream to the NPD in order to selectively detect and analyze the alkyl phosphates without deactivating the NPD bead; therefore, solving the problem of excess silicon and allowing for

the derivatization of mono- and di-alkyl phosphates by trimethylsilylation with subsequent detection by the NPD. Overall, the addition of the Deans switch increased the NPD bead life from approximately 5 chromatographic runs to over 1,000, which were performed over the course of 15 months.

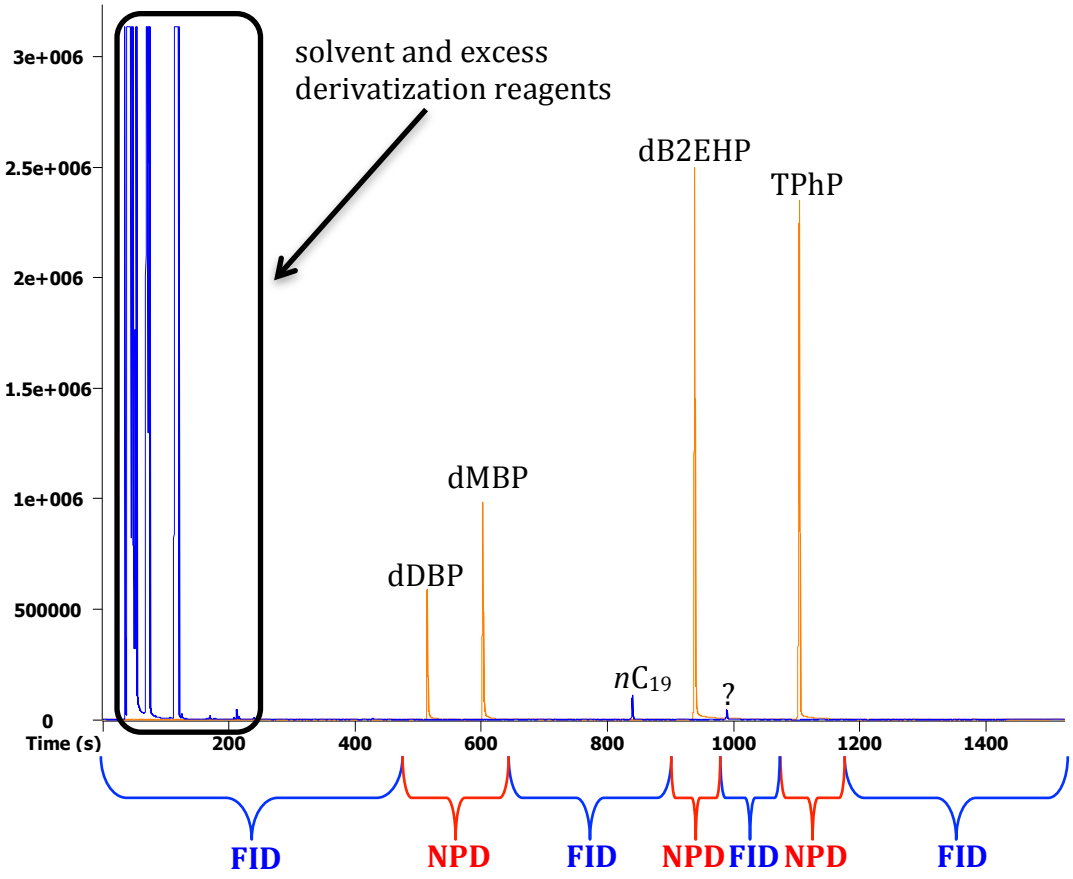

Figure 2-7. A GC-FID/NPD chromatogram exhibiting the early elution of the solvent and excess derivatization reagents, in addition to the capacity of the system to switch the effluent back and forth between the FID and NPD multiple times throughout a single run (blue signal = FID; red signal = NPD; dDBP = derivatized dibutyl phosphate; dMBP = derivatized monobutyl phosphate; nC$_{19}$ = nonadecane; dB2EHP = derivatized bis(2-ethylhexyl) phosphate; ? = unknown impurity; TPhP = triphenyl phosphate).

2.4 Optimization of Detector Gas Flows for the NPD

2.4.1 Overview

With post-column Deans switching yielding compatibility between trimethylsilylation derivatization and the nitrogen-phosphorus detector, the search for a derivatization method without the use of silicon was abandoned. However, before the NPD could be used for the analysis of alkyl phosphates in petroleum samples, the NPD gas flows (i.e. hydrogen, air, and makeup flows) required optimization, as they have been shown to have a significant impact on peak magnitude and peak asymmetry [91].

2.4.2 Experimental

2.4.2.1 Materials and Reagents

All reagents were used as received unless otherwise stated. The alkyl phosphate standards used for the optimization of the NPD gas flows included tributyl (Sigma–Aldrich) and trihexyl (Alfa Aesar) phosphate. CHROMASOLV® grade hexane (Sigma–Aldrich) was used as a solvent to prepare a solution containing 20.4 μg mL^{-1} tributyl phosphate and 21.4 μg mL^{-1} trihexyl phosphate. Tetradecane (Eastman Organic Chemicals, Rochester, NY, United States) was diluted in hexane to give a 1,036 μg mL^{-1} stock solution that was used as an internal standard at a concentration of 20.7 μg mL^{-1}. Sample solutions were prepared in 1.8 mL glass GC vials with PTFE-lined silicone septa (Chromatographic Specialties).

2.4.2.2 Instrumentation and Experimental Conditions

Analyses were conducted using the same instrumental setup and column configuration as previously described in **Section 2.3.2.2**. All injections were performed using 1 µL of sample with an Agilent 7683B Series autosampler and a split ratio of 50:1. The inlet temperature was 250 °C. The oven temperature program was 120 (0.2 min) – 235 °C at 10 °C min^{-1}. Ultra-high purity helium (Praxair) was used as the carrier gas with a ramped pressure program of 199.9 (0.2 min) – 265.2 kPa at 5.6 kPa min^{-1} for the inlet and 124.9 (0.2 min) – 167.7 kPa at 3.7 kPa min^{-1} for the Deans switch plate. The pressure programs were calculated using the Agilent Deans Switch Calculator and HP Flow Calculator. The Deans switch initially directed solvent and any excess derivatization reagents exiting the secondary column to the FID. The valve was actuated to direct each alkyl phosphate to the NPD for selective detection at 4.0 and 10.2 min with the internal standard, tetradecane, being sent to the FID for analysis.

Both detectors were kept at 325 °C. The NPD used a modified capillary-optimized jet (DETector Engineering & Technology, Inc.) and a TID-2 black ceramic bead (DETector Engineering & Technology, Inc.).

Data were acquired at a rate of 100 Hz and processed using ChromaTOF software (version 4.32; LECO). The data processing method used a baseline offset of 1, auto smoothing, expected peak width of 4 s, and a minimum S/N of 1,000 for peak detection.

2.4.3 Results and Discussion

NPD performance was optimized in terms of signal-to-noise ratio (S/N) by determining the optimal rates for hydrogen, makeup (i.e. helium), and air flows through the detector. This task was accomplished using a three-factor (i.e. hydrogen, air, and makeup flow rates), three-level (i.e. low, medium, and high) Box-Behnken statistical design of experiment [196,197], as previously completed in the literature by Ryan and Marriott for the optimization of NPD performance [91]. The Box-Behnken experimental design is a multivariate optimization technique that allows for all three NPD gas flows to be optimized simultaneously (i.e. accounting for any effects the factors may have on each other) with the fewest number of experiments (i.e. incomplete factorial). **Table 2-2** outlines the different levels investigated for each factor. The flow rates (i.e. levels) examined for hydrogen, makeup, and air were chosen based on recommendations from Agilent Technologies, DETector Engineering & Technology, Inc., and those flows tested in the literature [91].

Table 2-2. Factors and levels investigated in the optimization of the NPD gas flows using a Box-Behnken statistical design of experiment.

Factors	Levels		
	Low (–)	Medium (0)	High (+)
Hydrogen flow rate (mL min $^{-1}$)	1	3	5
Air flow rate (mL min $^{-1}$)	40	70	100
Makeup (helium) flow rate (mL min $^{-1}$)	1.5	2.5	3.5

Table 2-3 summarizes the experiments performed for the three-factor, three-level Box-Behnken statistical design as outlined in references [196,197]. Triplicate centre replicates were performed at flows of 3, 70, and 2.5 mL min^{-1} for hydrogen, makeup, and air, respectively. The experiments were performed in a random order (according to a random number generator used in Microsoft Excel) using 5 different sample vials in order to avoid correlated time effects and systematic errors. The results obtained in terms of normalized signal-to-noise ratio for tributyl (TBP) and trihexyl (THP) phosphate are also presented in **Table 2-3**. The overall performance reproducibility of the detector was confirmed based on the results obtained from the triplicate centre replicates, which yielded relative standard deviations of 6.6 and 3.2% for tributyl and trihexyl phosphate, respectively.

Table 2-3. List of experiments performed for the Box-Behnken statistical design of experiment and the resulting normalized S/N ratios for TBP and THP. Italic text highlights the experimental centre point replicates, while bold text highlights the experiment that resulted in the highest normalized S/N.

	NPD Flow Rates (mL min^{-1})			Normalized S/N	
Experiment	**Hydrogen**	**Air**	**Makeup**	**TBP**	**THP**
1	1	40	2.5	1.02	0.75
2	5	40	2.5	0.05	0.04
3	1	100	2.5	0.95	0.82
4	5	100	2.5	3.55	2.81
5	1	70	1.5	1.11	0.92
6	**5**	**70**	**1.5**	**5.34**	**4.76**
7	1	70	3.5	1.07	0.89
8	5	70	3.5	2.29	1.83
9	3	40	1.5	2.71	2.21
10	3	100	1.5	1.55	1.26
11	3	40	3.5	2.43	1.81
12	3	100	3.5	1.80	1.42
13	*3*	*70*	*2.5*	*2.34*	*1.87*
14	*3*	*70*	*2.5*	*2.11*	*1.76*
15	*3*	*70*	*2.5*	*2.39*	*1.84*

Figure 2-8 displays the response surface plots obtained for the Box-Behnken statistical design of experiment for both tributyl and trihexyl phosphate. The methodology (i.e. mathematical manipulations) for the construction of the response surface plots is described in reference [196]. Response surface plots displaying normalized S/N versus NPD hydrogen and air flows for TBP and THP (**Figures 2-8A** and **B** respectively) suggest optimal flows of 5 mL min^{-1} for hydrogen and 100 mL min^{-1} for air. **Figures 2-8C** and **D** display the response surface plots for normalized S/N versus NPD hydrogen and makeup flows for TBP and THP, respectively, which confirm an optimal flow of 5 mL min^{-1} for hydrogen and propose an optimal flow of 1.5 mL min^{-1} for makeup. Finally, the remaining response surface plots for normalized S/N versus NPD air and makeup flows for TBP and THP (**Figures 2-8E** and **F**, respectively) recommend an optimal flow of 70 mL min^{-1} for air and verify an optimal flow of 1.5 mL min^{-1} for makeup.

Therefore, the NPD gas flows that were found to result in optimal NPD performance (i.e. highest normalized signal-to-noise ratios, see **Table 2-3** and **Figure 2-8**) comprise 5 mL min^{-1} for hydrogen, 70 mL min^{-1} for air, and 1.5 mL min^{-1} for makeup (helium). A flow rate of 70 mL min^{-1} for air was chosen over 100 mL min^{-1} based on recommendations by DETector Engineering & Technology, Inc., the supplier of the NPD beads used herein. Unfortunately, shortly after implementing these flows for analysis, the NPD began producing a self-sustaining flame at the detector's jet structure due to

a flashback of hydrogen-air chemistry. As a result, the hydrogen flow had to be decreased to 3 mL min^{-1} for the remainder of this work.

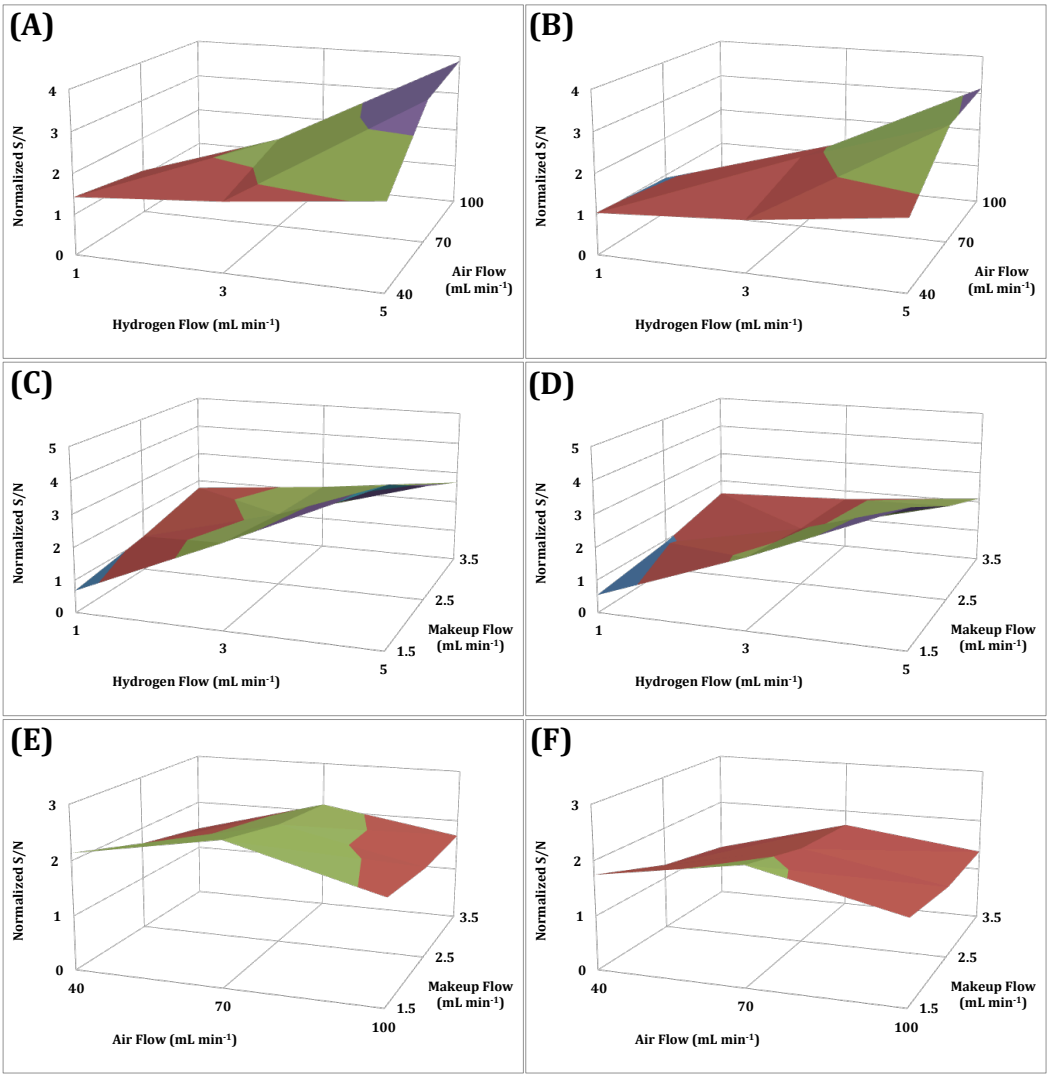

Figure 2-8. Response surface plots showing: normalized S/N versus NPD hydrogen and air flows for (A) TBP and (B) THP; normalized S/N versus NPD hydrogen and makeup flows for (C) TBP and (D) THP; and normalized S/N versus NPD air and makeup flows for (E) TBP and (F) THP.

Finally, throughout the experiments performed, the normalized analyte signal-to-noise ratio ranged from 0.05 to 5.3 for tributyl phosphate

(see **Table 2-3**), which is equivalent to a 100-fold difference in detector response. A similar difference can also be observed for trihexyl phosphate. These findings agree with those reported by Ryan and Marriott [91], further emphasizing the need for careful optimization of the NPD.

2.5 Optimization of Trimethylsilylation Derivatization Reaction

2.5.1 Overview

With the NPD performance optimized, the next and final step before alkyl phosphates could be analyzed by GC×GC-NPD was the optimization of the trimethylsilylation derivatization reaction. The trimethylsilylation derivatization reaction was previously optimized in the Harynuk Group in terms of reagent ratios such that a 50 µL solution of 10 parts BSTFA to 5 parts pyridine to 2 parts TMCS added to a 500 µL sample of phosphates results in optimal derivatization based on normalized peak response, precision, and peak asymmetry [16]. Herein, the optimization of the derivatization reaction in terms of reaction temperature and time, in addition to testing the stability of the derivatized products over a 48-hour period, is examined by means of normalized peak response (i.e. peak area).

2.5.2 Experimental

2.5.2.1 Materials and Reagents

All reagents were used as received unless otherwise stated. Derivatization was performed according to a previously established

protocol [16] as outlined in **Section 2.3.2.1**. The dialkyl phosphate standards used for the optimization of the derivatization reaction conditions consisted of dibutyl phosphate (Sigma–Aldrich) and bis(2-ethylhexyl) phosphate (Alfa Aesar). CHROMASOLV® grade hexane (Sigma–Aldrich) was used as a solvent. Triphenyl phosphate (Sigma–Aldrich) was dissolved and diluted in reagent-grade acetone (Caledon) to give a 1,020 μg mL^{-1} internal standard stock solution.

2.5.2.2 Instrumentation and Experimental Conditions

Analyses were conducted using the same instrumental setup and column configuration as previously described in **Section 2.3.2.2**. The inlet temperature was 250 °C. The oven temperature program was 50 (0.2 min) – 260 °C at 10 °C min^{-1}. Ultra-high purity helium (Praxair) was used as the carrier gas with a ramped pressure program of 159.5 (0.2 min) – 279.2 kPa at 5.7 kPa min^{-1} for the inlet and 99.1 (0.2 min) – 177.0 kPa at 3.7 kPa min^{-1} for the Deans switch plate. The pressure programs were calculated using the Agilent Deans Switch Calculator and HP Flow Calculator. The Deans switch initially directed solvent and any excess derivatization reagents exiting the secondary column to the FID. The valve was actuated to direct each dialkyl phosphate to the NPD for selective detection at 15.5 and 18.2 min.

Both detectors were kept at 325 °C. The NPD used a modified capillary-optimized jet (DETector Engineering & Technology, Inc.) and a TID-2 black ceramic bead (DETector Engineering & Technology, Inc.).

Data were acquired at a rate of 100 Hz and processed using ChromaTOF software (version 4.32; LECO). The data processing method used a baseline offset of 1, auto smoothing, expected peak width of 4 s, and a minimum S/N of 500 for peak detection.

Temperatures tested for the optimization of the derivatization reaction temperature included: 30, 40, 50, and 60 °C. Vials were maintained at temperature in an aluminum block inside a GC oven. The following reaction times were tested to determine the optimal derivatization reaction length: 10, 20, 30, 40, 50, 60, 120, 180, 240, 300, 1,440, and 2,880 minutes.

2.5.3 Results and Discussion

2.5.3.1 Derivatization Reaction Temperature Optimization

The compounds used to optimize the trimethylsilylation reaction temperature included dibutyl and bis(2-ethylhexyl) phosphates. The derivatization reaction was tested at temperatures ranging from 30 to 60 °C and times ranging from 10 minutes up to 48 hours. As described in the previously established protocol [16], 50 µL of derivatization reagent mixture was added to 500 µL aliquots of each sample in GC vials. The vials were then sealed, shaken, left to derivatize for a particular length of time at a set temperature, and then analyzed in triplicate using GC-FID/NPD. Samples were carefully prepared so that the time of injection on the GC corresponded as closely as possible with the appropriate length of time for the derivatization reaction.

Figure 2-9A displays a plot of the normalized response in terms of peak area on the y-axis for the trimethysilyl derivative of dibutyl phosphate versus the natural logarithm of the length of derivatization in minutes on the x-axis at 30, 40, 50, and 60 °C for the various derivatization reaction lengths tested. The resulting trend shows that, as the reaction temperature increases, the normalized response appears to decrease. The same trend is observed for the trimethylsilyl derivative of bis(2-ethylhexyl) phosphate (**Figure 2-9B**). As a result, 30 °C was deemed to be the optimal temperature for dialkyl phosphate derivatization.

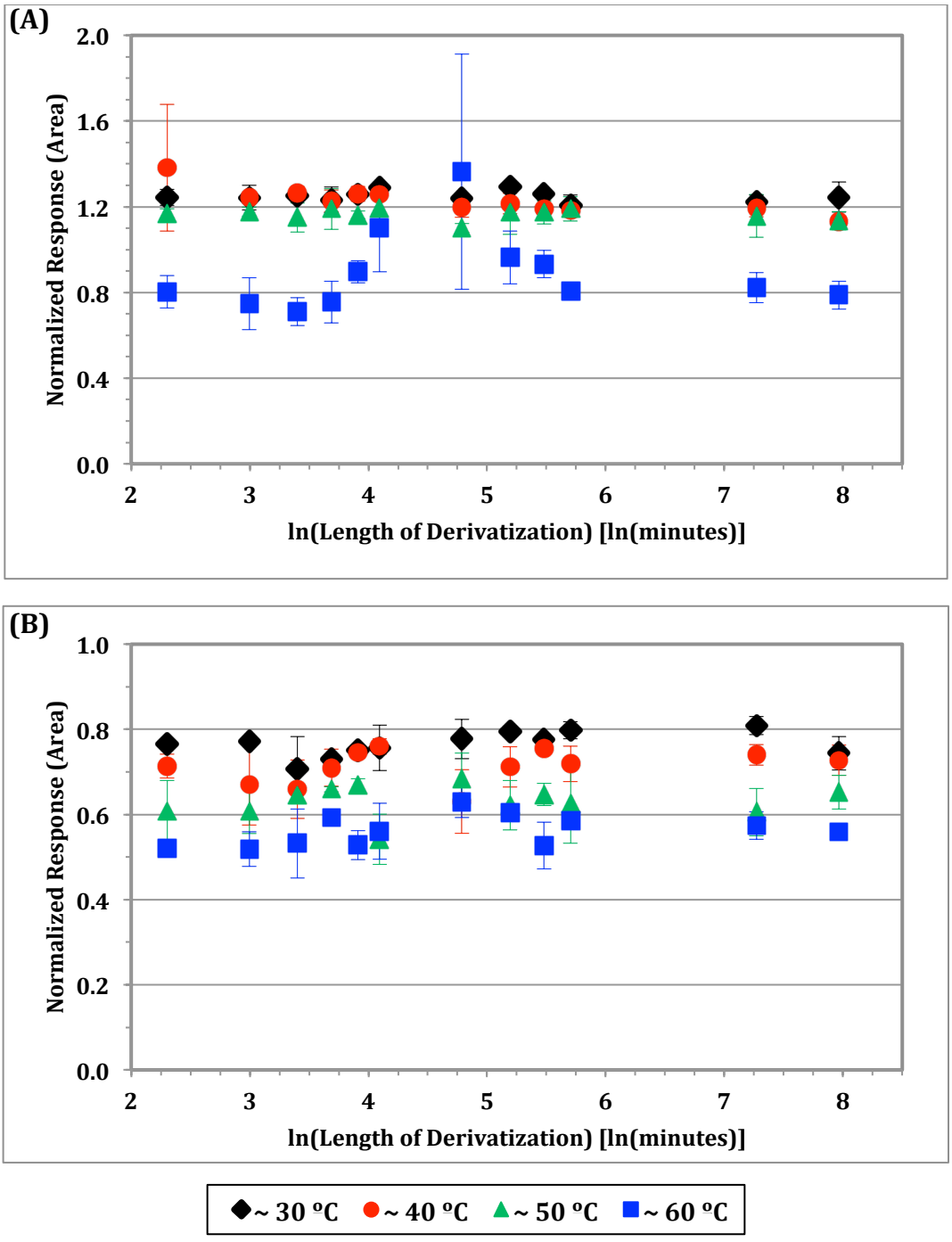

Figure 2-9. Plot of normalized response (area) versus the natural logarithm of the length of derivatization in minutes for: (A) derivatized dibutyl phosphate and (B) derivatized bis(2-ethylhexyl) phosphate at 30 (◆), 40 (●), 50 (▲), and 60 (■) °C. Error bars represent 1 standard deviation based on 3 replicates.

2.5.3.2 Derivatization Reaction Time Optimization and Stability Testing

The compounds used to optimize the trimethylsilylation reaction time included dibutyl and bis(2-ethylhexyl) phosphates. The derivatization reaction was tested at times ranging from 10 minutes up to 48 hours at the optimized temperature of 30 °C. Again 50 µL of derivatization reagent mixture was added to 500 µL aliquots of each sample in GC vials. The vials were then sealed, shaken, left to derivatize for a particular length of time at 30 °C, and then analyzed in triplicate using GC-FID/NPD. Samples were carefully prepared so that the time of injection on the GC corresponded as closely as possible with the appropriate length of time for the derivatization reaction.

The plot in **Figure 2-10** displays the normalized response in terms of peak area on the y-axis (for both dialkyl phosphates tested at the optimal temperature of 30 °C) versus the natural logarithm of the length of derivatization in minutes on the x-axis. Overall, maximum derivatization appears to be reached after only 10 minutes. Nevertheless, an optimal derivatization reaction length of 30 minutes was chosen to ensure complete derivatization. Furthermore, both of the dialkyl phosphates appear to be stable as their trimethylsilyl derivatives over the 48 hour period tested. Therefore, a batch of samples can be derivatized simultaneously for 30 minutes and left in an autosampler to be run on an instrument overnight without the response from the trimethylsilyl derivatives decreasing significantly over time. Additionally, the vials can be maintained at

temperature (i.e. 30 °C) by circulating heated water through the GC autosampler tray.

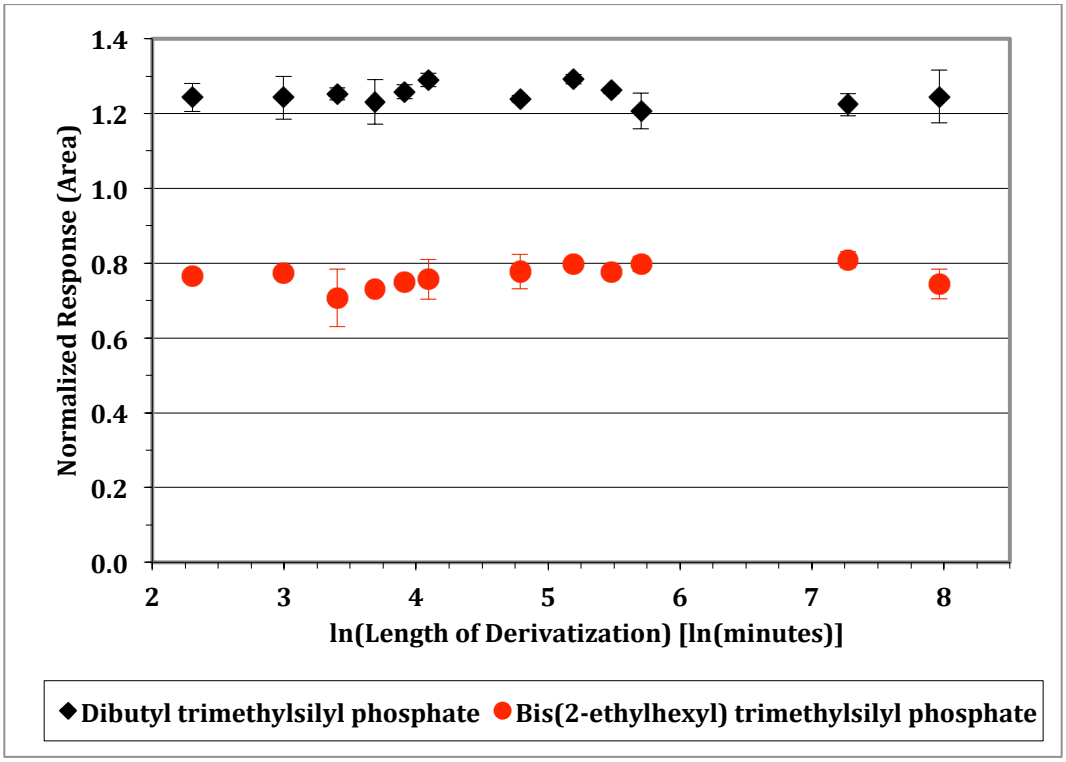

Figure 2-10. Plot of normalized response (area) versus the natural logarithm of the length of derivatization in minutes for dibutyl trimethylsilyl phosphate (◆) and bis(2-ethylhexyl) trimethylsilyl phosphate (●) at 30 °C. Error bars represent 1 standard deviation based on 3 replicates.

2.6 Conclusions

The first strategy investigated to solve the incompatibility between excess silicon (from the trimethylsilylation derivatization reaction) and the NPD was the use of a derivatization reaction that did not involve silicon. Overall, the derivatization reaction using 1-chloro-3-iodopropane was established to work well in acetonitrile as previously shown in the

literature [176]. Unfortunately, the derivatization reaction did not work well when the solvent system was switched to heptane, which was used to simulate the matrix of future petroleum samples. As a result, this derivatization approach was discarded while an attempt at the use of a Deans switch (installed post-column) to divert excess silicon away from the NPD was explored.

The trimethylsilyl derivatization reagents containing the excess silicon (which causes deactivation of the NPD bead) eluted early along with the solvent. Thus, at the beginning of a run, with the Deans switch solenoid valve closed, the effluent containing the solvent and excess derivatization reagents can be directed to an FID. Once the derivatization reagents have finished eluting, the valve can then be opened, directing the remaining effluent to the NPD in order to selectively detect and analyze the alkyl phosphates without deactivating the NPD bead. Overall, the addition of the Deans switch increased the NPD bead life from approximately 5 chromatographic runs to over 1,000, which were performed over the course of 15 months. NPD gas flow conditions of 5 mL min^{-1} for hydrogen, 70 mL min^{-1} for air, and 1.5 mL min^{-1} for makeup (helium) were found to result in optimal NPD performance based on peak signal-to-noise ratios. Unfortunately, these flows lead to the production of a self-sustained flame within the NPD, and the hydrogen flow had to be decreased to 3 mL min^{-1} for all remaining experiments.

With the installation of the Deans switch solving the problem of excess silicon and allowing for the use of trimethylsilylation derivatization in conjunction with the NPD, all other derivatization methods were abandoned, and final efforts to optimize the trimethylsilylation reaction were performed. A derivatization reaction temperature of 30 °C and derivatization reaction length of 30 minutes were established to be optimal. In addition, the trimethylsilyl derivatives were determined to be stable over the 48 hour period tested, therefore allowing for future samples to be derivatized simultaneously in a heated GC autosampler tray and left for analysis overnight.

Finally, with post-column Deans switching yielding compatibility between the trimethylsilylation derivatization reaction and the NPD in addition to the subsequent optimization of both the NPD performance and the trimethylsilylation derivation reaction, the next step towards the analysis of alkyl phosphates is the upgrade of the one-dimensional GC setup (i.e. GC-FID/NPD) to a comprehensive two-dimensional GC setup (i.e. GC×GC-FID/NPD).

CHAPTER THREE: Analysis of Alkyl Phosphates in Petroleum Samples by GC×GC with Nitrogen-phosphorus Detection and Post-column Deans Switching[2]

3.1 Introduction

Alkyl phosphate based gellants used as viscosity builders for fracture fluids used in the process of hydraulic fracturing have been implicated in numerous refinery-fouling incidents in North America. An inductively coupled plasma – optical emission spectroscopy (ICP-OES) based method has been developed by industry to monitor total volatile phosphorus in distillate fractions of crude oil [5,6]. However, this method is plagued with poor precision and a high limit of detection (0.5 ± 1 μg *phosphorus* mL^{-1}). Additionally, this method cannot speciate the phosphates, leaving industry incapable of studying this chemistry at a molecular level. Recently, the Harynuk Group has approached this challenge using comprehensive two-dimensional gas chromatography (GC×GC) [7].

GC×GC is a separations technique with numerous applications in many fields, especially petroleum. Its application to the petroleum field has been reviewed recently [10] and several other reviews cover broader aspects of the technique [9,70,71,72,73,74,75,76]. The Harynuk Group first introduced a method based on trimethylsilylation derivatization followed by GC×GC separation using a flame ionization detector (FID) for the speciation

[2] A version of this chapter has been published as K.D. Nizio, J.J. Harynuk, J. Chromatogr. A 1252 (2012) 171.

of di- and tri-alkyl phosphates in petroleum samples [16]. Although this analytical approach yielded detection limits and a level of precision that exceeded the capabilities of the currently-accepted ICP-OES methodology, the research demonstrated the necessity for selective detection in this application, which was achieved through the use of time-of-flight mass spectrometry (TOFMS) [17]. Overall, this method was capable of both speciating and quantifying alkyl phosphates in petroleum samples with better precision and lower limits of detection when compared to ICP-OES. However, TOFMS instrumentation is very expensive and therefore not suitable for use in on-line or at-line monitoring in a refinery environment. This chapter presents the use of nitrogen-phosphorus detection (NPD) in conjunction with GC×GC for alkyl phosphate measurement in petroleum samples. This is a much less expensive and more rugged detector (due to a larger dynamic range and the need for less frequent calibration) than the TOFMS detector, making this new method more attractive for implementation in an industrial setting.

3.2 Experimental

3.2.1 Materials and Reagents

Stock solutions were stored in glass vials and refrigerated at ~7 °C. Calibration, recovery study, and industrial petroleum sample solutions were prepared in 1.8 mL glass GC vials with polytetrafluoroethylene (PTFE)-lined

silicone septa (Chromatographic Specialties, Brockville, ON, Canada) for analysis by GC×GC-FID/NPD.

All reagents were used as received unless otherwise stated. Derivatization was performed according to a previously established protocol [16] using a mixture of *N,O*-bis(trimethylsilyl)trifluoroacetamide (BSTFA) (Sigma–Aldrich, Oakville, ON, Canada), pyridine (Caledon, Georgetown, ON, Canada), and trimethylchlorosilane (TMCS) (Sigma–Aldrich) in a 10:5:2 ratio by volume. A total of 50 µL of the derivatization reagent mixture was added to 500 µL of sample and left to derivatize at 30 °C for at least 30 min before analysis. Vials were maintained at temperature using the GC autosampler tray, which was kept at 30 °C by circulating heated water through the tray.

The alkyl phosphate standards used for the calibration and recovery studies consisted of triethyl, triisopropyl, tripropyl, dibutyl, and tributyl phosphate (Sigma–Aldrich), and bis(2-ethylhexyl), trihexyl, and trioctyl phosphate (Alfa Aesar, Ward Hill, MA, United States). CHROMASOLV® grade hexane (Sigma–Aldrich) was used as a solvent. Triphenyl phosphate (Sigma–Aldrich) was dissolved and diluted in reagent-grade acetone (Caledon) to give a 1,020 µg mL^{-1} stock solution that was used as an internal standard. A fracture fluid sample distilling at <250 °C (Wilson Analytical, Sherwood Park, AB, Canada) was diluted 10 times in hexane (Sigma–Aldrich), spiked with ~50 µg mL^{-1} of each alkyl phosphate, and derivatized for the recovery study. Four different industrial flowback samples (Imperial Oil, Sarnia, ON, Canada)

each comprising a mixture of crude oil and fracture fluid, were derivatized and spiked with internal standard before analysis.

3.2.2 Instrumentation and Experimental Conditions

3.2.2.1 Calibration and Recovery Study

Analysis was conducted using a consumable-free LECO GC×GC system (LECO Instruments, St. Joseph, MI, United States) equipped with a CFT (Capillary Flow Technology) Deans switch (Agilent Technologies, Mississauga, ON, Canada) and both FID and NPD detectors (**Figure 3-1**). The column configuration consisted of a 10 m × 0.18 mm, 0.18 μm Rxi-5Sil MS (Restek, Bellefonte, PA, United States) column in the first dimension and a 0.5 m × 0.18 mm, 0.18 μm Rxi-17Sil MS (Restek) column in the second dimension. The transfer lines consisted of 0.18 mm inner diameter deactivated fused silica (Agilent Technologies); 0.16 m connected the secondary column to the Deans switch and 0.20 m sections connected the Deans switch with the detectors.

All injections were performed in triplicate using 1 μL of sample with an Agilent 7683B Series autosampler and a split ratio of 50:1. The inlet temperature was 250 °C. The primary oven temperature program was 40 (2 min) – 280 °C at 30 °C min^{-1}. Relative to the primary oven, the secondary oven was programmed to have a constant offset of +30 °C and the modulator a constant offset of +45 °C. A modulation period of 1.5 s was used.

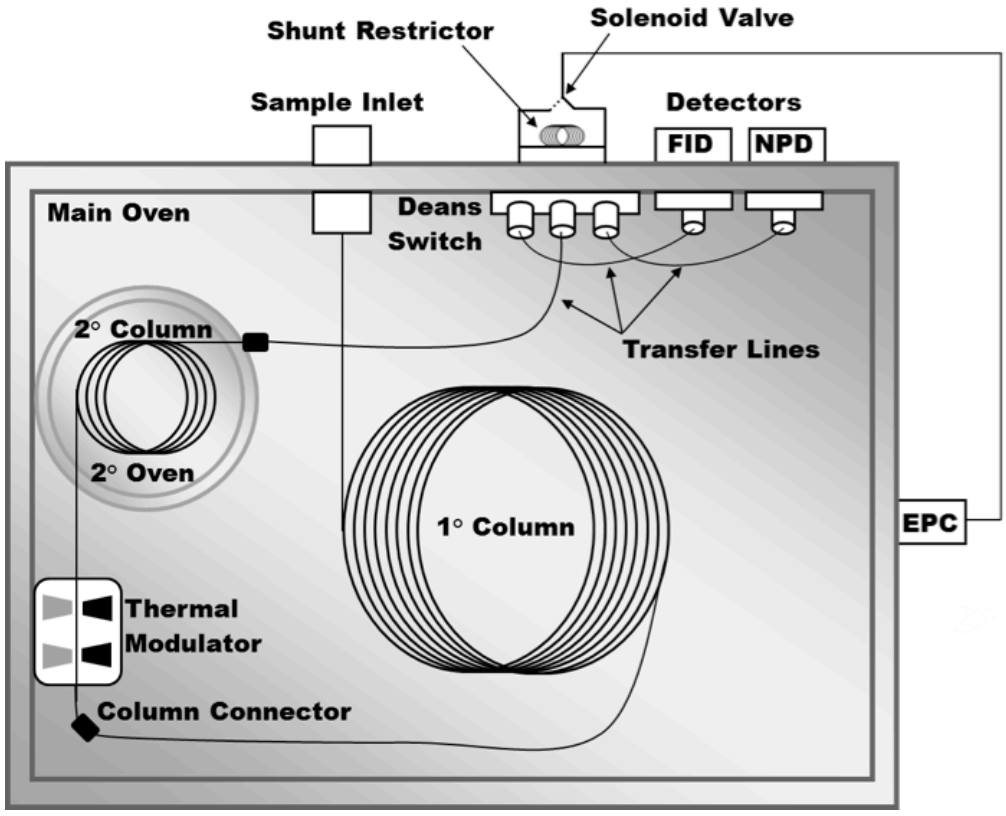

Figure 3-1. Schematic of the GC×GC-FID/NPD system with post-column Deans switch.

Ultra-high purity helium (Praxair, Edmonton, AB, Canada) was used as the carrier gas with a flow rate of ~1 mL min^{-1} and the following ramped pressure programs: 129.7 (2 min) – 249.3 kPa at 15.0 kPa min^{-1} for the inlet and 36.5 (2 min) – 62.8 kPa at 3.3 kPa min^{-1} for the Deans switch plate. The pressure programs were calculated using the Agilent Deans Switch Calculator and HP Flow Calculator. The Deans switch initially directed solvent and any excess derivatization reagents exiting the secondary column to the FID (**Figure 3-2A**). After 3.3 min, the valve was actuated to direct the effluent to the NPD for selective detection of the alkyl phosphates (**Figure 3-2B**).

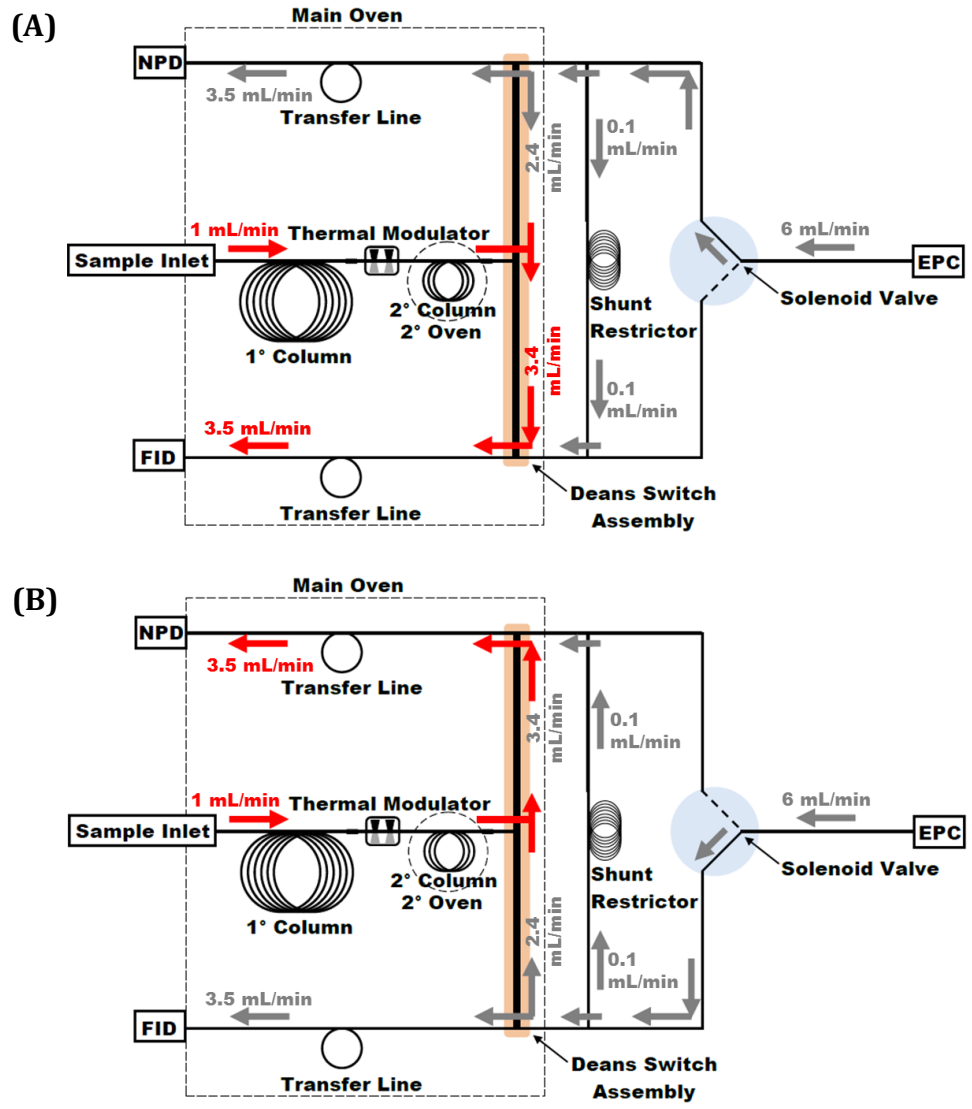

Figure 3-2. Deans switch schematic for GC×GC-FID/NPD: (A) effluent directed to FID (solenoid valve closed), (B) effluent directed to NPD (solenoid valve open).

Both detectors were kept at 325 °C. The NPD used a modified capillary-optimized jet (DETector Engineering & Technology, Inc., Walnut Creek, CA, United States) and a TID-2 black ceramic bead (DETector Engineering & Technology, Inc.). This NPD jet has a large enough bore to

permit the capillary column to pass through the jet and be positioned a few millimetres from the detector bead, improving the response characteristics of the detector over the conventional design [195].

Data were acquired at a rate of 100 Hz and processed using ChromaTOF software (version 4.42; LECO Instruments). The data processing method used a baseline offset of 0.5, auto smoothing, expected first-dimension peak width of 4.5 s, expected second-dimension peak width of 0.2 s, and a minimum signal-to-noise ratio (S/N) of 5 for peak detection.

3.2.2.2 Industrial Petroleum Samples

Analyses were conducted using the same instrumental setup and column configuration as previously stated. The method was modified as follows while all other parameters remained the same. Helium was used as the carrier gas with a ramped pressure program of 129.7 (2 min) – 273.6 kPa at 14.9 kPa min^{-1} for the inlet and 36.5 (2 min) – 68.9 kPa at 3.4 kPa min^{-1} for the pneumatic zone controlling the Deans switch. The primary oven temperature program was 40 (2 min) – 330 °C at 30 °C min^{-1}. The secondary oven temperature program was 70 (2 min) – 350 °C at 30 °C min^{-1}.

3.3 Results and Discussion

Previous research in our laboratory revealed the need for comprehensive multidimensional separations (i.e. GC×GC) coupled with selective detection for the speciation of alkyl phosphates in petroleum samples. The first selective detector tested was a nitrogen-phosphorus

detector; however, the excess silylation reagents from the derivatization mixture were found to coat the NPD bead in a layer of SiO_2, passivating the bead and fully quenching the signal after fewer than 10 chromatographic runs [7,16]. Thus, in early work the Harynuk Group turned to GC×GC-TOFMS, which was capable of quantifying the alkyl phosphates with better precision and lower limits of detection when compared to the currently-accepted ICP-OES method while also providing speciation information [17]. However, the NPD is a much more affordable and rugged detector than TOFMS instrumentation, and is therefore preferred for routine use in a refinery process laboratory.

A silicon-free derivatization method using 1-chloro-3-iodopropane [176] was investigated in this research; however, the reaction failed in hydrocarbon solvents, which were used to mimic a petroleum sample matrix (see **CHAPTER 2**; **Section 2.2**). Consequently, a strategy to divert excess silicon from the established derivatization protocol using post-column Deans switching to select detectors was implemented to allow the use of an NPD detector (see **CHAPTER 2**; **Section 2.3**).

Placing a Deans switch device after the secondary column allowed the effluent to be directed to the FID initially. After the derivatization reagents eluted, the pressure was switched and material directed to the NPD. Overall, the addition of the Deans switch increased the NPD bead life from approximately 5 chromatographic runs to over 1,000, which were performed over the course of 15 months.

Originally the Deans switch was installed on the oven wall (**Figure 3-3A**) as suggested by the installation manual. Initial testing showed the alkyl phosphate peaks to be extremely broad with severe tailing (**Figure 3-4A**). Some of this tailing is expected from the use of an NPD (known as "source tailing", although the mechanism of such tailing is unknown [93,146]); however, the severity of the tailing, as well as the peak broadness, was thought to be due to extra column band broadening occurring as a consequence of the lengthy transfer lines required to transfer the effluent from the secondary column to the Deans switch and then to the detector. As a result, the Deans switch was re-located from the oven wall to the oven roof (**Figure 3-3B**) in order to shorten the transfer lines. In total, the transfer lines from the end of the secondary column to the detector were initially 0.53 m in length, which is quite long, longer even than the secondary column, which is only about 0.38 m long inside the secondary oven. By moving the Deans switch to the oven roof, closer to the secondary oven and detectors, the transfer lines were shortened from a total of 0.53 m to 0.36 m, a reduction of 32%. **Figure 3-4B** demonstrates how this modification effectively reduced extra column band broadening resulting in narrower peaks with less tailing. The overall improved peak shape lead to an extended calibration range (by ~5×) and lower limit of quantification (reduced by ~50%) for most of the alkyl phosphate standards tested as revealed in **Table 3-1** where the low end of the calibration range is considered the "limit of quantification".

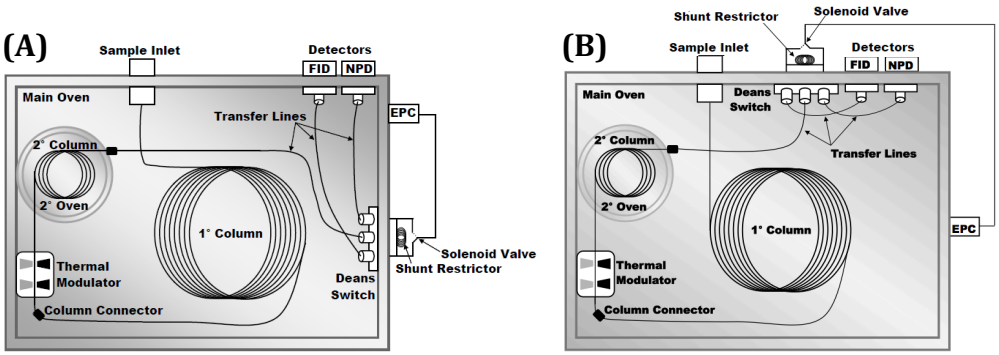

Figure 3-3. Schematic of the GC×GC-FID/NPD system with post-column Deans switch (A) before and (B) after moving the Deans switch to shorten transfer lines.

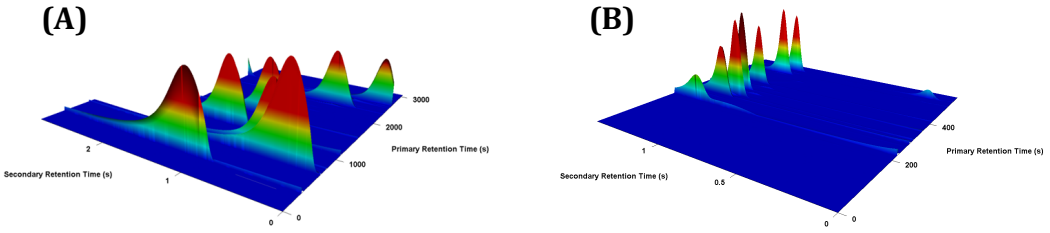

Figure 3-4. GC×GC-NPD chromatogram (A) before instrument modifications showing severe tailing and peak broadness and (B) after instrument modifications showing improved peak shape.

Table 3-1. Calibration data for each alkyl phosphate standard before and after instrument modifications showing an extension in calibration range (by ~5×) and lower limits of quantification (reduced by ~50%).

Phosphate	Overall Calibration Range (µg *alkyl phosphate* mL^{-1})	
	Before Modification	**After Modification***
triethyl	12 – 88	10 – 506
triisopropyl	5.2 – 77	5.0 – 501
tripropyl	6.3 – 95	5.1 – 509
dibutyl	1.1 – 84	0.5 – 131
tributyl	1.2 – 91	0.5 – 507
bis(2-ethylhexyl)	1.1 – 82	0.6 – 139
trihexyl	1.3 – 99	0.5 – 514
trioctyl	1.0 – 76	0.5 – 505

*The overall calibration range for each alkyl phosphate standard after modification is modeled effectively with two separate linear calibrations (high- and low-range) as described in **Section 3.3.1**.

3.3.1 Calibration Study

Solutions of approximately 500, 250, 125, 75, 50, 25, 10, 5, 1, 0.5, 0.1, and 0.05 μg mL^{-1} (weight per volume) of each phosphate were prepared in hexane. Two solutions for each concentration were prepared: one containing the six trialkyl phosphate standards and the other containing the two dialkyl phosphate standards. Triphenyl phosphate was added to each solution as an internal standard at a concentration of 51 μg mL^{-1} for normalization of the resulting peaks areas. As described in the previously established protocol [16], 50 μL of derivatization reagent mixture was added to 500 μL aliquots of each sample in GC vials. The vials were then sealed, shaken, left to derivatize for 30 min at 30 °C, and then analyzed in triplicate using GC×GC-FID/NPD.

Calibration data for the eight alkyl phosphates tested are presented in **Table 3-2**. The calibration curves were not linear over the entire calibration range, but could be modeled effectively with two separate linear calibrations (high- and low-range). As an example **Figure 3-5** shows the pair of calibration curves constructed for triethyl phosphate. The low and high concentration calibration regions overlapped by at least one concentration interval for all compounds. The cut-off points for each of the high and low concentration calibration regions were chosen based on the coefficient of determination (R^2), visual inspection of residuals, and errors of prediction for analyzed standard samples.

Table 3-2. Piece-wise linear fit calibration data.

Phosphate	Linear Calibration Equation (*High* Concentration Region)	R^2	*High* Concentration Calibration Range	
			(µg *alkyl phosphate* mL^{-1})	(µg *phosphorus* mL^{-1})
triethyl	$y = (2.66\times10^{-2}\pm2\times10^{-4})x - (5.7\times10^{-1}\pm5\times10^{-2})$	0.9997	51*(±3)* – 506*(±3)*	8.6*(±0.5)* – 86.0*(±0.5)*
triisopropyl	$y = (2.06\times10^{-2}\pm2\times10^{-4})x - (1\times10^{-2}\pm5\times10^{-2})$	0.9992	50*(±4)* – 501*(±6)*	6.9*(±0.5)* – 69.1*(±0.8)*
tripropyl	$y = (2.05\times10^{-2}\pm3\times10^{-4})x + (1.7\times10^{-1}\pm7\times10^{-2})$	0.9978	51*(±6)* – 509*(±6)*	7.0*(±0.8)* – 70.2*(±0.8)*
dibutyl	$y = (1.99\times10^{-2}\pm2\times10^{-4})x - (5\times10^{-2}\pm2\times10^{-2})$	0.9981	11*(±1)* – 131*(±1)*	1.2*(±0.2)* – 14.3*(±0.2)*
tributyl	$y = (1.92\times10^{-2}\pm2\times10^{-4})x - (1.6\times10^{-1}\pm5\times10^{-2})$	0.9988	51*(±4)* – 507*(±5)*	5.9*(±0.5)* – 59.0*(±0.6)*
bis(2-ethylhexyl)	$y = (1.28\times10^{-2}\pm2\times10^{-4})x - (4\times10^{-2}\pm1\times10^{-2})$	0.9981	11*(±1)* – 139*(±3)*	0.9*(±0.1)* – 10.9*(±0.2)*
trihexyl	$y = (1.322\times10^{-2}\pm6\times10^{-5})x + (4\times10^{-2}\pm1\times10^{-2})$	0.9997	26*(±2)* – 514*(±3)*	2.3*(±0.2)* – 45.4*(±0.3)*
trioctyl	$y = (1.090\times10^{-2}\pm7\times10^{-5})x + (2\times10^{-2}\pm2\times10^{-2})$	0.9996	25*(±3)* – 505*(±3)*	1.8*(±0.2)* – 36.0*(±0.2)*
Phosphate	**Linear Calibration Equation (*Low* Concentration Region)**	**R^2**	***Low* Concentration Calibration Range**	
			(µg *alkyl phosphate* mL^{-1})	**(µg *phosphorus* mL^{-1})**
triethyl	$y = (2.13\times10^{-2}\pm7\times10^{-4})x - (1.8\times10^{-1}\pm3\times10^{-2})$	0.9960	10*(±2)* – 76*(±2)*	1.7*(±0.3)* – 12.9*(±0.4)*
triisopropyl	$y = (2.11\times10^{-2}\pm2\times10^{-4})x - (6.6\times10^{-2}\pm9\times10^{-3})$	0.9986	5.0*(±0.7)* – 75.1*(±0.7)*	0.7*(±0.1)* – 10.4*(±0.1)*
tripropyl	$y = (2.11\times10^{-2}\pm2\times10^{-4})x - (4.1\times10^{-2}\pm6\times10^{-3})$	0.9990	5.1*(±0.4)* – 50.9*(±0.5)*	0.70*(±0.06)* – 7.03*(±0.07)*
dibutyl	$y = (1.40\times10^{-2}\pm2\times10^{-4})x - (6\times10^{-3}\pm1\times10^{-3})$	0.9983	0.5*(±0.1)* – 10.5*(±0.2)*	0.05*(±0.01)* – 1.15*(±0.02)*
tributyl	$y = (1.68\times10^{-2}\pm1\times10^{-4})x - (4\times10^{-3}\pm3\times10^{-3})$	0.9989	0.5*(±0.4)* – 50.7*(±0.5)*	0.06*(±0.05)* – 5.90*(±0.06)*
bis(2-ethylhexyl)	$y = (9.1\times10^{-3}\pm2\times10^{-4})x - (3.7\times10^{-3}\pm9\times10^{-4})$	0.9973	0.6*(±0.3)* – 11.2*(±0.3)*	0.05*(±0.02)* – 0.88*(±0.02)*
trihexyl	$y = (1.46\times10^{-2}\pm1\times10^{-4})x - (1\times10^{-3}\pm1\times10^{-3})$	0.9992	0.5*(±0.2)* – 25.7*(±0.2)*	0.04*(±0.02)* – 2.27*(±0.02)*
trioctyl	$y = (1.14\times10^{-2}\pm1\times10^{-4})x + (3\times10^{-3}\pm2\times10^{-3})$	0.9988	0.5*(±0.4)* – 50.5*(±0.6)*	0.04*(±0.03)* – 3.59*(±0.04)*

Calibration data based on 3 replicates (all from the same sample vial). Errors represent ± 1 standard deviation.

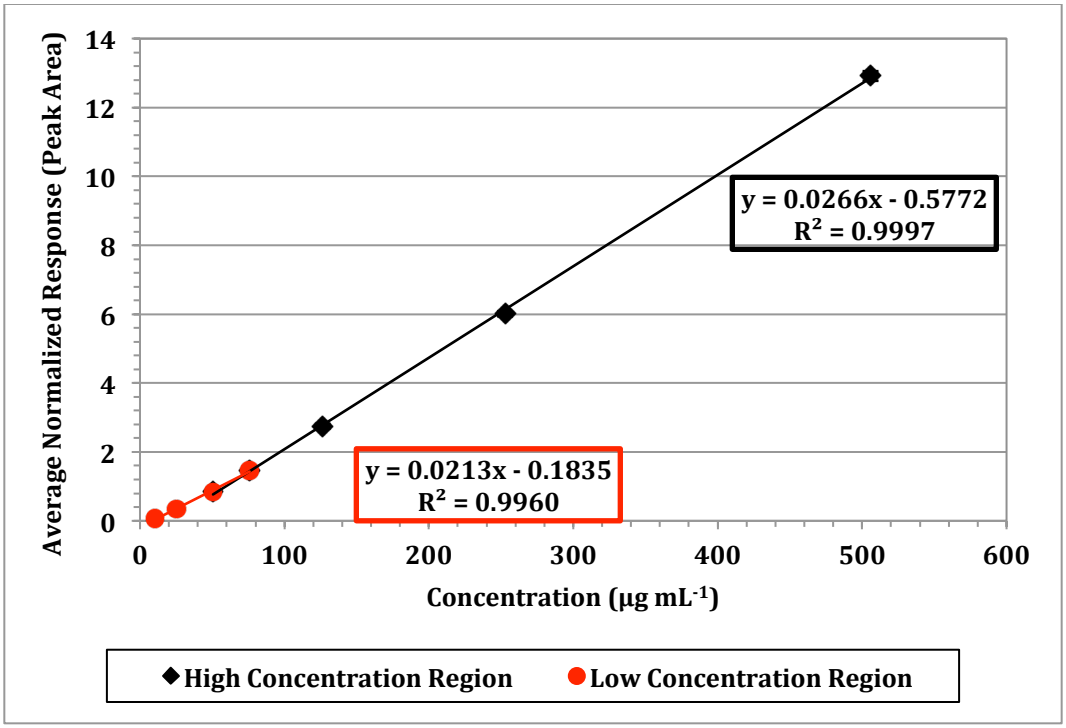

Figure 3-5. Piece-wise calibration curves for triethyl phosphate high (◆) and low (●) concentration ranges. Error bars represent 1 standard deviation.

To compare our GC×GC results with the currently-accepted ICP-OES method, GC×GC results were converted from µg *phosphate* mL^{-1} into µg *phosphorus* mL^{-1} using Equation (3-1):

$$\mu g\ phosphorus\ mL^{-1} = \left(\frac{30.974}{MW_{phosphate}}\right)(\mu g\ phosphate\ mL^{-1}) \qquad (3\text{-}1)$$

where 30.974 is the atomic mass of phosphorus (g mol^{-1}) and $MW_{phosphate}$ is the molecular weight of the alkyl phosphate (g mol^{-1}).

Most of the phosphate standards were easily quantifiable at concentrations as low as 0.5 µg *phosphate* mL^{-1}, while the analytes at 0.1 and 0.05 µg *phosphate* mL^{-1} were generally not detected. Limits of detection (LODs) and limits of quantification (LOQs) for this study have not been

provided because a strict definition of these terms, in the context of modulated multidimensional separations, has not yet been established [98] as previously described (see **CHAPTER 1**; **Section 1.4.3**). Although a theoretical study of these terms is ongoing in the Harynuk Group [154]. Nevertheless, judging by the lower end of the calibration range, in terms of μg *phosphorus* mL^{-1} (**Table 3-2**), the LOQs are likely to be comparable and in most cases much lower than the 0.5 μg *phosphorus* mL^{-1} LOD achievable using the currently-accepted ICP-OES method with the exception of triethyl phosphate. Furthermore, our method demonstrates an increased precision when compared to the ICP-OES method as revealed by the small errors in the calibration values (**Table 3-2**), which were calculated using Equation (3-2):

$$s_x = \frac{s_y}{|m|}\sqrt{\frac{1}{k} + \frac{x_u^2 n + \sum(x_i^2) - 2x_u \sum x_i}{n\sum(x_i^2) - (\sum x_i)^2}} \qquad (3\text{-}2)$$

where s_x is the estimated standard deviation in concentration based on the calibration curve, s_y is the standard deviation in y of the calibration curve, m is the calibration slope, k is the number of replicates of the sample that were measured, x_u is the average predicted concentration for the unknown based on k measurements, n is the number of xy pairs in the calibration curve, and x_i are the x values from the calibration curve.

3.3.2 Recovery Study

A sample of fracture fluid was diluted 10× in hexane and spiked with eight different alkyl phosphate standards to a concentration of ~50 μg *phosphate* mL^{-1} each. Triphenyl phosphate added as an internal

standard at a concentration of 51 μg mL^{-1}. A 500 μL aliquot of this sample was then derivatized and analyzed as previously described.

The diluted fracture fluid sample was found to have a native triethyl phosphate concentration of 16 ± 2 μg *phosphate* mL^{-1} (or 160 μg *phosphate* mL^{-1} in the undiluted sample) (**Figure 3-6**). After spiking the diluted sample with 50.6 μg *phosphate* mL^{-1} of triethyl phosphate, a concentration of 56 ± 2 μg *phosphate* mL^{-1} was measured suggesting that the recovered concentration of triethyl phosphate was 40 ± 2 μg *phosphate* mL^{-1} or 79%. **Table 3-3** presents the recovery data for all eight alkyl phosphates. Satisfactory recoveries between 79 and 105%, with relative standard deviations of 5.0% or less, were observed.

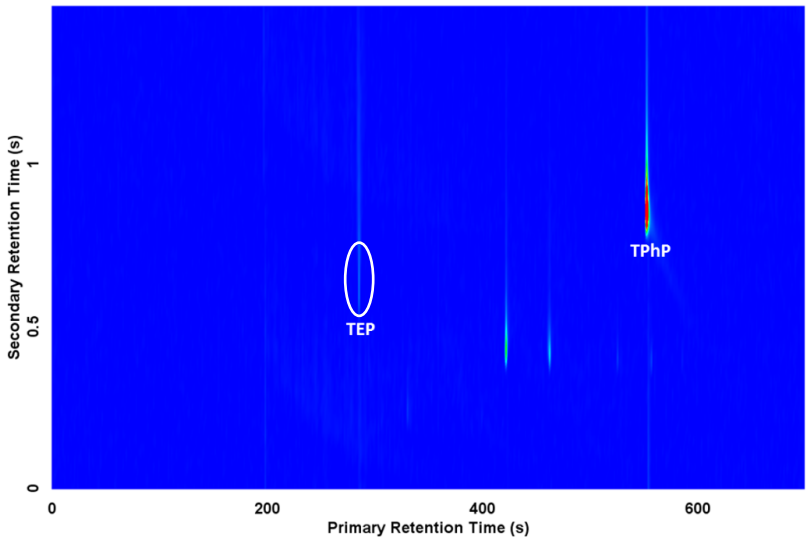

Figure 3-6. Fracture fluid sample diluted 10× in hexane, derivatized, and analyzed using GC×GC-NPD (TEP = triethyl phosphate (native); TPhP = triphenyl phosphate (internal standard)). Secondary dimension (^{2}D) offset of 0.8 s applied to plotted chromatogram.

Table 3-3. Results of recovery study in fracture fluid sample.

Phosphate	Spiked (μg *phosphate* mL^{-1})	Average Recovered (*n=3*) (μg *phosphate* mL^{-1})	%	RSD (%)
triethyl[a]	50.6	40 ± 2	79	5.0
triisopropyl	50.1	47.0 ± 0.7	94	1.5
tripropyl	50.9	48.5 ± 0.5	95	1.0
dibutyl	52.3	55 ± 1	105	2.4
tributyl	50.7	47.2 ± 0.5	93	1.1
bis(2-ethylhexyl)	55.8	58 ± 2	103	2.8
trihexyl	51.4	48 ± 2	93	4.4
trioctyl	50.5	50.8 ± 0.5	101	1.0

[a] Fracture fluid sample had a native concentration of triethyl phosphate of 16 ± 2 μg *phosphate* mL^{-1} (or 160 μg *phosphate* mL^{-1} in the undiluted sample). The actual measured concentration of the spiked sample was 56 ± 2 μg *phosphate* mL^{-1} of triethyl phosphate.

3.3.3 Qualitative and Quantitative Profiling of Industrial Samples

The derivatization and GC×GC-FID/NPD methods were used to profile alkyl phosphate contamination in four industrial flowback samples. Both triethyl phosphate and tributyl phosphate were identified in all four samples at concentrations ranging from 8.7 to 124 μg *phosphate* mL^{-1} (**Table 3-4**). Additionally, several other probable phosphorus (possibly nitrogen) compounds were also detected (**Figure 3-7**), yet remain unidentified due to a lack of available alkyl phosphate standards. As it has been shown that TOFMS with electron impact ionization is minimally informative for the identification of alkyl phosphates [17], the issue of unknown phosphate identification will likely require custom synthesis of standards in conjunction with a model of alkyl phosphate retention that is in the early stages of development [198,199].

Table 3-4. Quantification of native phosphates in four industrial flowback samples.

Sample	Phosphate	Concentration (µg *phosphate* mL^{-1}) (µ ± σ; *n=3*)	RSD (%)
1	triethyl	36 ± 2	5.0
	tributyl	27.9 ± 0.4	1.4
2	triethyl	25 ± 2	7.6
	tributyl	124 ± 4	3.2
3	triethyl	20 ± 2	9.4
	tributyl	8.7 ± 0.4	4.5
4	triethyl	32 ± 2	5.5
	tributyl	15.0 ± 0.4	2.6

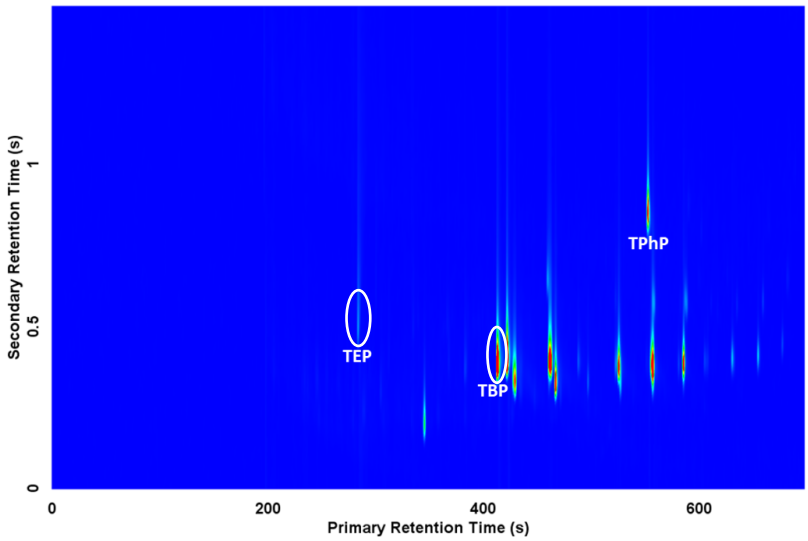

Figure 3-7. GC×GC-NPD chromatogram of a flowback sample (Sample 2, **Table 3-4**) (TEP = triethyl phosphate; TBP = tributyl phosphate; TPhP = triphenyl phosphate (internal standard)). ^{2}D offset of 0.8 s applied to plotted chromatogram.

3.4 Conclusions

The resulting GC×GC-FID/NPD system offers an approach that is capable of both quantifying and speciating individual alkyl phosphate compounds in industrial petroleum samples. In addition, this technique detected and quantified phosphate standards at levels comparable to or

below those achievable by the currently-accepted ICP-OES methodology, with improved precision. All of the industrial petroleum samples tested contained two known trialkyl phosphates, and numerous other compounds that were likely alkyl phosphates. Overall, this research represents a significant step forward in the development of a platform for the routine profiling of these contaminants in industrial samples. However, a further decrease in the limits of quantification of this technique would be preferred for trace analysis.

CHAPTER FOUR: Profiling Alkyl Phosphates in Industrial Petroleum Samples by GC×GC-NPD, Post-column Deans Switching, and Concurrent Backflushing[3]

4.1 Introduction

Several refinery-fouling incidents in North America have resulted due to the presence of alkyl phosphates in the crude oil feed. These phosphates originate in some cases from their use as gellants (viscosity builders) for fracture fluids used in the process of hydraulic fracturing in water-sensitive geologies. Industry has responded with an inductively coupled plasma – optical emission spectroscopy (ICP-OES) method for the analysis of total volatile phosphorus [5,6]. Applied to distillate fractions of crude oil, this method is plagued with poor precision and a high limit of detection (0.5 ± 1 μg *phosphorus* mL^{-1}). In addition, this approach provides only total phosphorus with no speciation information, thus it cannot be used to develop an understanding of alkyl phosphate fouling at a molecular level. **CHAPTER 3** presented an approach using comprehensive two-dimensional gas chromatography with nitrogen-phosphorus detection (GC×GC-NPD) and post-column Deans switching that provided qualitative and quantitative profiles of alkyl phosphates in industrial petroleum samples with increased precision and at levels comparable to or below those achievable by ICP-OES [18]. This chapter presents the further evolution of this method by

[3] A version of this chapter has been published as K.D. Nizio, J.J. Harynuk, Energy Fuels 28 (2014) 1709.

implementing splitless injection and concurrent backflushing in order to further lower the limits of quantification for trace analysis, while still maintaining the previously achieved precision. The use of concurrent backflushing has been shown to facilitate the exclusion of heavier, less-volatile matrix components from the system resulting in benefits of improved retention time reproducibility, improved detector stability, and decreased system maintenance, leading to less instrument downtime and improved sample throughput [200,201,202].

4.2 Experimental

4.2.1 Materials and Reagents

Stock solutions were stored in glass vials and refrigerated at ~7 °C. Calibration, recovery study, and industrial petroleum sample solutions were prepared in 1.8 mL glass GC vials with polytetrafluoroethylene (PTFE)-lined silicone septa (Chromatographic Specialties, Brockville, ON, Canada) for analysis by comprehensive two-dimensional gas chromatography with both flame ionization and nitrogen-phosphorus detection (GC×GC-FID/NPD).

All reagents were used as received unless otherwise stated. Derivatization was performed according to a previously established protocol [16] using a mixture of *N,O*-bis(trimethylsilyl)trifluoroacetamide (BSTFA) (Sigma-Aldrich, Oakville, ON, Canada), pyridine (Caledon, Georgetown, ON, Canada), and trimethylchlorosilane (TMCS) (Sigma-Aldrich) in a 10:5:2 ratio

by volume. A total of 50 μL of the derivatization reagent mixture was added to 500 μL of sample and left to derivatize at 30 °C for 30 min before analysis. Vials were maintained at temperature using the GC autosampler tray, which was kept at 30 °C by circulating heated water through the tray.

The alkyl phosphate standards used for the calibration and recovery studies consisted of triethyl, triisopropyl, tripropyl, dibutyl, and tributyl phosphate (Sigma-Aldrich), tripentyl phosphate (Tokyo Chemical Industry Co., Ltd., Toshima, Kita-Ku, Tokyo, Japan), and bis(2-ethylhexyl), trihexyl, and trioctyl phosphate (Alfa Aesar, Ward Hill, MA, United States). Triphenyl phosphate (Sigma-Aldrich) was dissolved and diluted in reagent-grade acetone (Caledon) to give a 1,020 μg mL^{-1} stock solution that was used as an internal standard. Isooctane (Sigma-Aldrich) was used as a solvent.

Two different industrial petroleum samples (Imperial Oil, Sarnia, ON, Canada) were diluted in isooctane (Sigma-Aldrich), spiked with ~0.2 and ~0.5 μg mL^{-1} of each alkyl phosphate, and derivatized for the recovery study. A total of 14 different industrial petroleum samples (Imperial Oil) were derivatized and spiked with internal standard before profiling. The industrial samples included a refinery process stream (catalyst feed stream), crude oil, mixtures of crude oil and fracture fluid, and mixtures of crude oil, fracture fluid, and "slop" (fracture fluid waste stream). The industrial petroleum samples were diluted from 50 to 20,000× in isooctane for splitless injections and 10× for split injections. Dilution factors were chosen in order to ensure that the alkyl phosphate concentration fell within the calibration range.

4.2.2 Instrumentation and Experimental Conditions

4.2.2.1 Splitless Injection

Analysis was conducted using a consumable-free LECO GC×GC system (LECO Instruments, St. Joseph, MI, United States) equipped with a post-column CFT (Capillary Flow Technology) Deans switch (Agilent Technologies, Mississauga, ON, Canada), a purged, deactivated stainless steel union (Agilent Technologies), and both FID and NPD detectors (**Figure 4-1**). The column configuration consisted of a 10 m × 0.18 mm, 0.18 µm Rxi-5Sil MS (Restek, Bellefonte, PA, United States) column in the first dimension (1 m of pre-column before the purged union and 9 m of analytical column after the purged union) and a 0.5 m × 0.18 mm, 0.18 µm Rxi-17Sil MS (Restek) column in the second dimension. The transfer lines consisted of 0.18 mm inner diameter deactivated fused silica (Agilent Technologies), 0.16 m connected the secondary column to the Deans switch and two 0.20 m segments connected the Deans switch with the detectors.

All injections were performed in triplicate using an Agilent 7683B Series autosampler. Injection conditions were 1 µL of sample with a 0.04 min post-injection delay at a temperature of 250 °C. The splitless injection purge time was 120 s at a flow of 100 mL min^{-1}. The primary oven temperature program was 60 °C (2 min) to 90 °C (2 min) to 330 °C at 30 °C min^{-1}. Relative to the primary oven, the secondary oven was programmed to have a constant offset of +35 °C and the modulator a constant offset of +50 °C. A modulation period of 1.6 s was used.

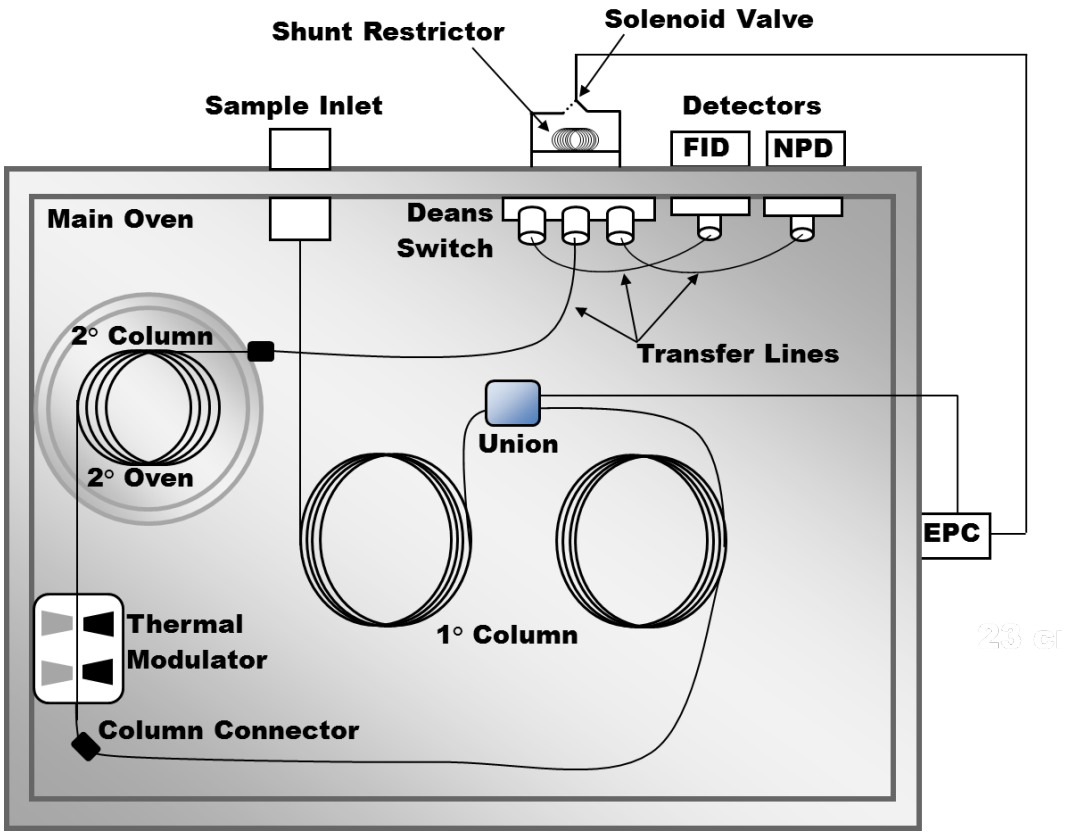

Figure 4-1. Schematic of the GC×GC-FID/NPD system with post-column Deans switch and purged union for concurrent backflushing.

Ultra-high purity helium (Praxair, Edmonton, AB, Canada) was used as the carrier gas with a flow rate of ~1.4 mL min^{-1} and the following ramped pressure programs: 139.3 kPa (2 min) to 154.1 kPa (2 min) to 230.0 kPa at a rate of 14.9 kPa min^{-1} for the inlet; 132.7 kPa (2 min) to 147.0 kPa (2 min) to 261.2 kPa at 14.3 kPa min^{-1} for the purged union; and 26.6 kPa (2 min) to 28.2 kPa (2 min) to 40.5 kPa at 1.5 kPa min^{-1} for the Deans switch plate. The pressure programs were calculated using the Agilent Deans Switch Calculator and HP Flow Calculator. The purged union initially permitted flow in the forward (analytical) direction (i.e. toward the detectors). After the last alkyl

phosphate standard passed the union (10.1 min), the pressure ramp for the inlet was interrupted and rapidly decreased to 34.5 kPa at 69.0 kPa min^{-1} in order to concurrently backflush the first 1 m of primary pre-column. When samples were analyzed using the NPD, the Deans switch initially directed solvent and any excess derivatization reagents exiting the secondary column to the FID. After 4 min, the valve was actuated to direct the effluent to the NPD for selective detection of the alkyl phosphates.

Both detectors were kept at 325 °C. The NPD used a modified capillary-optimized jet (DETector Engineering & Technology, Inc., Walnut Creek, CA, United States) and a TID-2 black ceramic bead (DETector Engineering & Technology, Inc.). This NPD jet has a large enough bore to permit the capillary column to pass through the jet and be positioned a few millimetres from the detector bead, improving the response characteristics of the detector over the conventional design [195].

Data were acquired at a rate of 100 Hz and processed using ChromaTOF software (version 4.42; LECO). The data processing method used a baseline offset of 0.5, auto smoothing, expected first-dimension peak width of 4.8 s, expected second-dimension peak width of 0.3 s, and a minimum signal-to-noise ratio (S/N) of 50 for base peak and 5 for sub-peak detection. A classification scheme, prepared with LECO's ChromaTOF software and the alkyl phosphate standards, was used for initial speciation of the industrial petroleum samples. Alkyl phosphate identification was confirmed using

retention times in both the first- and second-dimensions, as well as temperature-programmed retention indices in the first dimension ($^1I^T$).

4.2.2.2 Split Injection

Analyses were conducted using the same instrumental setup and column configuration as previously stated. The method was modified as follows while all other parameters remained the same. A split ratio of 50:1 was used for the split injections along with a modulation period of 4 s. The data processing method used an expected first-dimension peak width of 15 s and an expected second-dimension peak width of 2 s.

4.3 Results and Discussion

We have previously demonstrated the use of GC×GC with selective detection to quantify alkyl phosphates in petroleum samples. A time-of-flight mass spectrometer may be used directly for the measurement of alkyl phosphates [17], although it is expensive and not the best choice for routine monitoring in a refinery environment. For this situation, an NPD is a better choice, although it requires a Deans switch for detector selection to divert excess silylation reagents at the start of a chromatogram to an FID [18]. This protects the NPD bead, which would be rapidly (<10 injections) passivated with an inert layer of SiO_2 when exposed to excess silylation reagents [7,16]. Using the Deans switch after the secondary column in GC×GC for detector selection extended the lifetime of the NPD bead from approximately 5 injections to over 1,000, performed over the course of 15 months (see

CHAPTER 2; **Section 2.3**). The resulting GC×GC-FID/NPD system offered an approach that was capable of both quantifying and speciating individual alkyl phosphate compounds in industrial petroleum samples (see **CHAPTER 3** [18]). In addition, this technique detected and quantified phosphate standards at levels comparable to or below levels achievable by the currently-accepted ICP-OES methodology, with improved precision.

However, the fouling of refinery equipment is thought to be the result of chronic exposure to trace quantities of volatile phosphorus [67]. For example, at a level of 1 part per million (ppm) phosphorus, a refinery handling 120,000 barrels of oil per day (bpd) would be exposed to 0.12 bpd of phosphorus. Lowering the limits of quantification and detection for trace phosphorus will improve the ability of operators to monitor and plan for cumulative effects of phosphorus exposure in facilities. To address this need, we have adapted the GC×GC-FID/NPD system from split to splitless injection.

To protect the columns when performing splitless injections of derivatized heavy petroleum samples, a purged ultimate union was installed between the first 1 m of primary pre-column and 9 m of primary analytical column in order to allow for concurrent backflushing (**Figure 4-1**). Unlike with post-run backflushing configurations this setup is more time-effective because it allows backflushing to begin as soon as the last analyte of interest has passed the union. Backflushing helps to eliminate heavier, less volatile matrix components from the GC×GC-FID/NPD system by reversing column flow at the purged ultimate union, flushing the heavier, less volatile

components out the injector split vent. Overall, the addition of backflushing reduces the need for time-consuming, high-temperature bakeouts, which in turn cuts down on analytical time, increases column life, and minimizes column bleed and ghost peaks [200,201,202]. Furthermore, the heavier, less volatile matrix components do not reach the second portion of the primary column, the secondary column, or the detectors, therefore resulting in decreased system maintenance. This in turn leads to less instrument downtime, thus further improving sample throughput.

4.3.1 Calibration Study Using Splitless Injection

4.3.1.1 Splitless Injection Optimization

Splitless injection is used for trace analysis when the analytes of interest are in low ppm/μg mL^{-1} concentration. In split mode, only a small portion of the sample (usually 2% or less) is introduced to the column, while the remainder of the sample is swept out the split vent. Alternatively, in splitless mode, the split vent is closed during the first part of the injection; therefore, the bulk of the sample is sent to the column instead of out the split vent. As a result, analyte transfer in splitless injection is slow as the flow through the injector liner is equal to the column flow. The large injection volume and slow analyte transfer can result in substantial injection band broadening and poor peak shape if splitless injection is not properly optimized. In order to obtain reasonable peak shapes and widths in splitless injection, the split vent is opened a short time (usually about 30 – 120 s) after

injection to purge any left over residue from the liner. If the purge time is too short, compounds may not have enough time to vaporize completely resulting in poor transfer to the column and low peak areas. If the purge time is too long, the extended slow transfer of analytes from the liner to the column can result in poor peak shape (i.e. tailing).

To optimize the splitless injection purge time a phosphate standard sample containing all seven trialkyl phosphates was first prepared in isooctane at a concentration of 1 μg mL^{-1}, with triphenyl phosphate added as an internal standard at a concentration of 0.5 μg mL^{-1}. The standard sample was run in triplicate with inlet purge times of 30, 60, 70, 80, 90, 100, 110, and 120 s. **Figure 4-2A** displays a plot of normalized peak area versus front inlet purge time for all seven alkyl phosphate standards. Overall, 30 s was deemed too short a purge time. Next, two industrial petroleum samples (B and F) were chosen to help optimize the inlet purge time. Both samples were diluted in isooctane (50× and 100× respectively) and spiked with all seven trialkyl phosphate standards to concentrations of ~1 μg *phosphate* mL^{-1} each, with triphenyl phosphate added as an internal standard at a concentration of 0.5 μg mL^{-1}. As described in our previously established protocol [16], 50 μL of derivatization reagent mixture was added to 500 μL aliquots of each sample in GC vials. The vials were then sealed, shaken, left to derivatize for 30 min at 30 °C, and then analyzed in triplicate using GC×GC-FID/NPD. For the industrial samples, inlet purge times of 60, 70, 80, 90, 100, 110, 120, 130, 140, 150, and 180 s were tested as displayed in **Figure 4-2B** and **Figure 4-**

2C. An inlet purge time of 120 s was found to give acceptable peak shapes with maximum normalized peak area for sample B. Acceptable peak shapes were also achieved with a 120 s inlet purge time for sample F along with satisfactory peak areas.

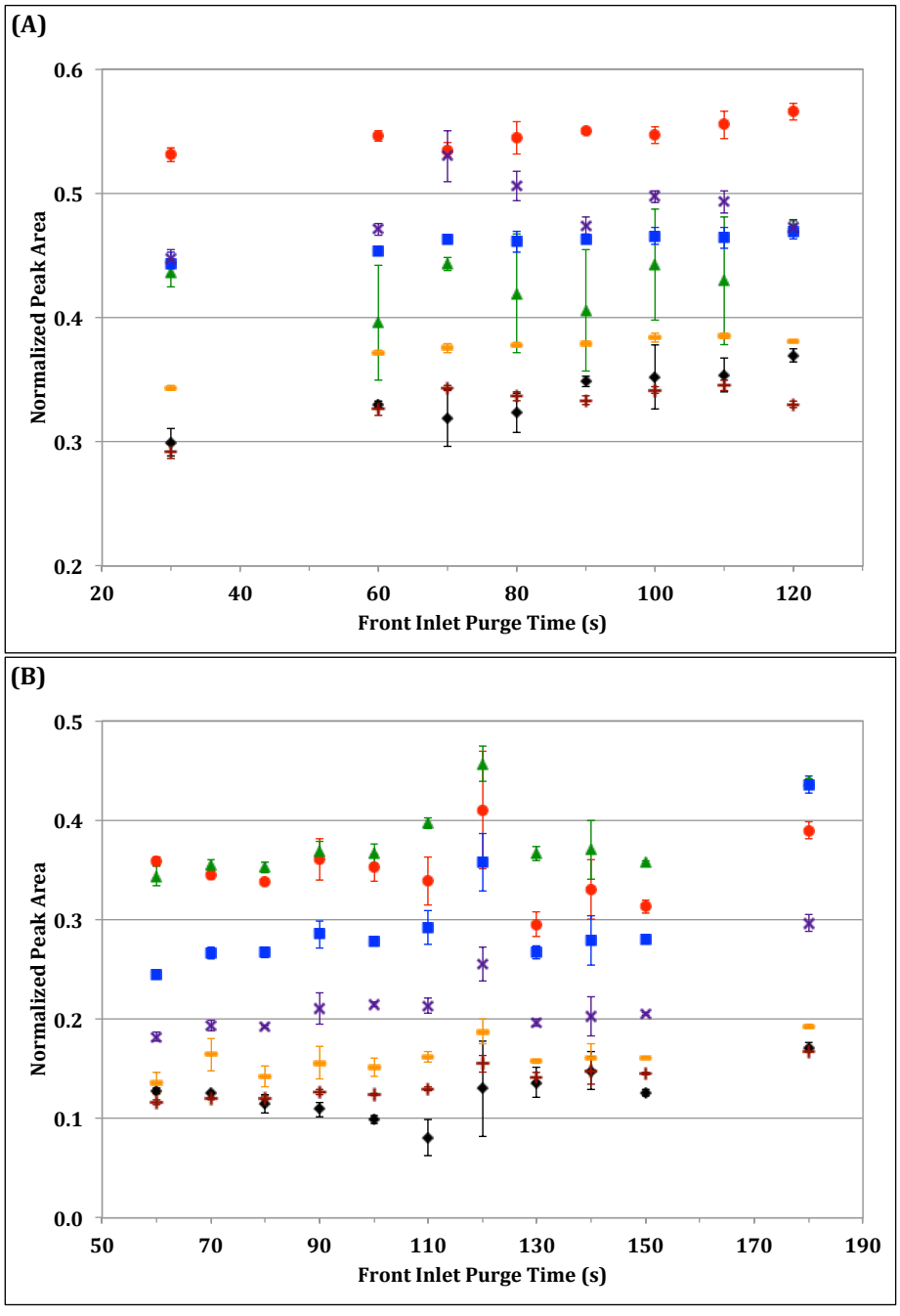

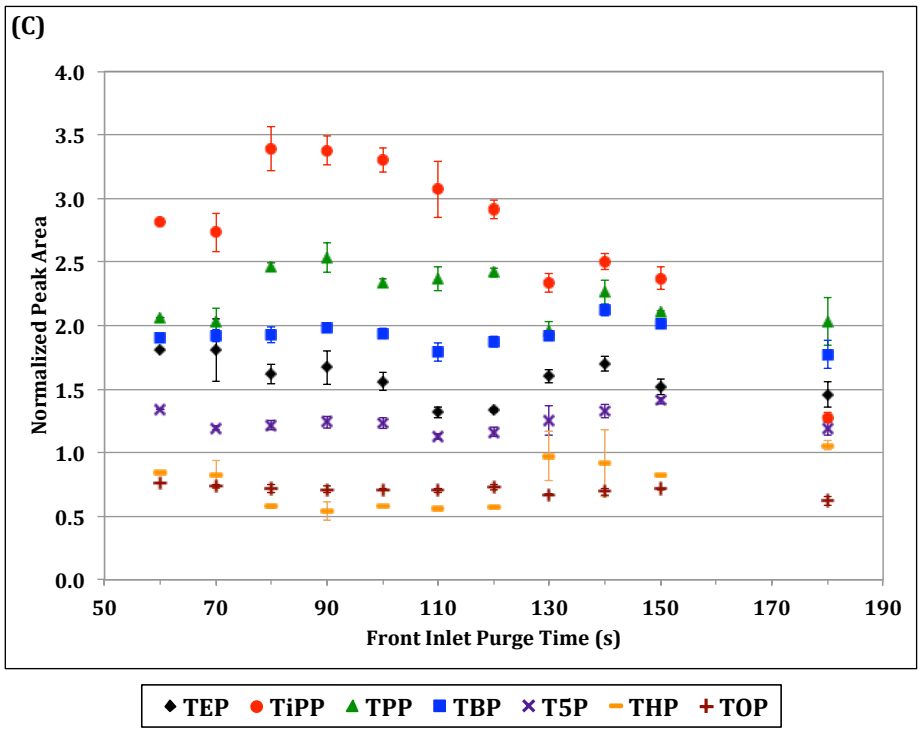

Figure 4-2. Plot of normalized peak area versus front inlet purge time for triethyl (TEP, ◆), triisopropyl (TiPP, ●), tripropyl (TPP, ▲), tributyl (TBP, ■), tripentyl (T5P, ×), trihexyl (THP, −), and trioctyl (TOP, +) phosphates in: (A) isooctane, (B) sample B diluted 50× in isooctane, and (C) sample F diluted 100× in isooctane. Error bars represent 1 standard deviation based on 3 replicates.

In addition to optimizing the splitless injection purge time, the injection was also optimized in terms of injection timing in order to ensure more efficient sample transfer from the needle to the inlet. Here, no injection delay, a pre-injection delay, and a post-injection delay were tested using the 120 s inlet purge time. A pre-injection delay allows the sample needle to be heated prior to injection, while a post-injection delay allows the sample needle to remain in the injector after the plunger has been depressed and the sample injected.

To optimize the injection timing, a sample of the seven trialkyl phosphate standards was prepared in isooctane, sample B and sample F as previously described. The samples were run in triplicate with no injection delay, 0.02 and 0.04 min pre-injection delays, and 0.02 and 0.04 min post-injection delays. **Figure 4-3** displays the results for each trialkyl phosphate. The presence or absence of a pre- or post-injection delay was found to have little effect on the normalized peak area of the later eluting phosphates (i.e. tripentyl, trihexyl and trioctyl phosphates). However, the earlier eluting phosphates had much higher normalized peak areas when a 0.04 min post-injection delay was used. This suggests that a post-injection delay of 0.04 min results in the most efficient transfer of sample from needle to inlet and was therefore used for all injections from this point on, along with a 120 s inlet purge time.

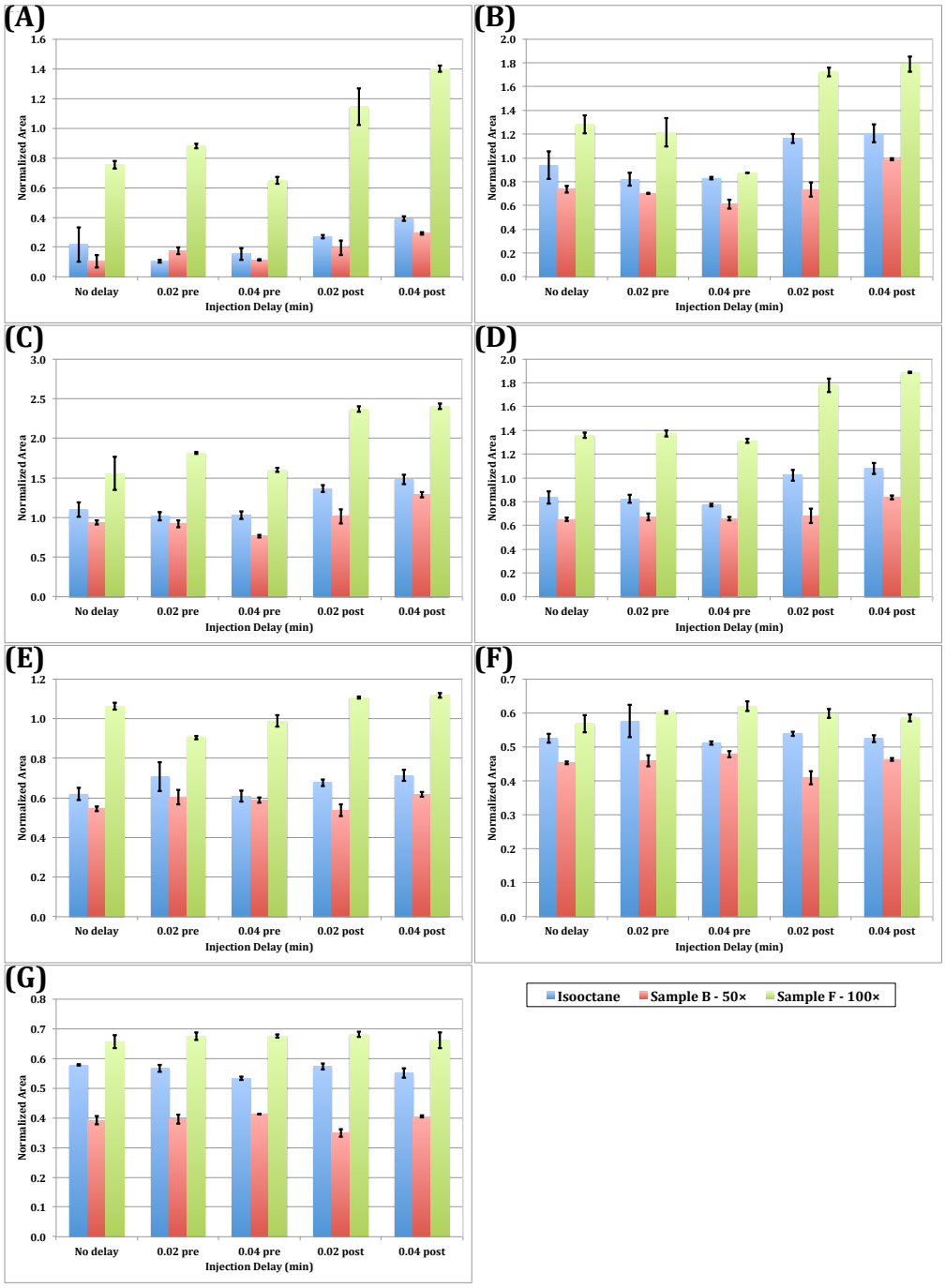

Figure 4-3. Plot of normalized peak area versus injection delay for: (A) triethyl, (B) triisopropyl, (C) tripropyl, (D) tributyl, (E) tripentyl, (F) trihexyl, and (G) trioctyl phosphates in isooctane (blue), sample B diluted 50× in isooctane (red), and sample F diluted 100× in isooctane (green). Error bars represent 1 standard deviation based on 3 replicates.

4.3.1.2 Splitless Injection Calibration

Solutions of approximately 1, 0.8, 0.6, 0.4, 0.2, 0.1, 0.05, 0.01, 0.005, and 0.001 μg mL^{-1} (weight per volume) of each alkyl phosphate were prepared in isooctane. Two solutions for each concentration were prepared: one containing the seven trialkyl phosphate standards and the other containing the two dialkyl phosphate standards. Triphenyl phosphate was added to each solution as an internal standard at a concentration of 0.5 μg mL^{-1} for normalization of the resulting peak areas. Samples were derivatized as previously described, then analyzed in triplicate using GC×GC-FID/NPD.

Calibration data for the nine alkyl phosphates tested are presented in **Table 4-1**. As was observed in our previously established method using split injection (**CHAPTER 3** [18]), the calibration curves were not linear over the entire calibration range, but could be modeled effectively with two separate linear calibrations (high- and low-range). The high and low concentration calibration regions overlapped by at least one concentration interval for all compounds. The cut-off points for each of the high and low concentration calibration regions were chosen based on the coefficient of determination (R^2), visual inspection of residuals, and errors of prediction for analyzed standard samples.

Table 4-1. Splitless injection piece-wise linear fit calibration data.

Phosphate	Linear Calibration Equation (*High* Concentration Region)	R^2	*High* Concentration Calibration Range	
			(µg *alkyl phosphate* mL^{-1})	(µg *phosphorus* mL^{-1})
triethyl	$y = (1.27\pm0.03)x - (0.17\pm0.02)$	0.9941	0.11*(±0.02)* – 1.15*(±0.02)*	0.019*(±0.003)* – 0.196*(±0.003)*
triisopropyl	$y = (1.11\pm0.04)x - (0.15\pm0.03)$	0.9969	0.42*(±0.02)* – 1.05*(±0.02)*	0.058*(±0.003)* – 0.145*(±0.003)*
tripropyl	$y = (2.11\pm0.07)x + (0.04\pm0.06)$	0.9901	0.46*(±0.02)* – 1.16*(±0.02)*	0.064*(±0.003)* – 0.160*(±0.003)*
dibutyl	$y = (0.82\pm0.02)x + (0.00\pm0.01)$	0.9991	0.21*(±0.03)* – 1.05*(±0.03)*	0.023*(±0.003)* – 0.115*(±0.003)*
tributyl	$y = (1.43\pm0.05)x + (0.07\pm0.04)$	0.9879	0.41*(±0.02)* – 1.02*(±0.02)*	0.047*(±0.002)* – 0.119*(±0.002)*
tripentyl	$y = (1.32\pm0.02)x + (0.05\pm0.02)$	0.9994	0.42*(±0.01)* – 1.05*(±0.01)*	0.042*(±0.001)* – 0.105*(±0.001)*
bis(2-ethylhexyl)	$y = (0.62\pm0.01)x - (0.059\pm0.008)$	0.9986	0.481*(±0.009)* – 1.07*(±0.01)*	0.0378*(±0.0007)* – 0.0840*(±0.0008)*
trihexyl	$y = (0.90\pm0.03)x + (0.00\pm0.02)$	0.9979	0.42*(±0.02)* – 1.06*(±0.02)*	0.0399*(±0.0002)* – 0.1006*(±0.0002)*
trioctyl	$y = (0.92\pm0.02)x - (0.04\pm0.02)$	0.9970	0.41*(±0.01)* – 1.02*(±0.02)*	0.0291*(±0.0007)* – 0.073*(±0.001)*
Phosphate	**Linear Calibration Equation (*Low* Concentration Region)**	**R^2**	***Low* Concentration Calibration Range**	
			(µg *alkyl phosphate* mL^{-1})	(µg *phosphorus* mL^{-1})
triethyl	----------	---	----------	----------
triisopropyl	$y = (0.86\pm0.03)x - (0.031\pm0.008)$	0.9965	0.05*(±0.01)* – 0.42*(±0.01)*	0.007*(±0.001)* – 0.058*(±0.001)*
tripropyl	$y = (2.10\pm0.02)x + (0.019\pm0.003)$	0.9996	0.006*(±0.003)* – 0.464*(±0.004)*	0.0008*(±0.0004)* – 0.0641*(±0.0005)*
dibutyl	$y = (0.54\pm0.02)x + (0.048\pm0.002)$	0.9950	0.010*(±0.006)* – 0.209*(±0.007)*	0.0011*(±0.0007)* – 0.0229*(±0.0008)*
tributyl	$y = (1.456\pm0.009)x + (0.042\pm0.002)$	0.9997	0.005*(±0.002)* – 0.407*(±0.003)*	0.0006*(±0.0002)* – 0.0473*(±0.0002)*
tripentyl	$y = (1.40\pm0.01)x + (0.007\pm0.002)$	0.9998	0.005*(±0.003)* – 0.420*(±0.006)*	0.0005*(±0.0003)* – 0.0422*(±0.0006)*
bis(2-ethylhexyl)	$y = (0.62\pm0.01)x - (0.059\pm0.008)$	0.9986	0.06*(±0.02)* – 0.48*(±0.01)*	0.005*(±0.002)* – 0.0378*(±0.0008)*
trihexyl	$y = (0.886\pm0.006)x + (0.004\pm0.001)$	0.9994	0.005*(±0.003)* – 0.420*(±0.003)*	0.0005*(±0.0003)* – 0.0399*(±0.0003)*
trioctyl	$y = (0.833\pm0.007)x - (0.002\pm0.001)$	0.9950	0.005*(±0.003)* – 0.408*(±0.004)*	0.0004*(±0.0002)* – 0.0291*(±0.0003)*

Calibration data based on 3 replicates (all from the same sample vial). Errors represent ± 1 standard deviation.

Limits of detection (LODs) and limits of quantification (LOQs) have not been provided for this study because a strict definition of these terms, in the context of modulated multidimensional separations, has not yet been established [98] as previously described (see **CHAPTER 1**; **Section 1.4.3**). Although a theoretical study of these terms is ongoing in the Harynuk Group [154]. As a result, the "LOQs" for this approach will be considered as the lowest value of the calibration range for the remainder of this thesis. These "LOQ" values are then converted from µg *phosphate* mL^{-1} to µg *phosphorus* mL^{-1} using Equation (4-1):

$$\mu g\ phosphorus\ mL^{-1} = \left(\frac{30.974}{MW_{phosphate}}\right)(\mu g\ phosphate\ mL^{-1}) \qquad (4\text{-}1)$$

where 30.974 is the atomic mass of phosphorus (g mol^{-1}) and $MW_{phosphate}$ is the molecular weight of the alkyl phosphate (g mol^{-1}). This conversion was made for the purpose of comparing the "LOQs" obtained from GC×GC-NPD with that of the currently-accepted ICP-OES method (0.5 ± 1 µg *phosphorus* mL^{-1}), which is only able to quantify total volatile phosphorus.

Table 4-2 presents the "LOQs" in terms of µg *phosphorus* mL^{-1} for the GC×GC-FID/NPD method for both split (**CHAPTER 3** [18]) and splitless injections using alkyl phosphate standards calibrated in solvent. There is no information for tripentyl phosphate with the split method, as that standard was not available when the initial study was conducted. Overall, splitless injection was found to produce "limits of quantification" two orders of magnitude lower than those achieved with split injection and two to three

orders of magnitude lower than that capable by ICP-OES, while still maintaining an increased precision over ICP-OES.

Table 4-2. Comparison of "limits of quantification" for split (**CHAPTER 3** [18]) versus splitless injection in solvent.

Phosphate	"LOQ" (µg *phosphorus* mL^{-1})	
	Split Injection	**Splitless Injection**
triethyl	1.7 ± 0.3	0.019 ± 0.003
triisopropyl	0.7 ± 0.1	0.007 ± 0.001
tripropyl	0.70 ± 0.06	0.0008 ± 0.0004
dibutyl	0.05 ± 0.01	0.0011 ± 0.0007
tributyl	0.06 ± 0.05	0.0006 ± 0.0002
tripentyl	*	0.0005 ± 0.0003
bis(2-ethylhexyl)	0.05 ± 0.02	0.005 ± 0.002
trihexyl	0.04 ± 0.02	0.0005 ± 0.0003
trioctyl	0.04 ± 0.03	0.0004 ± 0.0002
ICP-OES	0.5 ± 1	

*Standard was unavailable at the time of study.

4.3.2 Recovery Study

Table 4-3 presents the "LOQs" in terms of µg *phosphorus* mL^{-1} for the GC×GC-FID/NPD method for splitless injection using alkyl phosphate standards calibrated in two different industrial petroleum samples. Sample B is described as a crude oil sample, while sample F is a mixture of crude oil and fracture fluid. Sample B was diluted 50× in isooctane, while sample F was diluted 100×. Calibration standards were prepared as previously described. The calibrations performed in the industrial petroleum samples were found to yield "LOQs" approximately one order of magnitude higher than those obtained in solvent. In order to determine if the calibrations performed in solvent could be used to reliably quantify the alkyl phosphates in the real industrial petroleum samples, a recovery study was completed. The recovery

study was performed by spiking the real industrial petroleum samples with a known concentration of alkyl phosphate standards as described below. The sample was then analyzed using GC×GC-FID/NPD and each alkyl phosphate standard was quantified using the previously established calibration curve in order to determine if the calibration curve established in solvent recovered the same concentration of alkyl phosphate standards that was spiked into the real industrial petroleum sample.

Table 4-3. "Limits of quantification" for splitless injection in industrial petroleum samples B (50× dilution) and F (100× dilution).

Phosphate	"LOQ" (μg *phosphorus* mL^{-1})	
	B (50× dilution)	F (100× dilution)
triethyl	0.034 ± 0.005	*
triisopropyl	0.015 ± 0.003	0.007 ± 0.001
tripropyl	0.0007 ± 0.0001	0.001 ± 0.001
dibutyl	*	*
tributyl	0.001 ± 0.001	*
tripentyl	0.0011 ± 0.0006	0.001 ± 0.001
bis(2-ethylhexyl)	0.010 ± 0.002	0.005 ± 0.002
trihexyl	0.0010 ± 0.0008	0.0010 ± 0.0004
trioctyl	0.0036 ± 0.0003	0.0036 ± 0.0003

*Denotes phosphates that were native to industrial sample
(i.e. standard addition would have been required for calibration).

Industrial petroleum samples B and F were chosen for the recovery study. Both samples were diluted in isooctane (50× and 100× respectively) and spiked with all nine alkyl phosphate standards to concentrations of ~0.2 and ~0.5 μg *phosphate* mL^{-1} each, with triphenyl phosphate added as an internal standard at a concentration of 0.5 μg mL^{-1}. The two different spiking concentrations of alkyl phosphates were used in order to test the recoveries using both the high- and low-range calibration curves. A 500 μL aliquot of

each sample was derivatized and analyzed as previously described. Samples of B and F were also diluted in isooctane and analyzed without being spiked in order to determine what, if any, alkyl phosphates were native to each sample. Sample B was found to contain dibutyl phosphate, while sample F was found to contain triethyl, dibutyl and tributyl phosphates. The concentrations of the phosphates native to each sample were taken into account when calculating the recoveries.

Table 4-4 presents the results obtained from the recovery study. Satisfactory recoveries between 79 – 137% were obtained with relative standard deviations (RSDs) of 5% or lower. The errors associated with the recoveries are likely the result of matrix effects. These effects can be observed in **Figure 4-4**, where plots of NPD response factor (discussed in **Section 4.3.3.3**) versus the number of carbons per phosphate for trialkyl phosphates with straight chain alkyl groups show slight differences for isooctane, sample B, and sample F at both high (**Figure 4-4A**) and low (**Figure 4-4B**) calibration ranges (triethyl phosphate does not have a low calibration range, see **Table 4-1**). These matrix effects are also likely responsible for the higher "LOQs" (by approximately one order of magnitude) obtained with samples B and F compared to isooctane (**Table 4-2** and **Table 4-3**). However, the matrix effects appear to be minor and overall, the satisfactory results achieved from the recovery study demonstrate the reliability of calibrations performed in solvent when used for the quantification of alkyl phosphates in real samples.

Table 4-4. Results of recovery study performed in industrial petroleum samples B (50× dilution) and F (100× dilution).

Phosphate	B (50× dilution)				F (100× dilution)			
	Average (*n* = 3)				Average (*n* = 3)			
	Recovery 1		Recovery 2		Recovery 1		Recovery 2	
	%	RSD	%	RSD	%	RSD	%	RSD
triethyl	103	3	*	*	137	3	*	*
triisopropyl	110	4	122	5	103	4	115	5
tripropyl	79	5	100	1	106	3	128	1
dibutyl	105	4	118	4	104	3	117	3
tributyl	91	4	106	1	106	4	115	1
tripentyl	96	2	117	1	96	2	99	1
bis(2-ethylhexyl)	82	2	92	2	98	5	126	4
trihexyl	116	3	124	1	108	3	114	1
trioctyl	104	3	106	2	114	2	91	2

*Amount spiked is below the limit of quantification for triethyl phosphate.
Recovery 1: spiked 0.5 μg *phosphate* mL^{-1}.
Recovery 2: spiked 0.2 μg *phosphate* mL^{-1}.
Accounted for phosphates found to be native to samples B and F (**Table 4-5**).

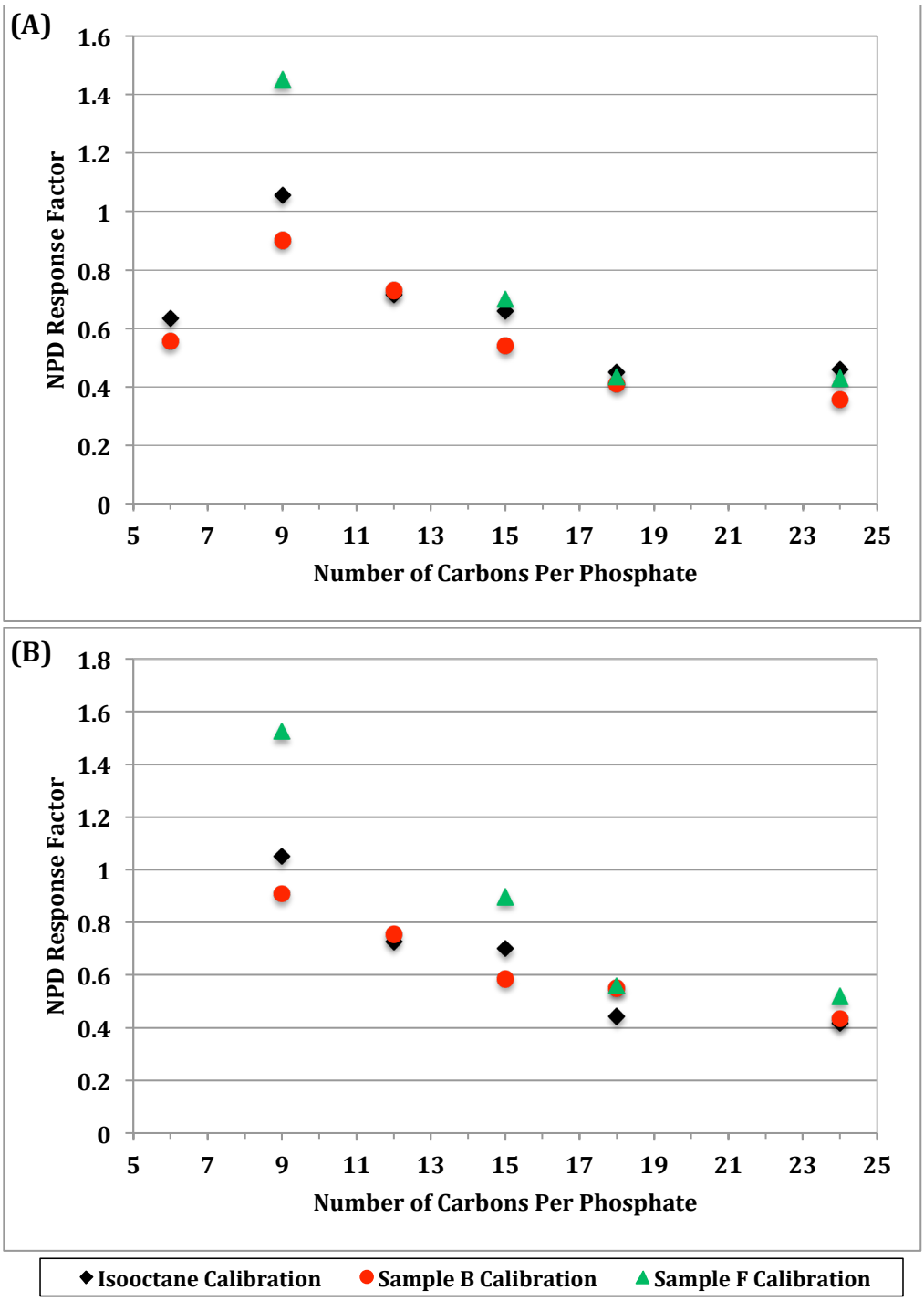

Figure 4-4. Plot of NPD response factor versus number of carbons per phosphate at (A) high and (B) low calibration ranges for trialkyl phosphates with straight chain alkyl groups calibrated in isooctane (◆), sample B (●), and sample F (▲). Triethyl phosphate does not have a low calibration range (see **Table 4-1**) and data for native phosphates (triethyl and tributyl phosphates) is not included for sample F.

4.3.3 Qualitative and Quantitative Profiling of Industrial Samples

4.3.3.1 Splitless Injection

The derivatization and GC×GC-FID/NPD method with splitless injection and concurrent backflushing was used to profile alkyl phosphate contamination in 14 different industrial petroleum samples provided by Imperial Oil. The industrial petroleum samples were each initially diluted 100× in isooctane, spiked with 0.5 μg mL^{-1} of internal standard, and derivatized as explained previously. Samples B, C, and D were found to contain phosphates at concentrations below the "LOQ" at 100× dilution and were therefore analyzed again with a dilution factor of 50×. Samples A, J, L, and N were too concentrated at 100× dilution. Various dilutions from 1,000× to 20,000× were required to bring these samples within the calibration range.

Alkyl phosphate identification was confirmed using retention times in both the first- and second-dimensions, as well as temperature-programmed retention indices in the first dimension ($^1I^T$), which were calculated using Equation (4-2):

$$^1I^T = 100\left[n + \left(N - n\right)\frac{^1t'_{r,phosphate} - {}^1t'_{r,n}}{^1t'_{r,N} - {}^1t'_{r,n}}\right] \qquad (4\text{-}2)$$

where n is the number of carbon atoms of the n-alkane eluting just before the phosphate of interest, N is number of carbon atoms of the n-alkane eluting just after the phosphate of interest, $^1t'_{r,phosphate}$ is the adjusted retention time of the phosphate of interest in the first dimension, $^1t'_{r,n}$ is the adjusted

retention time in the first dimension of the *n*-alkane eluting just before the phosphate of interest, and ${}^{1}t'_{r,N}$ is the adjusted retention time in the first dimension of the *n*-alkane eluting just after the phosphate of interest. The *n*-alkane retention times were obtained by analyzing each industrial petroleum sample using GC×GC-FID since each sample was found to contain the *n*-alkanes *n*-C_{11} to *n*-C_{27} (identification confirmed using standards and GC×GC peak patterns) as displayed in **Figure 4-5**. The adjusted retention times were calculated using the void time of the column, which was calculated using the LECO GC×GC Column Calculator. Alkyl phosphate identification was confirmed if ${}^{1}I^{T}$ was within ±15 retention index units since the internal standard, triphenyl phosphate, was found to be within ±15 retention index units in all 14 industrial petroleum samples tested. The temperature-programmed retention indices in the first dimension (Rxi-5Sil MS) for each alkyl phosphate are summarized in **Table 4-5.**

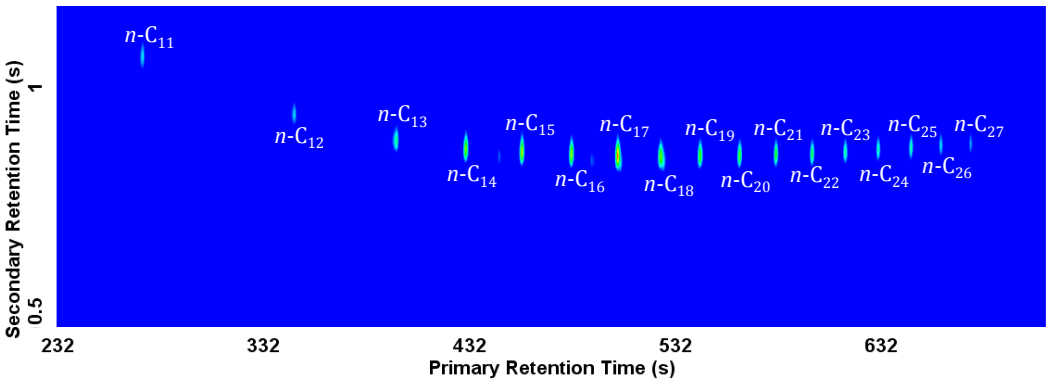

Figure 4-5. GC×GC-FID chromatogram of the *n*-alkanes, found to be native to the industrial petroleum samples, used to determine the retention indices of the alkyl phosphates in the first dimension.

Table 4-5. First dimension temperature-programmed retention indices collected on Rxi-5Sil MS.

Phosphate	n	N	${}^1t'_{r,n}$ (s)	${}^1t'_{r,N}$ (s)	${}^1t'_{r,phosphate}$ (s)	${}^1I^T$
triethyl	11	12	252.4	327.6	258.8	1109
triisopropyl	11	12	252.4	327.6	314.8	1183
tripropyl	13	14	377.2	410.8	402.8	1376
dibutyl	14	16	410.8	463.6	439.6	1509
tributyl	16	17	463.6	486.0	471.6	1636
tripentyl	19	20	526.0	545.2	527.6	1908
bis(2-ethylhexyl)	20	21	545.2	562.8	551.6	2036
trihexyl	21	22	562.8	580.4	578.8	2191
triphenyl	23	24	596.4	612.4	610.8	2390
trioctyl	24	25	612.4	628.4	618.8	2440

The final speciation results are shown in **Table 4-6**. All 14 samples were found to contain alkyl phosphate contamination of triethyl, dibutyl, tributyl, and/or tripentyl phosphates. Samples B, C, D, and E were all found to contain a total concentration of phosphorus below 1.5 μg *phosphorus* mL^{-1} demonstrating that the refined method using splitless injection is capable of quantifying and speciating individual and total alkyl phosphates at concentrations below the limit of detection of ICP-OES when the precision in this method is considered (0.5 ± 1 μg *phosphorus* mL^{-1}).

As expected, the crude oil samples were found to have the least contamination, while the samples containing a mixture of crude oil, fracture fluid and "slop" (fracture fluid waste stream) were found to have the highest contamination. **Figure 4-6** displays contour plots for samples A (refinery process stream, 10,000× dilution), B (crude, 50× dilution), F (crude/frac, 100× dilution), and L (crude/frac/slop, 20,000× dilution).

Table 4-6. Speciation and quantification of alkyl phosphates in 14 different industrial petroleum samples using SPLITLESS injection.

Sample Classification	Splitless Dilution Factor	Phosphates Identified	Concentration (µg *phosphorus* mL^{-1})		
			Per Phosphate ($\mu \pm \sigma$; $n = 3$)	Total P	RSD (%)
A: Refinery process stream	10,000×	dibutyl	30 ± 4	30	5
B: Crude	50×	dibutyl	0.54 ± 0.02	0.54	3
C: Crude	50×	dibutyl tripentyl	0.36 ± 0.02 0.47 ± 0.02	0.83	6 4
D: Crude	50×	dibutyl tripentyl	0.75 ± 0.02 0.37 ± 0.02	1.12	12 6
E: Crude	100×	dibutyl	0.32 ± 0.04	0.32	3
F: Crude/Frac	100×	triethyl dibutyl tributyl	0.147 ± 0.003 2.25 ± 0.05 2.58 ± 0.03	4.98	2 1 0.3
G: Crude/Frac	100×	dibutyl tributyl	1.97 ± 0.05 0.72 ± 0.02	2.69	0.2 2
H: Crude/Frac	100×	triethyl dibutyl tributyl	9.5 ± 0.5 1.60 ± 0.04 1.33 ± 0.02	12.43	1 1 0.7
I: Crude/Frac	100×	dibutyl tributyl	2.12 ± 0.05 0.81 ± 0.02	2.93	2 3
J: Crude/Frac/Slop	1,000× 100×	dibutyl tributyl	28.2 ± 0.5 Below LOQ	28.2	0.8 --------
K: Crude/Frac	100×	dibutyl tributyl	6.00 ± 0.05 3.49 ± 0.03	9.49	0.2 0.4
L: Crude/Frac/Slop	20,000×	dibutyl	908 ± 9	908	2
M: Crude/Frac	100×	dibutyl tributyl	2.82 ± 0.05 2.77 ± 0.03	5.59	1 0.8
N: Crude/Frac/Slop	10,000×	dibutyl	722 ± 5	722	0.3

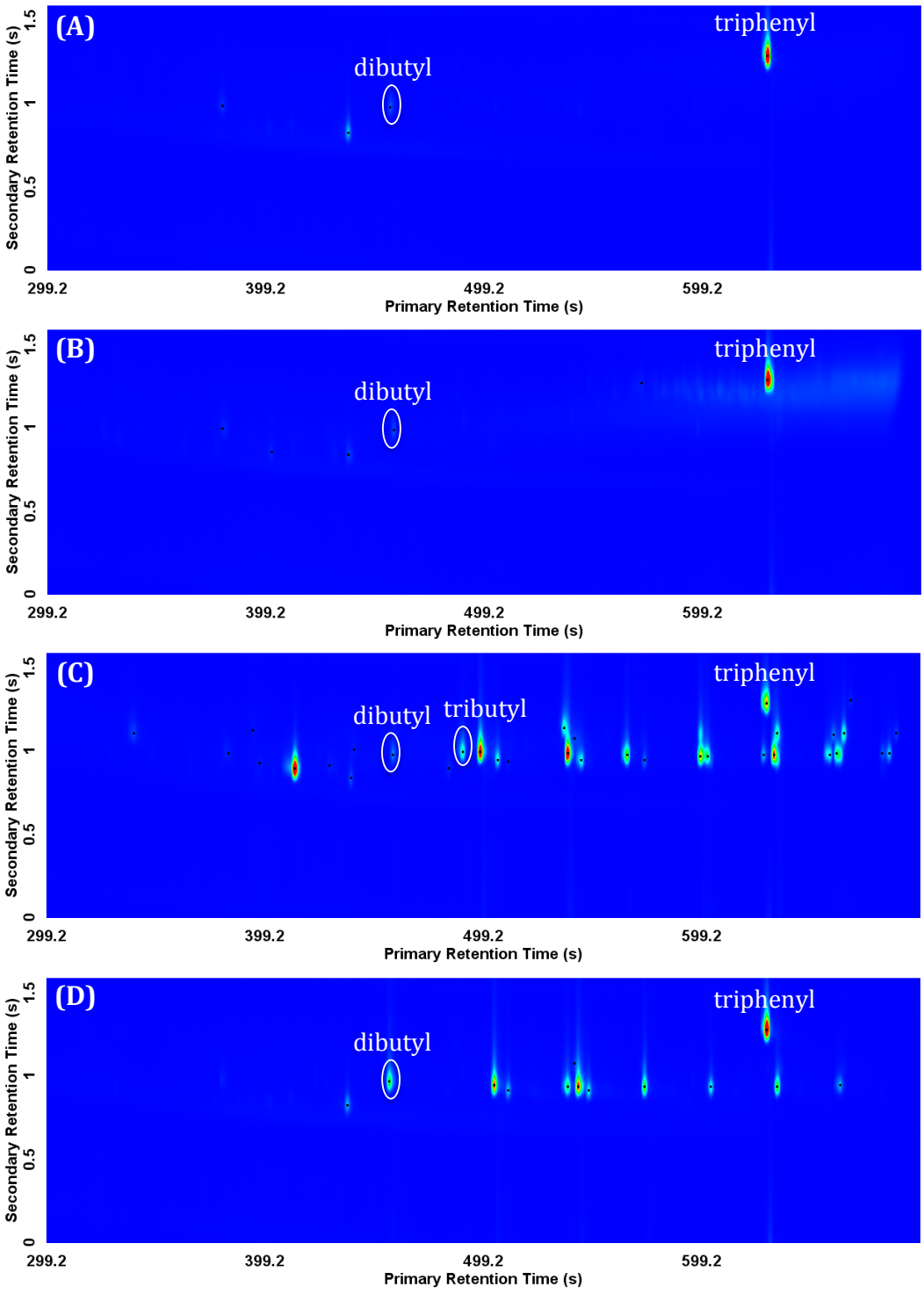

Figure 4-6. GC×GC-NPD chromatograms of industrial petroleum samples: (A) A (refinery process stream, 10,000× dilution), (B) B (crude, 50× dilution), (C) F (crude/frac, 100× dilution), and (D) L (crude/frac/slop, 20,000× dilution).

To demonstrate the stability of the retention times (provided by the addition of concurrent backflushing) with the splitless method, the alkyl phosphate standard mixture was injected and the retention times for the phosphates were recorded. Subsequently, 150 injections comprising 50 injections each of the crude/frac/slop samples (J, L, and N) each diluted 10,000× in isooctane were performed. Finally, the standard mixture was again injected and the retention times for the phosphates were recorded. The difference in retention times for all alkyl phosphates other than triethyl phosphate (TEP) and triisopropyl phosphate (TiPP) was ± 1 modulation period (P_M). For TEP and TiPP, which are very incompatible with the primary column chemistry and thus exhibit poor peak shapes and retention time reproducibility, the retention time shifts were ±4 and ±3 P_M, respectively.

4.3.3.2 Split Injection

In order to determine if splitless injection is necessary for the speciation of alkyl phosphates in real samples, the same 14 industrial petroleum samples were analyzed using the previously described split injection method from **CHAPTER 3** [18], with the addition of backflushing and 10× dilution in isooctane. The dilution in isooctane was used to help minimize viscosity effects when injecting the samples. **Table 4-7** shows the speciation results obtained using split injection.

Table 4-7. Speciation and quantification of alkyl phosphates in 14 different industrial petroleum samples using SPLIT injection.

Sample Classification	Split Dilution Factor	Phosphates Identified	Concentration (μg *phosphorus* mL^{-1})		
			Per Phosphate ($\mu \pm \sigma$; $n = 3$)	Total P	RSD (%)
A: Refinery process stream	10×	---------	---------	---------	--------
B: Crude	10×	---------	---------	---------	--------
C: Crude	10×	---------	---------	---------	--------
D: Crude	10×	---------	---------	---------	--------
E: Crude	10×	---------	---------	---------	--------
F: Crude/Frac	10×	tributyl	2.2 ± 0.7	2.2	4
G: Crude/Frac	10×	tributyl	1.0 ± 0.7	1.1	1
H: Crude/Frac	10×	tributyl	1.2 ± 0.7	1.2	5
I: Crude/Frac	10×	dibutyl	10 ± 2	10	3
J: Crude/Frac/Slop	10×	dibutyl	16 ± 2	16	9
K: Crude/Frac	10×	tributyl	2.9 ± 0.7	2.9	1
L: Crude/Frac/Slop	10×	dibutyl	1100 ± 200	1100	2
M: Crude/Frac	10×	tributyl	2.1 ± 0.7	2.1	1
N: Crude/Frac/Slop	10×	dibutyl	83 ± 2	83	9

Samples B through E, which contained only trace amounts of dibutyl phosphate contamination, were unable to be speciated using the split injection methodology. Samples C and D were found to contain trace contamination of tripentyl phosphate when analyzed using splitless injection; however, the split injection method was incapable of detecting or quantifying tripentyl phosphate in these samples. Triethyl phosphate, which was found in samples F and H using splitless injection, was also unable to be detected or quantified using split injection. Samples F, G, H, K, and M, which were found

to contain tributyl phosphate contamination using splitless injection, were also found to contain tributyl phosphate contamination using split injection. The contamination concentrations were found to agree within error between the two injection methods.

Samples I, J, L, and N were found to contain dibutyl phosphate contamination using both split and splitless injection; however, the two methods do not agree quantitatively. This is likely due to the fact that the samples containing high concentrations of dibutyl phosphate experienced a substantial dilution in the splitless method. When the samples were only diluted 10× for the split injection, there was likely such a high concentration of dialkyl phosphates (and other derivatizable groups) that the derivatization reaction could not proceed to completion. It is not likely the result of a viscosity or kinetic evaporative effect in the injector because of the fact that the results for tributyl phosphate agree reasonably well between the two injection methods. Finally, the splitless injection method also identified trace quantities of dibutyl phosphate in samples F, G, H, K, and M and trace quantities of tributyl phosphate in samples I and J, which were not detected using the split injection method.

4.3.3.3 Alkyl Phosphate Response Factors

As was observed in the previous chapter (**Figure 3-7**, **CHAPTER 3** [18]), several other probable phosphorus (possibly nitrogen) compounds were also detected in the GC×GC-NPD chromatograms of the industrial petroleum samples when analyzed using splitless injection (**Figure 4-6**);

however, these compounds remain unidentified due to a lack of available alkyl phosphate standards. Unfortunately, the nine alkyl phosphate standards used herein represent all of the alkyl phosphate standards that are currently commercially available. This lack of available standards makes the identification of suspect phosphates difficult. Furthermore, it has been shown that time-of-flight mass spectrometry (TOFMS) with electron impact ionization is minimally informative for the identification of alkyl phosphates [17]. Therefore, the issue of unknown phosphate identification will likely require custom synthesis of standards in conjunction with a model of alkyl phosphate retention that is in the early stages of development [198,199].

As previously stated, GC×GC separations can provide ordered chromatograms where structurally-related compounds elute with distinct patterns on the retention plane aiding in sample characterization (i.e. speciation) [11,12,13], which is further aided in this case by the use of a selective detector. However, even if the unidentified peaks in the industrial petroleum samples (**Figure 4-6**) could be classified as suspect phosphates (based on GC×GC elution patterns) the quantification of these analytes is challenging as a result of the nitrogen-phosphorus detector producing a different response to each analyte (i.e. each alkyl phosphate requires a separate calibration curve). Nevertheless, if the response factor for the suspect phosphate was known the concentration could then be determined.

Unfortunately, the experimental determination of gas chromatographic response factors (i.e. a measure of the chromatographic

response of a target analyte compared to an internal standard) is routine but requires the availability of standards for each compound of interest, as well as the preparation of standard solutions at specific concentrations and their analysis by gas chromatography. In the event of a complex mixture containing numerous compounds the experimental determination of individual response factors can be time-consuming and in some cases impossible due to the vast number of compounds unavailable as standards, as is the case with the alkyl phosphates. Therefore, a theoretical method for predicting or estimating gas chromatographic response factors would be quite valuable for quantifying suspect alkyl phosphates. Consequently, Katrizky *et al*. developed a method for the prediction of FID response factors using an applied multivariate statistical partial least-square method [203,204]. Jalali-Heravi and Fatemi later developed an artificial neural network (ANN) for modeling FID response factors [205].

Herein the calibration data for all nine alkyl phosphate standards has already been collected; therefore we can determine the NPD response factor, *F*, for each standard analyte using Equation (4-3):

$$\frac{A_X}{[X]} = F\left(\frac{A_S}{[S]}\right) \tag{4-3}$$

where A_X is the peak area of the analyte signal, A_S is the peak area of the internal standard signal, [*X*] is the concentration of the analyte, and [*S*] is the concentration of the internal standard. Equation (4-3) can also be rearranged to equal the slope of a calibration curve (normalized area versus analyte concentration) multiplied by the internal standard concentration. A plot of

each alkyl phosphate NPD response factor versus the number of carbons per phosphate can then be constructed to see if a trend exists between alkyl phosphate NPD response and the number of carbons per phosphate. Such a trend would allow for the prediction/estimation of approximate values for the NPD response factors for those alkyl phosphates that do not have commercially available standards (e.g. triheptyl phosphate or mixed phosphates where the alkyl chains are not all the same length).

Only two dialkyl phosphate standards (dibutyl phosphate and bis(2-ethylhexyl)phosphate) exist commercially, therefore no trend could be obtained for dialkyl phosphate response factors. In addition, only those trialkyl phosphates with straight chain alkyl groups were included (i.e. triisopropyl phosphate was left out).

Figure 4-7A displays a plot of NPD response factor versus the number of carbons per phosphate for trialkyl phosphates with straight chain alkyl groups for splitless injection in isooctane at high and low calibration ranges (triethyl phosphate does not have a low calibration range, see **Table 4-1**). **Figure 4-7B** shows the same plot for the split injection method in hexane (data from **CHAPTER 3** [18]). Tripentyl phosphate was unavailable at the time of this study and is therefore missing from the plot. Unfortunately, a clear trend to allow for the prediction of NPD response factors is not observed for either the high or low calibration ranges for the splitless injection method (**Figure 4-7A**). Alternatively, the split injection method (**Figure 4-7B**) does appear to have an overall trend of decreasing alkyl

phosphate NPD response factor with increasing number of carbons per phosphate for both high and low calibration ranges. Predictions of approximate NPD response factors for suspect phosphates could potentially be attained from this relationship; however, the split injection method has been proven to be inadequate for speciating trace alkyl phosphate contamination in industrial petroleum samples. Furthermore, as a result of the trialkyl phosphate standards that do not exist commercially, some of the desirable predictions (e.g. trinonyl and tridecyl phosphate) would involve extrapolation, which is ill advised. Therefore, the custom synthesis of standards, in conjunction with a model of alkyl phosphate retention [198,199], still remains necessary for the identification and quantification of suspect phosphates as previously stated.

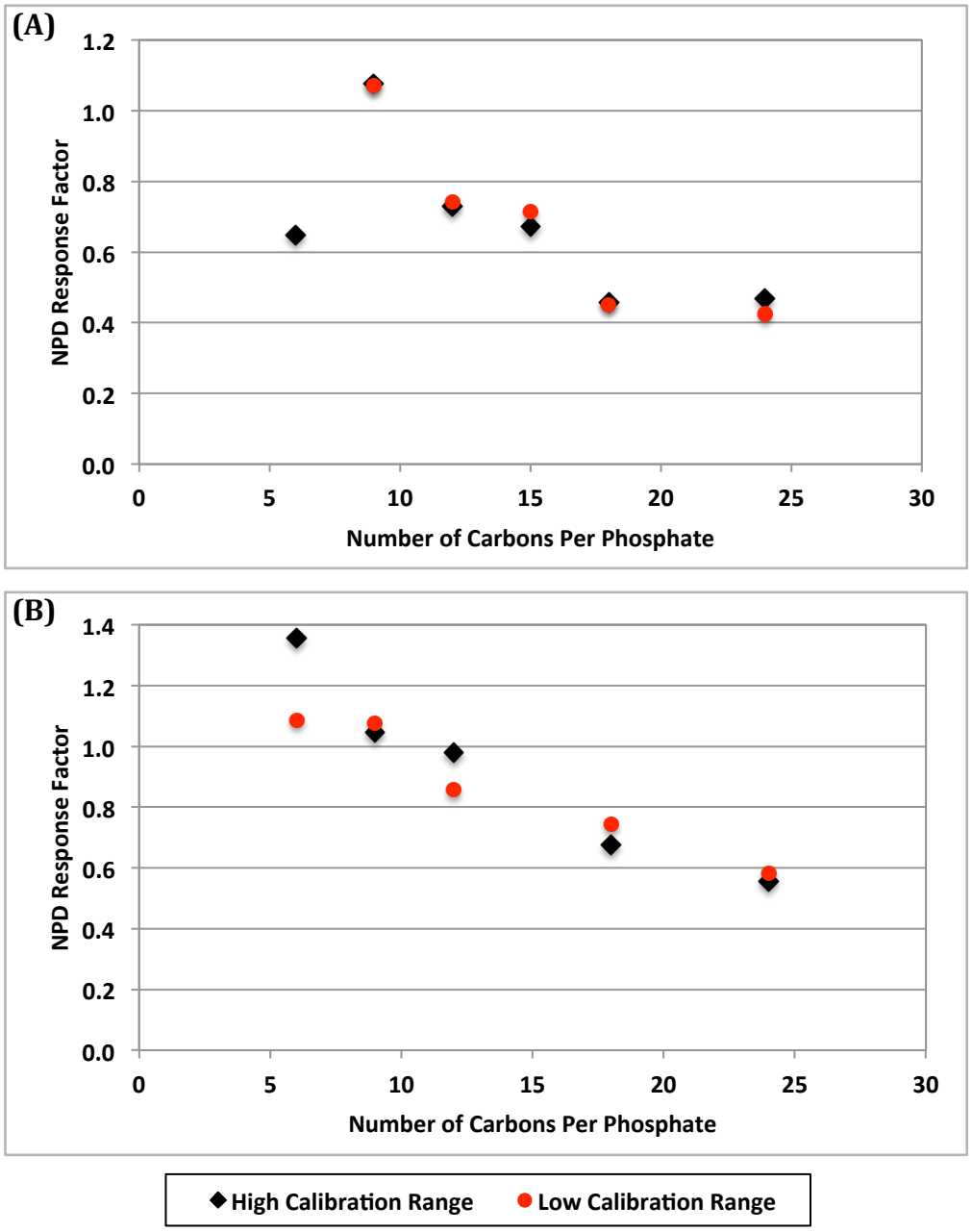

Figure 4-7: Plot of NPD response factor versus number of carbons per phosphate at high (◆) and low (●) calibration ranges for trialkyl phosphates with straight chain alkyl groups for: (A) splitless injection in isooctane (triethyl phosphate does not have a low calibration range, see **Table 4-1**) and (B) split injection in hexane (tripentyl phosphate was unavailable at the time of study, data from **CHAPTER 3** [18]).

4.4 Conclusions

In this chapter, the GC×GC-FID/NPD method with post-column Dean switching from **CHAPTER 3** was refined to incorporate splitless injection and concurrent backflushing. Overall, this approach provided lower "limits of quantification" and the speciation of alkyl phosphates in industrial petroleum samples at concentrations that are not capable by ICP-OES methodology or GC×GC-FID/NPD with split injection. Furthermore, the addition of concurrent backflushing allowed a reduction in instrument downtime for system maintenance by eliminating heavier, less volatile matrix components from the system.

A recovery study performed in two different industrial petroleum samples provided results demonstrating the reliability of calibrations performed in solvent for use in quantifying alkyl phosphate contamination in real samples. When split injection was compared with splitless injection for the speciation of 14 real industrial petroleum samples, split injection was unable to fully speciate samples containing only trace amounts of alkyl phosphate contamination, exposing the need for splitless injection. Additionally, the splitless method likely provides more accurate results for high concentrations of dialkyl phosphates than the split injection method due to the fact that the samples can be substantially diluted, resulting in a more complete derivatization reaction. Overall, the splitless injection method allowed for the identification and quantification of individual alkyl phosphates in real industrial petroleum samples at concentrations below the

limit of detection of the currently-accepted ICP-OES methodology. With the establishment of this method the next step is to use this method to profile crude oil entering a refinery, as well as petroleum product streams exiting the refinery. Such information is important in order to determine which alkyl phosphate species are causing distillation tower fouling in the hopes of one day developing a mitigation strategy.

CHAPTER FIVE: Profiling Alkyl Phosphate Contamination in a Western Canadian Refinery

5.1 Introduction

As previously described, alkyl phosphates have a variety of uses in the petroleum industry. From additives used in well fracture processes to corrosion inhibitors, there are many routes by which traces of these phosphorus-containing compounds can enter into petroleum processing facilities. The presence of alkyl phosphates in crude oils causes numerous problems including the fouling of refinery equipment, the poisoning of catalysts, and impacts for downstream processes/consumers if the phosphates enter petroleum product streams [1,2]. Overall, this contamination has resulted in decreased and unpredictable lifespans of refinery equipment, in addition to more unplanned and recurrent maintenance shutdowns. These issues have occurred at a number of facilities across Canada since 1995, with impacts measured in the tens of millions of dollars.

In order to mitigate these issues, one must study the chemistry of alkyl phosphates in a refinery environment. This is a challenge because the family of alkyl phosphates that could be present comprises dozens of different molecular structures. Additionally the molecules could undergo chemical reactions in the refinery (e.g. within the distillation tower), making them even more difficult to identify. Finally, the phosphates are present (in

trace quantities) in crude oil, which is among the most chemically complex sample types one will encounter.

The method developed in **CHAPTER 4** [19] of this thesis represents the only analytical method/technology that is capable of: 1) separating these phosphates from each other and from the crude oil matrix; and 2) speciating and quantifying the phosphates reproducibly in petroleum samples at trace levels. Using this method/technology, this chapter presents some preliminary results from the first-ever detailed study of alkyl phosphate contamination in a refining environment. As nobody has ever been able to track the species of phosphates in a refinery, this phase of the project is very exciting and largely discovery-based. By profiling the phosphates that are entering the refinery in crude oil, as well as the phosphates that are found in various petroleum product streams, these findings will hopefully begin to shed some light on possible routes to mitigating the issue of alkyl phosphate contamination and solving this multimillion-dollar problem.

5.2 Experimental

5.2.1 Materials and Reagents

Stock solutions were stored in glass vials and refrigerated at ~7 °C. Calibration and refinery sample solutions were prepared in 1.8 mL glass GC vials with polytetrafluoroethylene (PTFE)-lined silicone septa (Chromatographic Specialties, Brockville, ON, Canada) for analysis by

comprehensive two-dimensional gas chromatography with both flame ionization and nitrogen-phosphorus detection (GC×GC-FID/NPD).

All reagents were used as received unless otherwise stated. Derivatization was performed according to a previously established protocol [16] using a mixture of *N,O*-bis(trimethylsilyl)trifluoroacetamide (BSTFA) (Sigma-Aldrich, Oakville, ON, Canada), pyridine (Caledon, Georgetown, ON, Canada), and trimethylchlorosilane (TMCS) (Sigma-Aldrich) in a 10:5:2 ratio by volume. A total of 50 µL of the derivatization reagent mixture was added to 500 µL of sample and left to derivatize at 30 °C for 30 min before analysis. Vials were maintained at temperature using the GC autosampler tray, which was kept at 30 °C by circulating heated water through the tray.

GC×GC-NPD calibration was performed as described in **CHAPTER 4** [19] with splitless injection using the following standards: triethyl, triisopropyl, tripropyl, dibutyl, and tributyl phosphate (Sigma-Aldrich), tripentyl phosphate (Tokyo Chemical Industry Co., Ltd., Toshima, Kita-Ku, Tokyo, Japan), and bis(2-ethylhexyl), trihexyl, and trioctyl phosphate (Alfa Aesar, Ward Hill, MA, United States). Isooctane (Sigma-Aldrich) was used as a solvent. Triphenyl phosphate (Sigma-Aldrich) was dissolved and diluted in reagent-grade acetone (Caledon) to give a 1,020 µg mL^{-1} stock solution that was used as an internal standard. A diesel range organics mix (Certified Reference Material, Restek, Bellefonte, PA, United States) containing even numbered *n*-alkanes from *n*-C_{10} to *n*-C_{28} (at ~2,000 µg mL^{-1} each in

methylene chloride) was diluted in isooctane to give a 50 μg mL^{-1} stock solution.

Samples from two atmospheric distillation units at a Western Canadian Refinery were collected by company personnel and mailed to the University of Alberta for analysis. Samples were collected from the two separate distillation units (with different feed slates) every three days (April 30, May 3 and May 6, 2014) until a total of six sample sets were collected (i.e. three sample sets per distillation unit). Each set of samples included both raw and desalted crude oil, as well as three different distillate product cuts (referred to as distillate 1, distillate 2, and distillate 3). The refinery samples were diluted 10 to 100× in isooctane and derivatized as previously described prior to injection. The diesel range organics mix stock solution was added to distillate samples 1 and 2 at a concentration of 0.5 μg mL^{-1} for the purpose of calculating temperature-programmed retention indices in the first dimension. The raw crude oil, desalted crude oil, and distillate 3 samples were all found to contain the *n*-alkanes *n*-C_{11} to *n*-C_{27} and therefore it was not necessary to add the diesel range organics mix to these samples.

5.2.2 Instrumentation and Experimental Conditions

Analyses were conducted using the same instrumental setup and column configuration as previously described in **CHAPTER 4**; **Section 4.2.2.1** [19]. A classification scheme, prepared with LECO's ChromaTOF software (LECO Instruments, St. Joseph, MI, United States) and

the alkyl phosphate standards, was used for initial speciation of the refinery samples. Alkyl phosphate identification was confirmed using retention times in both the first- and second-dimensions, as well as temperature-programmed retention indices in the first dimension ($^1I^T$).

5.3 Results and Discussion

Herein, the preliminary results of a study profiling alkyl phosphate contamination in petroleum streams at various points during the refining process are presented. Sampling was performed on raw crude oil, desalted crude oil, and three distinct distillate product cuts (referred to as distillate 1, 2, and 3) from two separate atmospheric distillation units (referred to as unit A and unit B) of a Western Canadian Refinery that has suffered from phosphorus issues in the past. The sampling program was initially organized to collect samples from the two distillation units (with different feed slates) every three days (resulting in a total of six sets of five samples or 30 total samples) for the collection of phosphate profiles passing through the refinery. **CHAPTER 6**; **Section 6.2.2** outlines the continuation of this sample collection and the analyses that will take place as a part of the future work of this long-term profiling study.

The analytical methodology that was used for this study is based on the published method developed in **CHAPTER 4** [19]. Briefly, the method relies on the use of comprehensive two-dimensional gas chromatography (GC×GC) with selective detection (provided by a nitrogen-phosphorus

detector (NPD)). This method has been used to profile alkyl phosphate contamination in industrial petroleum samples at trace levels (~0.0005 ± 0.0003 µg *phosphorus* mL^{-1}) as described in **CHAPTER 4** [19]. These impressive results are realized because of the advantages provided by GC×GC in combination with the selective detection of the NPD. One of the earliest industries to enthusiastically exploit GC×GC for research and development (R&D) activities is the oil industry, particularly the laboratories of Exxon Mobil [206], Shell [207], and the *Institut français du pétrole* near Paris, France [208,209]. Here, GC×GC is employed for the first-ever detailed study of alkyl phosphate contamination in a refining environment, where both crude oil streams entering the refinery as well as petroleum product streams exiting the refinery, are inspected.

5.3.1 Qualitative and Quantitative Profiling of Refinery Samples

The GC×GC-FID/NPD method, with splitless injection and concurrent backflushing, described in **CHAPTER 4** [19], was used to profile alkyl phosphate contamination in 30 different refinery samples provided by a Western Canadian Refinery. The raw and desalted crude samples were diluted 50× in isooctane while distillate samples 1, 2, and 3 were diluted 10×, 50×, and 100×, respectively. Dilution factors were chosen based on the sample's overall analyte concentration, chromatographic appearance, and previous experience gained from the industrial petroleum samples profiled

in **CHAPTER 4**. Each sample was spiked with 0.5 μg mL^{-1} of internal standard (i.e. triphenyl phosphate) and derivatized as previously explained.

Overall, the 18 refinery distillate samples were discovered to be quite clean in terms of alkyl phosphate contamination. The only known/standard alkyl phosphate that was identified in the distillate samples was dibutyl phosphate, which was determined to be due to the use of a contaminated derivatization mixture. As a result, dibutyl phosphate was also identified in the 12 refinery raw and desalted crude oil samples. **Figure 5-1A** displays a GC×GC-NPD chromatogram of the dibutyl phosphate peak found in a sample containing the derivatization mixture in isooctane, while **Figures 5-2B** and **C** show the dibutyl phosphate peak identified in the derivatized distillate 1 samples collected on April 30, 2014 from unit A and unit B, respectively. Similar results were uncovered for all of the refinery samples, with the dibutyl phosphate peak appearing with a constant peak area corresponding to a concentration well below dibutyl phosphate's "limit of quantification".

When the dibutyl phosphate contamination was first discovered in the derivatization mix, a new source of pyridine and TMCS was obtained from a laboratory at the University of Alberta that does not work with alkyl phosphates. Unfortunately, a new source of BSTFA could not be obtained on short notice. The new supplies of pyridine and TMCS, however, were employed for refinery sample derivatization throughout this chapter, as well as for the collection of the derivatization mix chromatogram shown in **Figure 5-1A**. Therefore, the source of the dibutyl phosphate contamination was

traced back to the bottle of BSTFA. A new bottle of this reagent will be essential for future studies. In addition, the previous supplies of pyridine and TMCS will be tested for dibutyl phosphate contamination before being put back to use for derivatization.

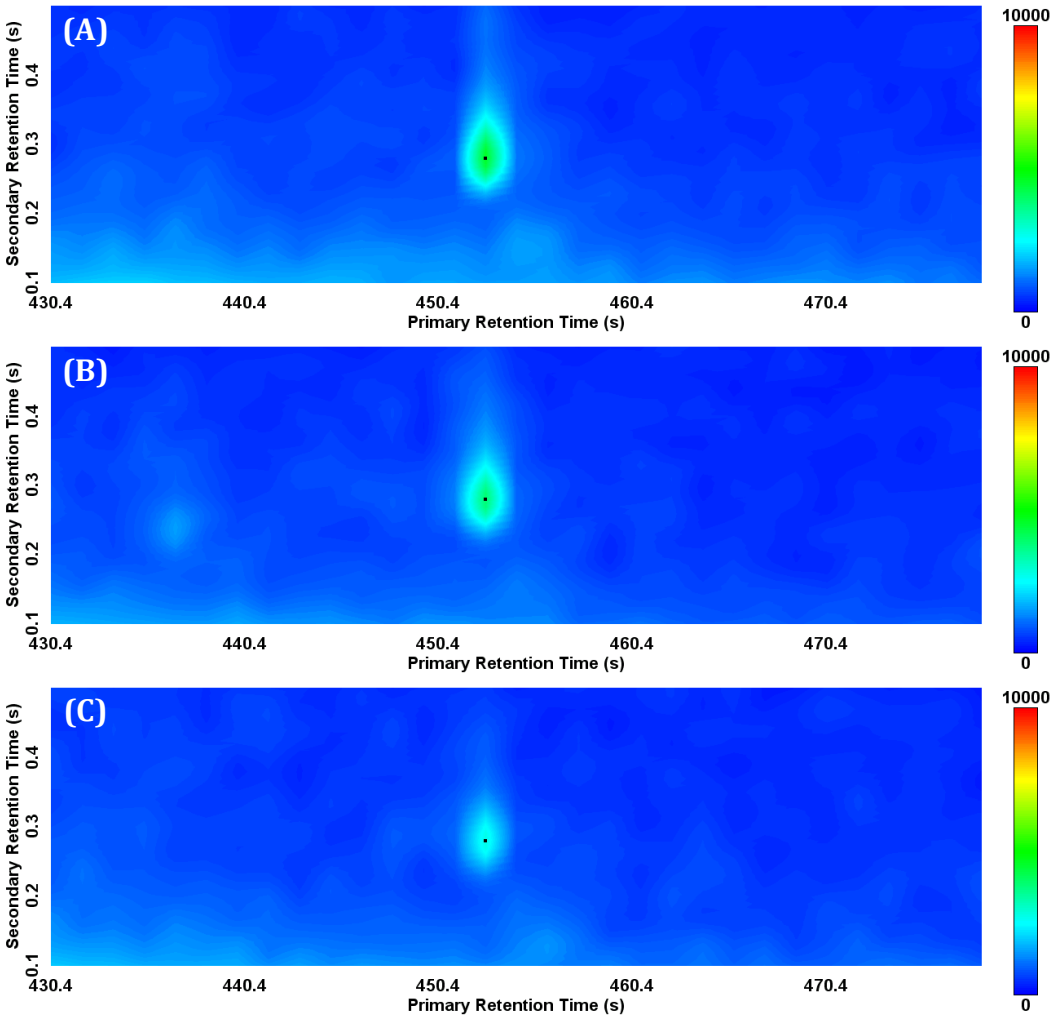

Figure 5-1. GC×GC-NPD chromatograms of the dibutyl phosphate peak identified in: (A) isooctane containing the derivatization mixture, (B) derivatized distillate 1 sample (diluted 10× in isooctane) collected from unit A on April 30, 2014, and (C) derivatized distillate 1 sample (diluted 10× in isooctane) collected from unit B on April 30, 2014. Secondary dimension (^{2}D) offset of 0.8 s applied to plotted chromatograms.

In addition to dibutyl phosphate, the classification scheme (prepared using LECO's ChromaTOF software and the alkyl phosphate standards, **Figure 5-2**) also identified possible tripentyl and trioctyl phosphate peaks in all 12 of the raw and desalted crude oil samples. The identification of these peaks was confirmed using retention times in both the first- and second-dimensions, as well as temperature-programmed retention indices in the first dimension ($^1I^T$), which were calculated using Equation (5-1):

$$^1I^T = 100\left[n + \left(N - n\right)\frac{^1t'_{r,phosphate} - {}^1t'_{r,n}}{^1t'_{r,N} - {}^1t'_{r,n}}\right] \qquad (5\text{-}1)$$

where n is the number of carbon atoms of the n-alkane eluting just before the phosphate of interest, N is number of carbon atoms of the n-alkane eluting just after the phosphate of interest, $^1t'_{r,phosphate}$ is the adjusted retention time of the phosphate of interest in the first dimension, $^1t'_{r,n}$ is the adjusted retention time in the first dimension of the n-alkane eluting just before the phosphate of interest, and $^1t'_{r,N}$ is the adjusted retention time in the first dimension of the n-alkane eluting just after the phosphate of interest. The n-alkane retention times were obtained by analyzing each refinery sample using GC×GC-FID. The raw and desalted crude oil samples were all found to contain the n-alkanes n-C_{11} to n-C_{27} (identification confirmed using standards and GC×GC peak patterns). The adjusted retention times were calculated using the void time of the column, which was calculated using the LECO GC×GC Column Calculator. Alkyl phosphate identification is considered to be confirmed if the $^1I^T$ is within ±15 retention index units of the standard value,

since the internal standard, triphenyl phosphate, was always found to be within ±15 retention index units in the industrial petroleum samples tested in **CHAPTER 4** [19]. The peak suspected to be tripentyl phosphate was found to have a first dimension temperature-programmed retention index of 1900, while the peak suspected to be trioctyl phosphate produced a first dimension temperature-programmed retention index of 2430. When compared to the alkyl phosphate standard ${}^{1}I^{T}$ values (summarized in **Table 4-5** of **CHAPTER 4** [19]) both the suspected tripentyl phosphate and the suspected trioctyl phosphate peaks were discovered to be within ±15 retention index units, confirming their identities. The identity of the dibutyl phosphate peak was also confirmed with a first dimension temperature-programmed retention index of 1503.

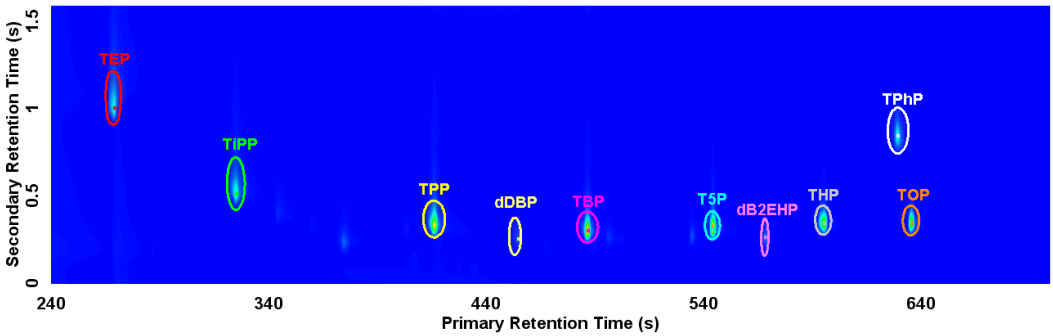

Figure 5-2. Classification scheme, prepared with LECO's ChromaTOF software and the phosphate standards, used for initial speciation of the refinery samples (TEP = triethyl; TiPP = triisopropyl; TPP = tripropyl; dDBP = derivatized dibutyl; TBP = tributyl; T5P = tripentyl; dB2EHP = derivatized bis(2-ethylhexyl); THP = trihexyl; TPhP = triphenyl; TOP = trioctyl). ^{2}D offset of 0.8 s applied to plotted chromatogram.

With each of the raw and desalted crude oil samples diluted 50× in isooctane, the overall concentration of tripentyl and trioctyl phosphate was determined to be near or below the "limit of quantification" for each of these alkyl phosphates (which corresponds to ~0.005 µg *phosphate* mL^{-1} or ~0.0005 µg *phosphorus* mL^{-1}). These samples will need to be re-analyzed at a lower dilution factor in order to bring the tripentyl and trioctyl phosphate peaks within their respective calibration ranges for quantification. This task will be performed as a part of the future work of this study.

As was observed in the previous two chapters (see **Figure 3-7** in **CHAPTER 3** [18] and **Figure 4-6** in **CHAPTER 4** [19]), several other probable phosphorus (possibly nitrogen) compounds were also detected in the GC×GC-NPD chromatograms of the refinery samples profiled herein. These peaks remain unidentified due to a lack of available alkyl phosphate standards, however potential strategies to identify these unknown peaks are outlined in **CHAPTER 6**; **Section 6.2.1**. As an example, **Figure 5-3** displays chromatograms for raw crude oil samples collected from unit A on April 30, May 3, and May 6, 2014 where a number of unidentified peaks are present. In addition, **APPENDIX A** compiles GC×GC-NPD chromatograms for all 30 refinery samples profiled, emphasizing the number of unidentified peaks/compounds in these samples. It is important to note however, that these unidentified compounds are all present in very trace concentrations. One exception to this, is the compound appearing inside the oval in **Figure 5-3C** at a first dimension retention time of 318 s and a second dimension

retention time of 0.25 s. What is even more interesting about this compound is that its concentration is greatly reduced in the desalted crude oil sample collected from the same unit (A) on the same day (May 6, 2013), as illustrated in **Figure 5-4**.

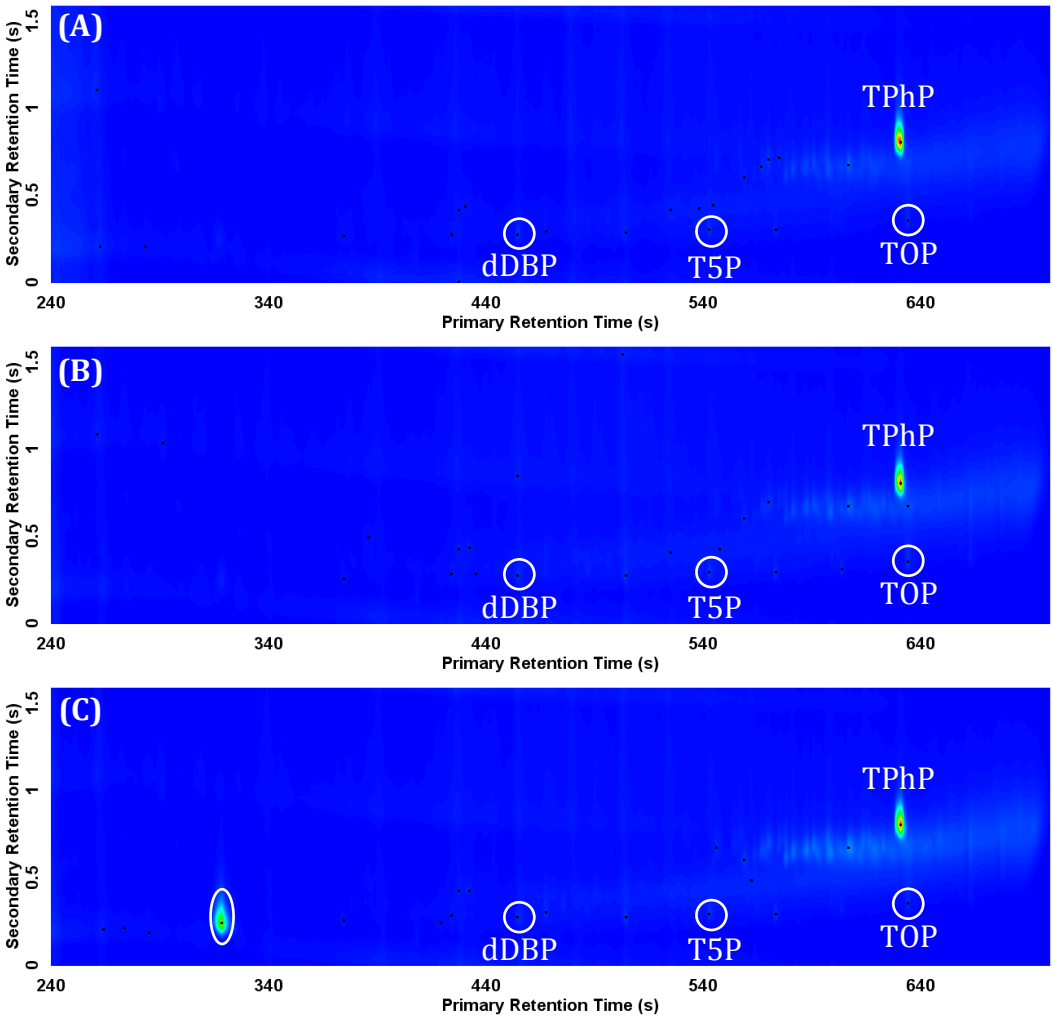

Figure 5-3. GC×GC-NPD chromatograms of raw crude oil samples (diluted 50× in isooctane) collected from unit A on: (A) April 30, (B) May 3, and (C) May 6, 2014 (dDBP = derivatized dibutyl phosphate; T5P = tripentyl phosphate; TOP = trioctyl phosphate). The oval in (C) identifies the most concentrated compound found in all 30 of the refinery samples. Triphenyl phosphate (TPhP) added as an internal standard at 0.5 μg mL^{-1}. ^{2}D offset of 0.8 s applied to plotted chromatograms.

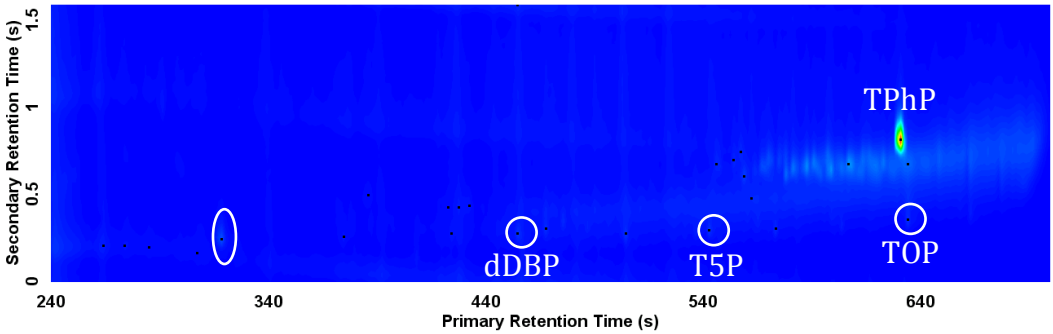

Figure 5-4. GC×GC-NPD chromatogram of a desalted crude oil sample (diluted 50× in isooctane) collected from unit A on May 6, 2014 (dDBP = derivatized dibutyl phosphate; T5P = tripentyl phosphate; TOP = trioctyl phosphate). The oval identifies a compound showing a greatly reduced concentration when compared to the same compound found in the raw crude oil sample collected from the same distillation unit on the same day (see **Figure 5-2C**). Triphenyl phosphate (TPhP) added as an internal standard at 0.5 μg mL^{-1}. ^{2}D offset of 0.8 s applied to plotted chromatogram.

5.4 Conclusions

A profiling study, such as that begun herein, has never been performed as the technology is only just now becoming available. Overall, this chapter previews some very preliminary results of this refinery profiling study. A more thorough description of the remaining research for this study is outlined in the subsequent chapter (see **CHAPTER 6**; **Section 6.2.2**). The final results of this profiling study will hopefully provide the chemical information needed to contemplate future mitigation strategies for handling the "phosphate problem". This will be important to refineries across Canada that struggle with issues of equipment fouling. A mitigation strategy would be, quite literally, a multimillion-dollar idea for the Canadian petroleum industry.

CHAPTER SIX: Conclusions and Future Work

6.1 Conclusions

As discussed throughout this thesis, alkyl phosphates are employed as additives during crude oil extraction and production processes in the Western Canadian Sedimentary Basin (WCSB). Unfortunately, residual phosphates can contaminate the crude oil once the well goes into production. These compounds then wreak havoc within refineries causing problems such as premature fouling of distillation towers and poisoning of catalysts [1,2]. Furthermore, the phosphates can also enter petroleum product streams, impacting downstream processes or consumers. Overall, this contamination has resulted in decreased and unpredictable lifespans of refinery equipment, in addition to more unplanned and recurrent maintenance shutdowns, costing refineries tens of millions of dollars.

In response, the Canadian Crude Quality Technical Association (CCQTA) and the Canadian Association of Petroleum Producers (CAPP) set a limit of 0.5 μg mL^{-1} of total volatile phosphorus within distillate fractions [2,4]. This limit is monitored using an inductively coupled plasma – optical emission spectroscopy (ICP-OES) based method developed by industry [5,6]. Unfortunately, this method is plagued with poor precision and a high limit of detection (0.5 ± 1 μg *phosphorus* mL^{-1}). More importantly, this method cannot provide speciation information, which is critical for developing an understanding of the challenge of alkyl phosphates at a molecular level.

Consequently, the preliminary objective of this research was to develop an innovative method capable of providing lower limits of detection and quantification, improved precision and reproducibility, as well as the speciation and thus quantification (i.e. profiling) of individual alkyl phosphates in petroleum samples. The Harynuk Group first developed a method capable of profiling alkyl phosphates using comprehensive two-dimensional gas chromatography – time-of-flight mass spectrometry (GC×GC-TOFMS) [17]. However, the use of a phosphate-selective detector, such as the nitrogen-phosphorus detector (NPD), would mark an improvement over TOFMS instrumentation in terms of cost and ruggedness (due to a larger dynamic range and the need for less frequent calibration), resulting in a detection system suitable for widespread deployment in refining environments. As a result, the use of GC×GC with nitrogen-phosphorus detection for the speciation of alkyl phosphates in petroleum samples was investigated herein.

Unfortunately, only trialkyl phosphates are volatile enough to be analyzed by gas chromatography (GC). In order to monitor levels of mono- and di-alkyl phosphates using GC these samples must first be derivatized. A trimethylsilylation derivatization reaction was previously optimized in the Harynuk Group in terms of reagent ratios such that a 50 µL solution of a derivatization mixture containing 10 parts *N,O*-bis(trimethylsilyl)trifluoroacetamide (BSTFA) to 5 parts pyridine to 2 parts trimethylchlorosilane (TMCS) added to a 500 µL sample of alkyl phosphates

results in optimal derivatization [16]. However, when a derivatized sample was analyzed using GC×GC-NPD the excess silylation reagents from the derivatization mixture were found to coat the NPD bead in a layer of SiO_2, passivating the bead and fully quenching the signal after fewer than 10 chromatographic runs.

As a result, **CHAPTER 2** explored three possible strategies for solving this problem of excess silicon. The first approach considered was the use of a different phosphorus-selective detector that would not be deactivated by excess silicon. Here, the use of a flame photometric detector (FPD), selective for sulfur and phosphorus, was proposed (see **CHAPTER 2**; **Section 2.1**). Unfortunately, continuous-mode FPDs are known to have severe complications with quenching in the presence of co-eluting hydrocarbons [82,83,84] (i.e. problematic for the analysis of petroleum samples), while pulsed-mode FPDs are only capable of data collection rates on the order of 3 – 5 Hz (i.e. too slow for GC×GC). Finally, the multiple flame photometric detector [85,86], which is resistant to hydrocarbon quenching and is capable of GC×GC compatible data collection rates, is not yet commercially available. Consequently, the prospect of using a different phosphorus-selective detector to solve the problem of excess silicon was rejected.

The second solution investigated was the use of a silicon-free derivatization method using 1-chloro-3-iodopropane [176] (see **CHAPTER 2**; **Section 2.2**). Overall, the reaction was found to perform well in acetonitrile as described in the literature; however, the reaction failed to consistently

derivatize mono- and di-alkyl phosphates when performed in heptane, which was used to simulate the matrix of future petroleum samples. As a result, this alternative derivatization approach was abandoned while the third and final strategy, the use of a Deans switch (installed post-column) to divert excess silicon away from the NPD, was examined (see **CHAPTER 2**; **Section 2.3**).

The post-column placement of the Deans switch device permitted the column effluent to be directed to either a flame ionization detector (FID) or a nitrogen-phosphorus detector using a solenoid valve and an external pressure control (EPC) system. With this setup the effluent containing the highly volatile silylation reagents could be directed to the FID initially before switching the pressure in the Deans switch and directing the remaining sample material to the NPD, for selective detection. Overall, the addition of the Deans switch effectively resolved the incompatibility between the excess silicon from the derivatization reagents and the NPD, increasing the NPD bead life from approximately 5 chromatographic runs to over 1,000, which were performed over the course of 15 months [18]. The next and final steps before the alkyl phosphates could be analyzed using GC×GC-FID/NPD included the optimization of both the NPD performance and the trimethylsilylation derivatization reaction conditions.

NPD performance was optimized in terms of signal-to-noise ratio (S/N) by determining the optimal detector gas flow rates for hydrogen, makeup (i.e. helium), and air using a three-factor, three-level Box-Behnken statistical design of experiment [196,197] (see **CHAPTER 2**; **Section 2.4**).

Overall, NPD gas flow conditions of 5 mL min^{-1} for hydrogen, 70 mL min^{-1} for air, and 1.5 mL min^{-1} for makeup (helium) were found to produce optimal NPD performance; however, these flows lead to the production of a self-sustained flame within the NPD and as a result, the hydrogen flow had to be decreased to 3 mL min^{-1} for all remaining experiments.

As previously mentioned the trimethylsilylation derivatization reaction was previously optimized in terms of reagent ratios [16]. Herein the reaction conditions were optimized in terms of reaction temperature (30 °C) and derivatization reaction length (30 minutes) (see **CHAPTER 2**; **Section 2.5**). In addition, the trimethylsilyl derivatives were determined to be stable over the 48 hour period tested therefore allowing for future samples to be derivatized simultaneously in a heated GC autosampler tray and left for analysis overnight.

Using both the optimized NPD gas flows and trimethylsilylation derivation reaction conditions, **CHAPTER 3** presented the development of a method for the analysis of alkyl phosphates in petroleum samples using GC×GC-FID/NPD with post-column Deans switching and split injection [18]. The resulting GC×GC-FID/NPD system revealed an approach that is capable of both quantifying and speciating individual alkyl phosphate compounds in real industrial petroleum samples with increased precision and at levels comparable to or below those achievable with the currently-accepted ICP-OES method. In addition, a recovery study performed in a fracture fluid

sample demonstrated the reliability of calibrations performed in solvent when used for quantification of alkyl phosphates in real samples.

The overall fouling of refinery equipment is thought to be the result of chronic exposure to trace quantities of volatile phosphorus [67]. Consequently, the GC×GC-FID/NPD method developed in **CHAPTER 3** was further refined in **CHAPTER 4** [19] for trace analysis. The implementation of splitless injection and concurrent backflushing resulted in limits of quantification two orders of magnitude lower than those achieved with split injection (**CHAPTER 3** [18]) and two to three orders of magnitude lower than what is possible by ICP-OES, while still maintaining an increased precision over ICP-OES. The addition of concurrent backflushing facilitated the elimination of heavier, less volatile matrix components from the system resulting in excellent retention time reproducibility (~± 1 modulation period (P_M)) and a reduction in system maintenance leading to less instrument downtime and improved sample throughput. In addition, a recovery study performed in two different industrial petroleum samples again demonstrated the reliability of calibrations performed in solvent when used for quantification of alkyl phosphates in real samples.

A profiling study of alkyl phosphates in 14 different industrial petroleum samples (crude oil and mixtures of crude oil and fracture fluid) using both the split injection method (**CHAPTER 4**; **Section 4.3.3.2**) and the refined splitless injection method (**CHAPTER 4**; **Section 4.3.3.1**) revealed that split injection is unable to fully speciate samples containing only trace

amounts of alkyl phosphate contamination, thus exposing the need for splitless injection. Furthermore, the splitless method will likely provide more accurate results for samples containing high concentrations of mono- and di-alkyl phosphates than the split method due to the fact that the samples can be substantially diluted, resulting in a more complete derivatization reaction. Finally, several of the industrial petroleum samples profiled in **CHAPTER 4** were also found to contain both individual and/or total phosphorus concentrations below 1.5 μg *phosphorus* mL^{-1}, demonstrating that the refined GC×GC-FID/NPD method is capable of both speciating and quantifying individual and total alkyl phosphates at phosphorus concentrations below the limit of detection of the ICP-OES method, when the precision in this method is considered (0.5 ± 1 μg *phosphorus* mL^{-1}).

CHAPTER 5 applied the refined GC×GC-FID/NPD methodology, developed in **CHAPTER 4** [19], to a preliminary study profiling alkyl phosphate contamination in a Western Canadian Refinery. Both crude oil (raw and desalted) entering the refinery, as well as three different petroleum product distillate streams exiting the refinery, were inspected. Trace quantities of tripentyl and trioctyl phosphate were identified in all of the crude oil samples tested, while the distillate samples were found to be free of any known/standard alkyl phosphate contamination. Dibutyl phosphate however, was identified in all 30 refinery samples tested (i.e. both crude and distillate samples), though its presence was discovered to be due to the use of contaminated derivatization reagent(s). In addition, several unidentified

probable phosphorus (possibly nitrogen) compounds were also discovered in the crude oil and distillate samples. GC×GC-NPD chromatograms for each of the refinery samples exhibiting both the identified and unidentified compounds can be found in **APPENDIX A**. Plenty of future work remains for this long-term profiling study, which is detailed in **Sections 6.2.1** and **6.2.2** below.

Overall, the GC×GC-FID/NPD method developed in **CHAPTER 4** [19] represents the only analytical method/technology that is currently capable of: 1) separating the alkyl phosphates from each other and from a crude oil matrix; and 2) speciating and quantifying the alkyl phosphates reproducibly in petroleum samples at trace levels. Thus, in conclusion, this thesis presents a significant step towards a routine, robust method for profiling (i.e. speciating and quantifying) alkyl phosphate contamination in petroleum and process samples in a production environment using comprehensive two-dimensional gas chromatography with nitrogen-phosphorus detection.

6.2 Future Work

6.2.1 Alkyl Phosphate Speciation

CHAPTERS 3, **4**, and **5** revealed the presence of a number of unidentified peaks in the GC×GC-NPD chromatograms of the various industrial petroleum samples profiled throughout this thesis (see **Figures 3-7**, **4-6**, and **APPENDIX A**). These peaks signify probable phosphorus

(possibly nitrogen) compounds that remain unidentified due to a lack of available alkyl phosphate standards.

It has been mentioned a number of times throughout this thesis that structurally-related compounds elute with distinct patterns in GC×GC, resulting in ordered chromatograms, which can assist in sample characterization and compound identification [11,12,13]. Pattern recognition becomes a challenge here, because the family of alkyl phosphates that could be present comprises dozens of different molecular structures (e.g. pure phosphates versus mixed phosphates). Additionally, the molecules could undergo chemical reactions in the refinery (e.g. within the distillation tower), making them even more difficult to identify. Unfortunately, the current collection of alkyl phosphate standards consists mostly of pure, non-branched trialkyl phosphates. This lack of variety in the available alkyl phosphate standards makes pattern recognition (and thus the identification of unknown (i.e. non-standard) phosphates) nearly impossible within the GC×GC-NPD chromatograms. An increase in the assortment of phosphate standards accessible (including mono- and di-alkyl phosphates as well as branched and mixed phosphates), in conjunction with a model of alkyl phosphate retention (that is in the early stages of development [198,199]), may provide the potential for pattern/compound identification within the GC×GC-NPD chromatograms. The further development of this alkyl phosphate retention model however, also relies on an increase in the alkyl phosphate standard collection.

The Harynuk laboratory is an analytical chemistry laboratory and is therefore not equipped with the appropriate synthetic apparatus, materials, methods or personnel to conduct/handle in-house synthesis and purification of alkyl phosphate standards. A quick inquiry into outsourcing the custom synthesis to an industrial laboratory revealed prices ranging from $1,400 (Toronto Research Chemicals, Inc.) to $10,000 (TCI America) per alkyl phosphate requested. This endeavor could become quite expensive depending on the number of alkyl phosphate standards required to increase the collection enough to allow for pattern recognition and the advancement of the alkyl phosphate retention model.

Alternatively, mass spectrometry (MS) could be employed for the identification of suspect phosphates (for which standards do not exist) or other unidentified, possible phosphorus-containing compounds (that may result from reactions within the distillation tower). Previous work in the Harynuk Group [17] has determined that TOFMS with electron impact ionization is minimally informative for the identification of alkyl phosphates. However, the use of a softer (i.e. lower energy) ionization technique (such as chemical ionization) that results in an easily identifiable, intact molecular ion peak is likely to be more informative but has not yet been explored. Other MS techniques that may be considered in the future include: gas chromatographic or targeted two-dimensional gas chromatographic analyses with tandem mass spectrometry (MS/MS), GC or GC×GC with high-resolution time-of-flight mass spectrometry, and GC with ion-mobility spectrometry –

tandem mass spectrometry. The GC×GC-NPD analyses will help suggest locations in the chromatogram and approximate molecular formulae (estimated using GC×GC peak patterns if possible) of suspect phosphates to target with MS/MS.

6.2.2 Profiling Alkyl Phosphate Contamination in a Refinery

The sampling program initiated in **CHAPTER 5** will be continued for a total of six months (end of April to end of October, 2014), however sample collection will be reduced to once every two weeks. This will provide a series of 12 time points for the collection of phosphate profiles passing through the refinery. The phosphate profiles will be collected as performed in **CHAPTER 5** using the published GC×GC-FID/NPD method developed in **CHAPTER 4** [19].

The ultimate goal of this profiling study will be to determine: 1) the distribution and variation in concentration and speciation of phosphates throughout a refinery; 2) whether any phosphates are consumed or generated as part of the refining process; 3) the long-term stability of alkyl phosphates in storage (to be determined by re-analyzing samples periodically); and 4) the long-term stability of instrument calibrations. This research will allow the refinery to assess the extent of exposure that their facility experiences to phosphorus-containing compounds and to observe variations in phosphorus profiles over a period of several months. The outcome of this research has the potential to inform future projects and

needs of the refinery/company. These include the potential of equipping their laboratory with the equipment required to perform the analysis in-house (~$80,000 – 100,000 in equipment) or the potential of sponsoring the development of compact, on-line, automated monitoring equipment for alkyl phosphates in a production environment.

A profiling study, such as that proposed here, has never been performed as the technology is just now becoming available. The results of this study will begin to provide the chemical information needed to contemplate future mitigation strategies for handling the "phosphate problem". This will be important to refineries across North America that struggle with issues of equipment fouling. A mitigation strategy would, quite literally, be a multimillion-dollar idea for the petroleum industry.

References

[1] S.C. Lawrence, A.C. Kalenchuk, K. Ranicar, S. Dhillon, A. Baig, SPE Prod. Oper. (2009) 556.

[2] R.S. Taylor, P.S. Stemler, A. Lemieux, G.C. Fyten, A. Cheng, J. Can. Petro. Technol. 46 (2007) 16.

[3] B. Kennedy, Phosphorus in Crude, Maxxam Analytics, Calgary, Alberta, Canada (2007) available online at http://www.ccqta.com/files/june2007.pdf, accessed on May 27, 2014.

[4] The Canadian Crude Quality Technical Association (CCQTA), Phosphorus in Crude Oil, available online at http://www.ccqta.com/projects.php?project_id=6, accessed on May 27, 2014.

[5] P. Unruh, Letter to Pipelines. Canadian Association of Petroleum Producers, Calgary, Alberta, Canada (2006).

[6] Test Method for Determination of Organo-Phosphorus in Volatile Distillates of Crude Oil by Inductively Coupled Plasma (ICP) Optical Emission Spectrometry, available online at http://www.ccqta.com/files/sept2006revised.pdf, accessed on May 27, 2014.

[7] A.D. Rossé, J.J. Harynuk, The Column 6 (2010) 3.

[8] C. von Mühlen, C.A. Zini, E.B. Caramão, P.J. Marriott, J. Chromatogr. A 1105 (2006) 39.

[9] M. Adahchour, J. Beens, R.J.J. Vreuls, U.A.Th. Brinkman, Trends Anal. Chem. 25 (2006) 726.

[10] K.D. Nizio, T.M. McGinitie, J.J. Harynuk, J. Chromatogr. A 1255 (2012) 12.

[11] J. Beens, J. Blomberg, P.J. Schoenmakers, J. High Resol. Chomatogr. 23 (2000) 182.

[12] J. Dallüge, J. Beens, U.A.Th. Brinkman, J. Chromatogr. A 1000 (2003) 69.

[13] P.J. Marriott, T. Massil, H. Hugel, J. Sep. Sci. 27 (2004) 1273.

[14] H.J. de Geus, J. de Boer, J.B. Phillips, E.B. Ledford Jr., U.A.Th. Brinkman, J. High Resol. Chromatogr. 21 (1998) 411.

[15] A.L. Lee, K.D. Bartle, A.C. Lewis, Anal. Chem. 73 (2001) 1330.

[16] A.D. Rossé, J.J. Harynuk, Anal. Methods 2 (2010) 1176.

[17] J.J. Harynuk, A.D. Rossé, G.B. McGarvey, Anal. Bioanal. Chem. 401 (2011) 2415.

[18] K.D. Nizio, J.J. Harynuk, J. Chromatogr. A 1252 (2012) 171.

[19] K.D. Nizio, J.J. Harynuk, Energy Fuels 28 (2014) 1709.

[20] J. Blomberg, E.P.C. Mes, P.J. Schoenmakers, J.J.B. van der Does, J. High Resol. Chromatogr. 20 (1997) 125.

[21] J.B. Phillips, J. Xu, J. Chromatogr. A 703 (1995) 327.

[22] J.M. Davis, J.C. Giddings, Anal. Chem. 55 (1983) 418.

[23] J.C. Giddings, J. Chromatogr. A 703 (1995) 3.

[24] S.T. Teng, A.D. Williams, K. Urdal, J. High Resol. Chromatogr. 17 (1994) 469.

[25] ASTM D 6733-01: Standard test method for determination of individual components in spark ignition engine fuels by 50-meter capillary high resolution gas chromatography, Annual Book of ASTM Standard, vol. 05.03 (2006).

[26] H. Boer, P. van Arkel, W.J. Boersma, Chromatographia 13 (1980) 500.

[27] J. Curvers, P. van der Sluys, J. Chromatogr. Sci. 26 (1988) 267.

[28] J. Curvers, P. van den Engel, J. Chromatogr. Sci. 26 (1988) 271.

[29] F.P. Di Sanzo, J.L. Lane, R.E. Yoder, J. Chromatogr. Sci. 26 (1988) 206.

[30] P. van Arkel, J. Beens, H. Spaans, D. Grutterink, R. Verbeek, J. Chromatogr. Sci. 25 (1987) 141.

[31] C. Vendeuvre, F. Bertoncini, D. Espinat, D. Thiébaut, M.-C. Hennion, J. Chromatogr. A 1090 (2005) 116.

[32] E. Furimsky, Appl. Catal. A 199 (2000) 147.

[33] J. Blomberg, P.J. Schoenmakers, U.A.Th. Brinkman, J. Chromatogr. A 972 (2002) 137.

[34] J. Blomberg, T. Riemersma, M. van Zuijlen, H. Chaabani, J. Chromatogr. A 1050 (2004) 77.

[35] P. Zeuthen, K.G. Knudsen, D.D. Whitehurst, Catal. Today 65 (2001) 307.

[36] M. Dorbon, C. Bernasconi, Fuel 68 (1989) 1067.

[37] F. Adam, F. Bertoncini, N. Brodusch, E. Durand, D. Thiébaut, D. Espinat, M.-C. Hennion, J. Chromatogr. A 1148 (2007) 55.

[38] F. Adam, F. Bertoncini, C. Dartiguelongue, K. Marchand, D. Thiébaut, M.-C. Hennion, Fuel 88 (2009) 938.

[39] R. van der Westhuizen, A. Crouch, P. Sandra, J. Sep. Sci. 31 (2008) 3423.

[40] F. Bertoncini, C. Vendeuvre, D. Thiébaut, Oil Gas Sci. Technol. 60 (2005) 937.

[41] F. Bertoncini, M.C. Marion, N.E.S. Brodusch, Oil Gas Sci. Technol. 64 (2009) 79.

[42] Off. J. Eur. Union L140 (2009) 16.

[43] F. Adam, F. Bertoncini, V. Coupard, N. Charon, D. Thiébaut, D. Espinat, M.-C. Hennion, J. Chromatogr. A 1186 (2008) 236.

[44] J.A. DeMello, C.A. Carmichael, E.E. Peacock, R.K. Nelson, J.S. Arey, C.M. Reddy, Mar. Pollut. Bull. 54 (2007) 894.

[45] Z. Wang, S.A. Stout, M. Fingas, Environ. Forensics 7 (2006) 105.

[46] G.S. Frysinger, R. B. Gaines, J. Sep. Sci. 24 (2001) 87.

[47] A. Aguiar, A.I.S. Júnior, D.A. Azevedo, F.R.A. Neto, Fuel 89 (2010) 2760.

[48] Y. Kojima, K. Inazu, Y. Hisamatsu, H. Okochi, T. Baba, T. Nagoya, Atmos. Environ. 44 (2010) 2873.

[49] O. Amador-Muñoz, R. Villalobos-Pietrini, A. Aragón-Piña, T.C. Tran, P. Morrison, P.J. Marriott, J. Chromatogr. A 1201 (2008) 161.

[50] J.M. Carpentier, Our Energy Heritage Oil and Gas, Meridian Press, Montreal (1989) 73.

[51] W.M. Harms in: J.K. Borchardt, T.F. Yen (Eds.), Oil Field Chemistry: Enhanced Recovery and Production Stimulation, American Chemical Society, Washington, DC (1989) 55.

[52] S. Schubarth, D. Milton-Tayler, SPE Annual Technical Conference and Exhibition, Houston, Texas, 26–29 September 2004, Paper 90562-MS.

[53] J.I. DiStasio (Ed.), Chemicals for Oil Field Operations Recent Developments, Noyes Data Corporation, New Jersey (1981) 141.

[54] L.J. Maberry, S.B. McConnell, K.V. Tanner, J.J. Hinkel, SPE Production & Facilities 13 (1998) 236.

[55] S.H. Rose, B.P. Block, J. Am. Chem. Soc. 87 (1965) 2076.

[56] J.I. Fukasawa, H. Tsutsumi, J. Colloid Interface Sci. 143 (1991) 69.

[57] M.G. Page, G.G. Warr, J. Phys. Chem. B 108 (2004) 16983.

[58] M.G. Page, G.G. Warr, Langmuir 25 (2009) 8810.

[59] National Northeast British Columbia's Ultimate Potential for Conventional Natural Gas Fact Sheet 2006, available online at http://www.neb-one.gc.ca/clf-nsi/rnrgynfmtn/nrgyrprt/ntrlgs/nbcltmtptntl2006/fctsht0609-eng.html, accessed on May 27, 2014.

[60] G.P. Funkhouser, US Patent 7066262 B2 (2006).

[61] B. Lukocs, S. Mesher, T.P. Wilson Jr., T. Garza, W. Mueller, F. Zamora, L.W. Gatlin, US Patent 2007/0173413 A1 (2007).

[62] A. Lemieux, Crude Quality Concern, Phosphorus in Light Sweet Canadian Crude, Canadian Crude Quality Technical Association Project Summary available online at http://www.ccqta.com/files/june1999.pdf, accessed on May 27, 2014.

[63] S.M.A.M. Bouwens, J.P.R. Vissers, V.H.J. de Beer, R. Prins, J. Catal. 112 (1988) 401.

[64] S.M.A.M. Bouwens, A.M. van der Kraan, V.H.J. de Beer, R. Prins, J. Catal. 128 (1991) 559.

[65] The Canadian Crude Quality Technical Association, Phosphorus in Crude, available online at http://www.ccqta.com/phosphoruslist.php, accessed on May 27, 2014.

[66] R.S. Taylor, P.S. Stemler, A. Cheng, C. Tamayo, G.P. Funkhouser, A. Lemieux, Refinery Plugging by Residual Oil Gellant Chemicals in Crude: Understanding and Preventing the Problem Through New Oil Gellant Chemistry, 5th Canadian International Petroleum Conference (2004) 1.

[67] G. Fyten, P. Houle, R.S. Taylor, P.S. Stemler, A. Lemieux, J. Can. Petrol. Technol. 46 (2007) 17.

[68] R.S. Taylor, P.S. Stemler, A. Lemieux, G.P. Funkhouser, G.C. Fyten, A. Cheng, S. Stadnyk, J. Can. Petrol. Technol. 44 (2005) 16.

[69] R.S. Taylor, A. Lemieux, T. Blackmore, G.C. Fyten, C. Tamayo, G. P. Funkhouser, J. Can. Petrol. Technol. 47 (2008) 50.

[70] T. Górecki, J. Harynuk, O. Panić, J. Sep. Sci. 27 (2004) 359.

[71] M. Adahchour, J. Beens, R.J.J. Vreuls, U.A.Th. Brinkman, Trends Anal. Chem. 25 (2006) 438.

[72] M. Adahchour, J. Beens, R.J.J. Vreuls, U.A.Th. Brinkman, Trends Anal. Chem. 25 (2006) 540.

[73] M. Adahchour, J. Beens, R.J.J. Vreuls, U.A.Th. Brinkman, Trends Anal. Chem. 25 (2006) 821.

[74] H.J. Cortes, B. Winniford, J. Luong, M. Pursch, J. Sep. Sci. 32 (2009) 883.

[75] P.Q. Tranchida, G. Purcaro, P. Dugo, L. Mondello, Trends Anal. Chem. 30 (2011) 1437.

[76] M. Edwards, A. Mostafa, T. Górecki, Anal. Bioanal. Chem. 401 (2011) 2335.

[77] P.J. Marriott, S.-T. Chin, B. Maikhunthod, H.-G. Schmarr, S. Bieri, Trends Anal. Chem. 34 (2006) 1.

[78] J.V. Seeley, S.K. Seeley, Anal. Chem. 85 (2013) 557.

[79] G.K.H.D. Alwis, L.L. Needham, D.B. Barr, J. Chromatogr. B 843 (2006) 34.

[80] S.-T. Chin, Z.-Y. Wu, P.D. Morrison, P.J. Marriott, Anal. Methods 2 (2010) 243.

[81] X. Liu, B. Mitrevski, D. Li, J. Li, P.J. Marriott, Microchem. J. 111 (2013) 25.

[82] P.L. Patterson, Anal. Chem. 50 (1978) 345.

[83] M. Dressler, Selective Gas Chromatographic Detectors, Elsevier, Amsterdam (1986) 152.

[84] W.A. Aue, X.-Y. Sun, J. Chromatogr. A 641 (1993) 291.

[85] T.C. Hayward, K.B. Thurbide, Anal. Chem. 81 (2009) 8858.

[86] K.B. Thurbide, Apparatus and Method for Quenching-Resistant Multiple Flame Photometric Detector, US Patent 20110239737 (2011).

[87] A.T. James, A.J.P. Martin, Biochem. J. 50 (1952) 679.

[88] H. Carlsson, G. Robertsson, A. Colmsjo, Anal. Chem. 73 (2001) 5698.

[89] P.L. Patterson, J. Chromatogr. 167 (1978) 381.

[90] P.L. Patterson, J. Chromatogr. Sci. 24 (1986) 41.

[91] D. Ryan, P. Marriott, J. Sep. Sci. 29 (2006) 2375.

[92] K. Olah, A. Szoke, Z. Vajta, J. Chromatogr. Sci. 17 (1979) 497.

[93] W.M. Draper, J. Agric. Food Chem. 43 (1995) 2077.

[94] L.A. Colón, L.J. Baird in: R.L. Grob, E.F. Barry (Eds.), Modern Practice of Gas Chromatography 4th ed., John Wiley & Sons, New Jersey (2004) 315.

[95] M.C. Simmons, L.R. Snyder, Anal. Chem. 30 (1958) 32.

[96] J.C. Giddings, Anal. Chem. 56 (1984) 1258A.

[97] J.C. Giddings, J. High Resol. Chromatogr. 10 (1987) 319.

[98] J.J. Harynuk, A.H. Kwong, P.J. Marriott, J. Chromatogr. A 1200 (2008) 17.

[99] L. Blumberg, M.S. Klee, J. Chromatogr. A 1217 (2010) 99.

[100] W. Khummueng, J. Harynuk, P.J. Marriott, Anal. Chem. 78 (2006) 4578.

[101] P.Q. Tranchida, P. Dugo, G. Dugo, L. Mondello, J. Chromatogr. A. 1054 (2004) 3.

[102] P.Q. Tranchida, P. Donato, F. Cacciola, M. Beccaria, P. Dugo, L. Mondello, Trends Anal. Chem. 52 (2013) 186.

[103] A.W. Culbertson, W.B. Williams, A.G. McKee, X. Zhang, K.L. March, S. Naylor, S.J. Valentine, LC GC N. Am. (2008) 74.

[104] M.F. Almstetter, P.J. Oefner, K. Dettmer, Anal. Bioanal. Chem. 402 (2012) 1993.

[105] M. Kallio, T. Hyötyläinen, M. Lehtonen, M. Jussila, K. Hartonen, M. Shimmo, M.L. Riekkola, J. Chromatogr. A 1019 (2003) 251.

[106] O. Panić, T. Górecki, Anal. Bioanal. Chem. 386 (2006) 1013.

[107] G.S. Frysinger, R.B. Gaines, C.M. Reddy, Environ. Forensics 3 (2002) 27.

[108] G.S. Frysinger, R.B. Gaines, J. Forensic Sci. 47 (2002) 471.

[109] R.K. Nelson, B.M. Kile, D.L. Plata, S.P. Sylva, L. Xu, C.M. Reddy, R.B. Gaines, G.S. Frysinger, S.E. Reichenbach, Environ. Forensics 7 (2006) 33.

[110] First International Symposium on Comprehensive Multidimensional Gas Chromatography, Volendam, The Netherlands, March 6-7, 2003.

[111] P.Q. Tranchida, D. Sciarrone, P. Dugo, L. Mondello, Anal. Chim. Acta 716 (2012) 66.

[112] Z. Liu, J.B. Phillips, J Chromatogr. Sci. 29 (1991) 227.

[113] M. Adahchour, J. Beens, R.J.J. Vreuls, A.M. Batenburg, U.A.Th. Brinkman, J. Chromatogr. A 1054 (2004) 47.

[114] T.C. Tran, G.A. Logan, E. Grosjean, J. Harynuk, D. Ryan, P. Marriott, Org. Geochem. 37 (2006) 1190.

[115] A. Kohl, J. Cochran, D.M. Cropek, J. Chromatogr. A 1217 (2010) 550.

[116] R. van der Westhuizen, R. Crous, A. de Villiers, P. Sandra, J. Chromatogr. A 1217 (2010) 8334.

[117] L. Mahé, T. Dutriez, M. Courtiade, D. Thiébaut, H. Dulot, F. Bertoncini, J. Chromatogr. A 1218 (2011) 534.

[118] R. van der Westhuizen, M. Ajam, P. De Coning, J. Beens, A. de Villiers, P. Sandra, J. Chromatogr. A 1218 (2011) 4478.

[119] P.M. Harvey, R.A. Shellie, P.R. Haddad, J. Chromatogr. Sci. 48 (2010) 245.

[120] R.E. Murphy, M.R. Schure, J.P. Foley, Anal. Chem. 70 (1998) 1585.

[121] N.J. Micyus, S.K. Seeley, J.V. Seeley, J. Chomatogr. A 1086 (2005) 171.

[122] C.A. Bruckner, B.J. Prazen, R.E. Synovec, Anal. Chem. 70 (1998) 2796.

[123] J.V. Seeley, F. Kramp, C.J. Hicks, Anal. Chem. 72 (2000) 4346.

[124] C.G. Fraga, B.J. Prazen, R.E. Synovec, Anal. Chem. 73 (2001) 5833.

[125] J.W. Diehl, F.P. Di Sanzo, J. Chromatogr. A 1080 (2005) 157.

[126] P.A. Bueno, J.V. Seeley, J. Chromatogr. A 1027 (2004) 3.

[127] J.V. Seeley, N.J. Micyus, J.D. McCurry, S.K. Seeley, Am. Lab. 38 (2006) 24.

[128] J.V. Seeley, N.J. Micyus, S.V. Bandurski, S.K. Seeley, J.D. McCurry, Anal. Chem. 79 (2007) 1840.

[129] P.Q. Tranchida, G. Purcaro, A. Visco, L. Conte, P. Dugo, P. Dawes, G. Dugo, L. Mondello, J. Chromatogr. A 1218 (2011) 3140.

[130] J.B. Phillips, E.B. Ledford, Field Anal. Chem. Technol. 1 (1996) 23.

[131] H.J. de Geus, J. de Boer, U.A.Th. Brinkman, J. Chromatogr. A 767 (1997) 137.

[132] R.M. Kinghorn, P.J. Marriott, J. High Resolut. Chromatogr. 21 (1998) 620.

[133] E.B. Ledford Jr., C. Billesbach, J. High Resolut. Chromatogr. 21 (2000) 202.

[134] J. Beens, M. Adahchour, R.J.J. Vreuls, K. van Altena, U.A.Th. Brinkman, J. Chromatogr. A 919 (2001) 127.

[135] T. Hyötyläinen, M. Kallio, K. Hartonen, M. Jussila, S. Palonen, M.L. Riekkola, Anal. Chem. 74 (2002) 4441.

[136] J. Harynuk, T. Górecki, J. Chromatogr. A 1019 (2003) 53.

[137] R.A. Shellie, P.J. Marriott, Analyst 128 (2003) 879.

[138] R.A. Shellie, P.J. Marriott, C.W. Hule, J. Sep. Sci. 26 (2003) 1185.

[139] B.J.G. Silva, P.Q. Tranchida, G. Purcaro, M.E.C. Queiroz, L. Mondello, F.M. Lanças, J. Chromatogr. A 1255 (2012) 177.

[140] C. von Mühlen, W. Khummueng, C.A. Zini, E.B. Caramão, P.J. Marriott, J. Sep. Sci. 29 (2006) 1909.

[141] L. Mondello (Ed.), Comprehensive Chromatography in Combination with Mass Spectrometry (1st Ed.), John Wiley & Sons, Inc., Hoboken, New Jersey (2011).

[142] ISO/IEC, Guide 99: International vocabulary of metrology- Basic and general concepts and associated terms (VIM). ISO: Geneva, 2007.

[143] A.D. McNaught, A. Wilkinson (Eds.), IUPAC, Compendium of Chemical Terminology. 2nd ed., Blackwell Scientific Publications: Oxford (1997) 399.

[144] IUPAC. Pure Appl. Chem. 67 (1995) 1699.

[145] T.T. Truong, P.J. Marriott, N.A. Porter, J. AOAC Int. 84 (2001) 323.

[146] W. Khummueng, C. Trenerry, G. Rose, P.J. Marriott, J. Chromatogr. A 1131 (2006) 203.

[147] R.L. Bordajandi, L. Ramos, M.J. González, J. Chromatogr. A 1125 (2006) 220.

[148] D. Kocak, M.Z. Ozel, F. Gogus, J.F. Hamilton, A.C. Lewis, Food Chem. 135 (2012) 2215.

[149] J. Beens, H. Boelens, R. Tijssen, J. Blomberg, J. High Resol. Chromatogr. 21 (1998) 47.

[150] B.S. Mitrevski, J.T. Brenna, Y. Zhang, P.J. Marriott, J. Chromatogr. A. 1214 (2008) 134.

[151] J. de Vos, P. Gorst-Allman, E. Rohwer, J. Chromatogr. A 1218 (2011) 3282.

[152] M.Z. Ozel, F. Gogus, S. Yagci, J.F. Hamilton, A.C. Lewis, Food Chem. Toxicol. 48 (2010) 3268.

[153] M.Z. Ozel, J.F. Hamilton, A.C. Lewis, Environ. Sci. Technol. 45 (2011) 1497.

[154] A.P. de la Mata, J.J. Harynuk, Anal. Chem. 84 (2012) 6646.

[155] W. Bertsch, J. High Resol. Chromatogr. 23 (2000) 167.

[156] K.M. Pierce, L.F. Wood, B.W. Wright, R.E. Synovec, Anal. Chem. 77 (2005) 7735.

[157] B.V. Hollingsworth, S.E. Reichenbach, Q. Tao, A. Visvanathan, J. Chromatogr. A 1105 (2006) 51.

[158] M. Ni, S.E. Reichenbach, A. Visvanathan, J. TerMaat, J.E.B. Ledford, J. Chromatogr. A 1086 (2005) 165.

[159] S.E. Reichenbach, V. Kottapalli, M. Ni, A. Visvanathan, J. Chromatogr. A 1071 (2005) 263.

[160] S.E. Reichenbach, M. Ni, V. Kottapalli, A. Visvanathan, Chemometr. Intell. Lab. 71 (2004) 107.

[161] S.E. Reichenbach, M. Ni, D. Zhang, E.B. Ledford, J. Chromatogr. A 985 (2003) 47.

[162] S.E. Reichenbach, X. Tian, Q. Tao, D.R. Stoll, P.W. Carr, J. Sep. Sci. 33 (2010) 1365.

[163] R.E. Synovec, B.J. Prazen, K.J. Johnson, C.G. Fraga, C.A. Bruckner, Adv. Chromatogr. 42 (2003) 1.

[164] A.E. Sinha, B.J. Prazen, R.E. Synovec, Anal. Bioanal. Chem. 378 (2004) 1948.

[165] K.M. Pierce, J.C. Hoggard, R.E. Mohler, R.E. Synovec, J. Chromatogr. A 1184 (2008) 341.

[166] Z.D. Zeng, H.M. Hugel, P.J. Marriott, Anal. Bioanal. Chem. 401 (2011) 2373.

[167] Z. Zheng, J. Li, H.M. Hugel, G. Xu, P.J. Marriott, Trends Anal. Chem. 53 (2014) 150.

[168] J.J. Harynuk, T. Górecki, Am. Lab. 39 (2007) 36.

[169] A. Mostafa, M. Edwards, T. Górecki, J. Chromatogr. A 1255 (2012) 38.

[170] D.R. Knapp, Handbook of Analytical Derivatization Reactions, John Wiley & Sons, New York (1979) 390.

[171] C.F. Poole, J. Chromatogr. A. 1296 (2013) 2.

[172] A.E. Pierce, Silylation of Organic Compounds, Pierce Chemical Company, Rockford, IL (1968).

[173] K. Blau, G.S. King (Eds.), Handbook of Derivatives for Chromatography, Heyden, London (1978).

[174] K. Blau, J. Halket (Eds.), Handbook of Derivatives for Chromatography, John Wiley & Sons, Chichester (1993).

[175] A.P. Bento, F.M. Bickelhaupt, J. Org. Chem. 72 (2007) 2201.

[176] G.K.H. De Alwis, L.L. Needham, D.B. Barr, J. Chromatogr. B 843 (2006) 34.

[177] D.R. Deans, J. Chromatogr. 18 (1965) 477.

[178] J. Blomberg, U.A.Th. Brinkman, J. Chromatogr. A 831 (1999) 257.

[179] P. Apps, J. Sep. Sci. 29 (2006) 2338.

[180] C.-H. Wang, C.-C. Chang, J.-L. Wang, J. Chromatogr. A 1163 (2007) 298.

[181] A. Ghosh, C.T. Bates, S.K. Seeley, J.V. Seeley, J. Chromatogr. A. 1291 (2013) 146.

[182] Agilent Technologies, Capillary Flow Technology, http://www.chem.agilent.com/en-US/products-services/Instruments-Systems/Gas-Chromatography/Capillary-Flow-Technology/Pages/default.aspx, accessed on May 27, 2014.

[183] SGE, SilFlow™ – micro-fluidic platform, http://www.sge.com/products/silflow-stainless-steel-micro-fluidic-platform, accessed on May 27, 2014.

[184] Shimadzu, Advanced Flow Technology Series, http://www.shimadzu.com.au/advanced-flow-technology-series, accessed on May 27, 2014.

[185] PerkinElmer, Swafer Micro-Channel Wafer Technology, http://www.perkinelmer.com/Catalog/Family/ID/Swafer%20MicroChannel%20Wafer%20Technology, accessed on May 27, 2014.

[186] Gerstel, Multicolumn Switching MCS, http://www.gerstel.com/en/multidimensional-gc-mcs.htm, accessed on May 27, 2014.

[187] SGE, Leak Free SilTite™ metal ferrules for GC & GC-MS, http://www.az-analyt.eu/files/downloads/br-0093-a-rev05-nd.pdf, accessed on May 27, 2014.

[188] J.V. Seeley, J. Chromatogr. A 1255 (2012) 24.

[189] D.R. Deans, Chromatographia 1 (1968) 18.

[190] R. Gras, J. Luong, M. Hawryluk, M. Monagle, J. Chromatogr. A. 1217 (2010) 348.

[191] P.L. Wylie, LC GC N. Am. (2007) 40.

[192] B. Mitrevski, P.J. Marriott, Anal. Chem. 84 (2012) 4837.

[193] F. Chainet, C.-H. Lienemann, J. Ponthus, M. Courtiade, O. François, X. Donard, J. Chromatogr. A. 1264 (2012) 80.

[194] Agilent, Capillary Flow Technology: Deans Switch, https://www.chem.agilent.com/Library/brochures/5989-9384EN.pdf, accessed on May 27, 2014.

[195] DETector Engineering & Technology, Inc., DET Report, No. 48 (July 2004) 3.

[196] G.E.P. Box, D.W. Behnken, Technometrics 2 (1960) 455.

[197] S.L.C. Ferreira, R.E. Bruns, H.S. Ferreira, G.D. Matos, J.M. David, G.C. Brandão, E.G.P. da Silva, L.A. Portugal, P.S. dos Reis, A.S. Souza, W.N.L. dos Santos, Anal. Chim. Acta 597 (2007) 179.

[198] B.M. Weber, J.J. Harynuk, J. Chromatogr. A. 1271 (2013) 170.

[199] B.M. Weber, J.J. Harynuk, J. Sep. Sci. 37 (2014) 1460.

[200] M.S. Klee, J. Sep. Sci. 32 (2009) 88.

[201] B.P. Gray, P. Teale, J. Chromatogr. A. 1217 (2010) 4749.

[202] K. Mastovska, P.L. Wyli, J. Chromatogr. A. 1265 (2012) 155.

[203] A.R. Katritzky, E.V. Gordeeva, J. Chem. Inf. Comput. Sci. 33 (1993) 835.

[204] A.R. Katritzky, E.S. Ignatchenko, R.A. Barcock, V.S. Lobanov, M. Karelson, Anal. Chem. 66 (1994) 1799.

[205] M. Jalali-Heravi, M.H. Fatemi, J. Chromatogr. A. 825 (1998) 161.

[206] F.C. Wang, W.K. Robbins, M.A. Greaney, J Sep. Sci. 27 (2004) 468.

[207] J. Blomberg, P.J. Schoenmakers, J. Beens, R. Tijssen, J. High Resol. Chromatogr. 20 (1997) 539.

[208] C. Vendeuvre, R. Ruiz-Guerrero, F. Bertoncini, L. Duval, D. Thiébaut, M.-C. Hennion, J. Chromatogr. A 1086 (2005) 21.

[209] T. Dutriez, J. Borras, M. Courtiade, D. Thiébaut, H. Dulot, F. Bertoncini, M.-C. Hennion, J. Chromatogr. A 1218 (2011) 1390.

APPENDIX A: GC×GC-NPD Chromatograms for the Western Canadian Refinery Samples Profiled in **CHAPTER 5**

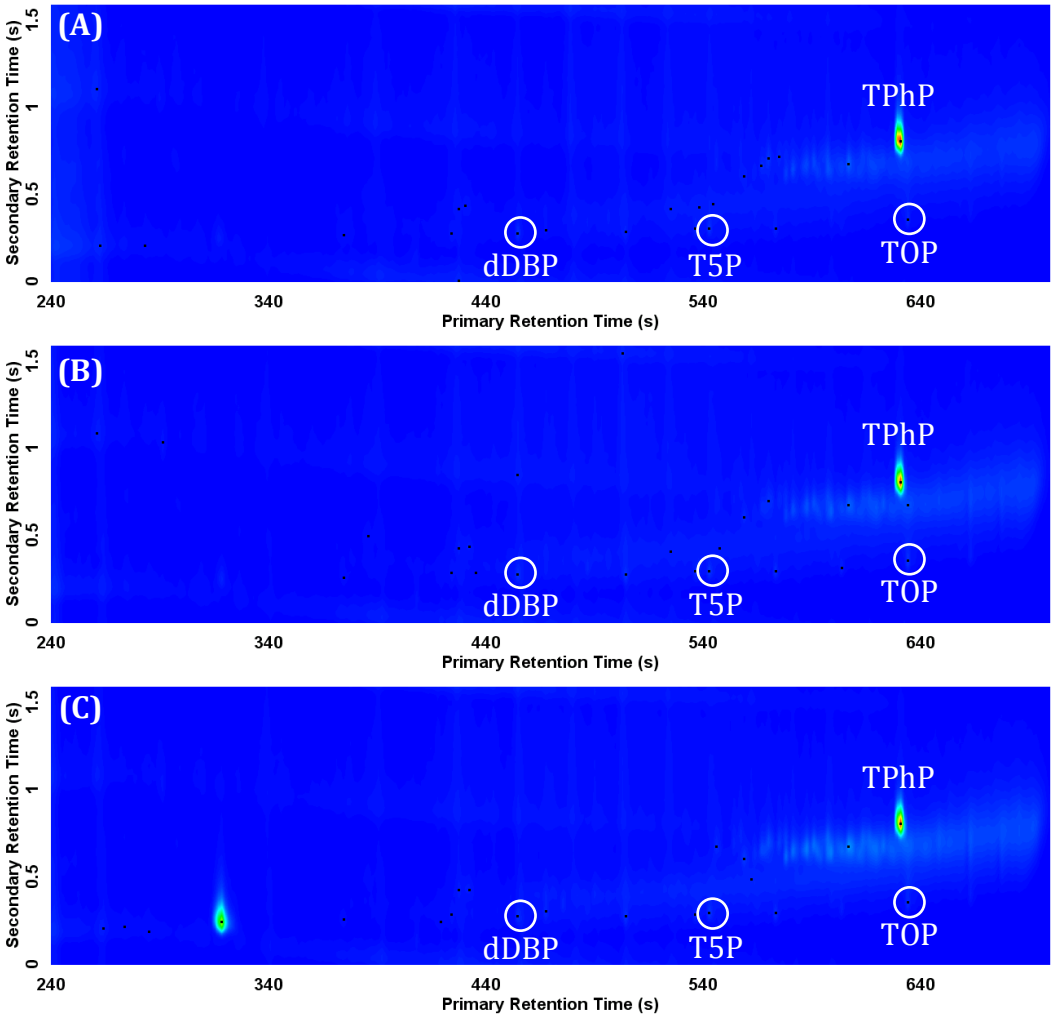

Figure A-1. GC×GC-NPD chromatograms of raw crude oil samples (diluted 50× in isooctane) collected from unit A on: (A) April 30, (B) May 3, and (C) May 6, 2014 (dDBP = derivatized dibutyl phosphate; T5P = tripentyl phosphate; TOP = trioctyl phosphate). Triphenyl phosphate (TPhP) added as an internal standard at 0.5 μg mL^{-1}. Secondary dimension (^2D) offset of 0.8 s applied to plotted chromatograms.

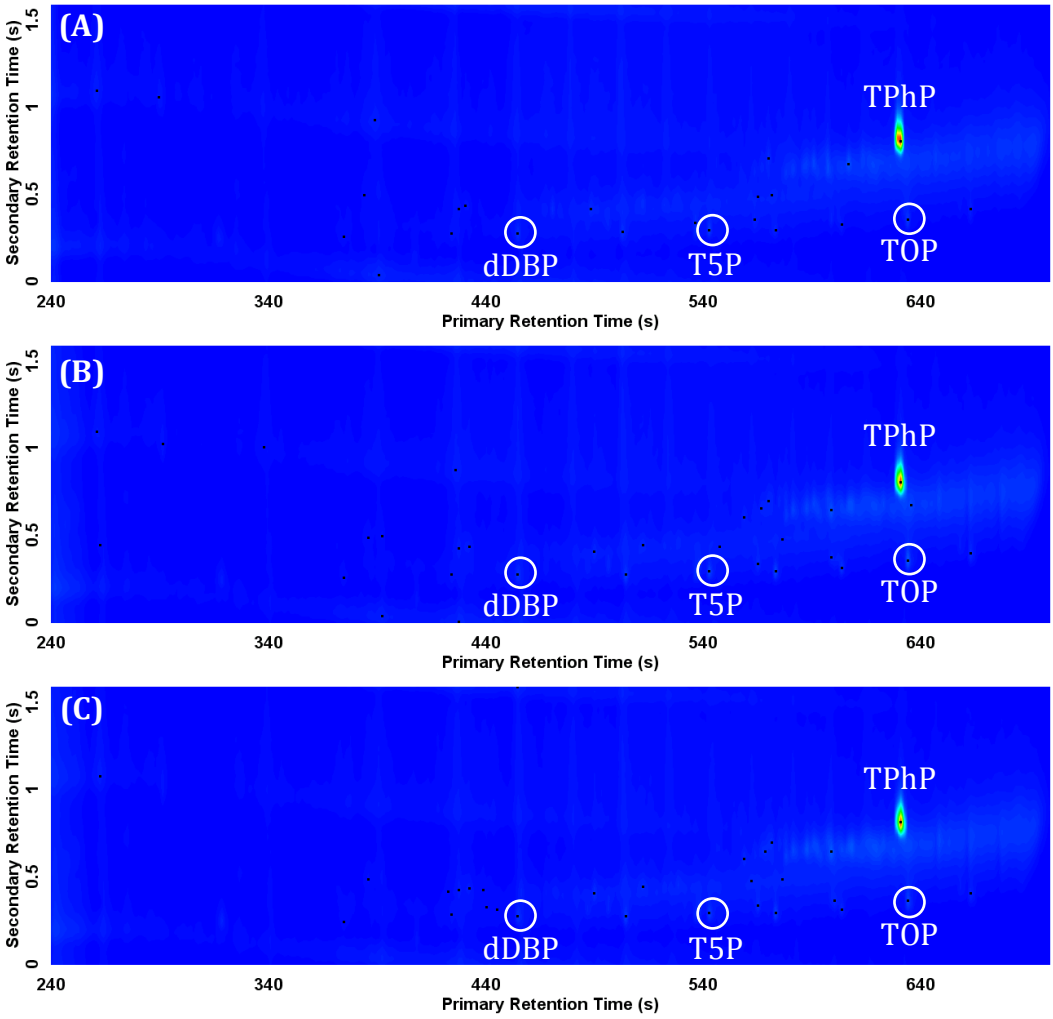

Figure A-2. GC×GC-NPD chromatograms of raw crude oil samples (diluted 50× in isooctane) collected from unit B on: (A) April 30, (B) May 3, and (C) May 6, 2014 (dDBP = derivatized dibutyl phosphate; T5P = tripentyl phosphate; TOP = trioctyl phosphate). Triphenyl phosphate (TPhP) added as an internal standard at 0.5 µg mL^{-1}. ^{2}D offset of 0.8 s applied to plotted chromatograms.

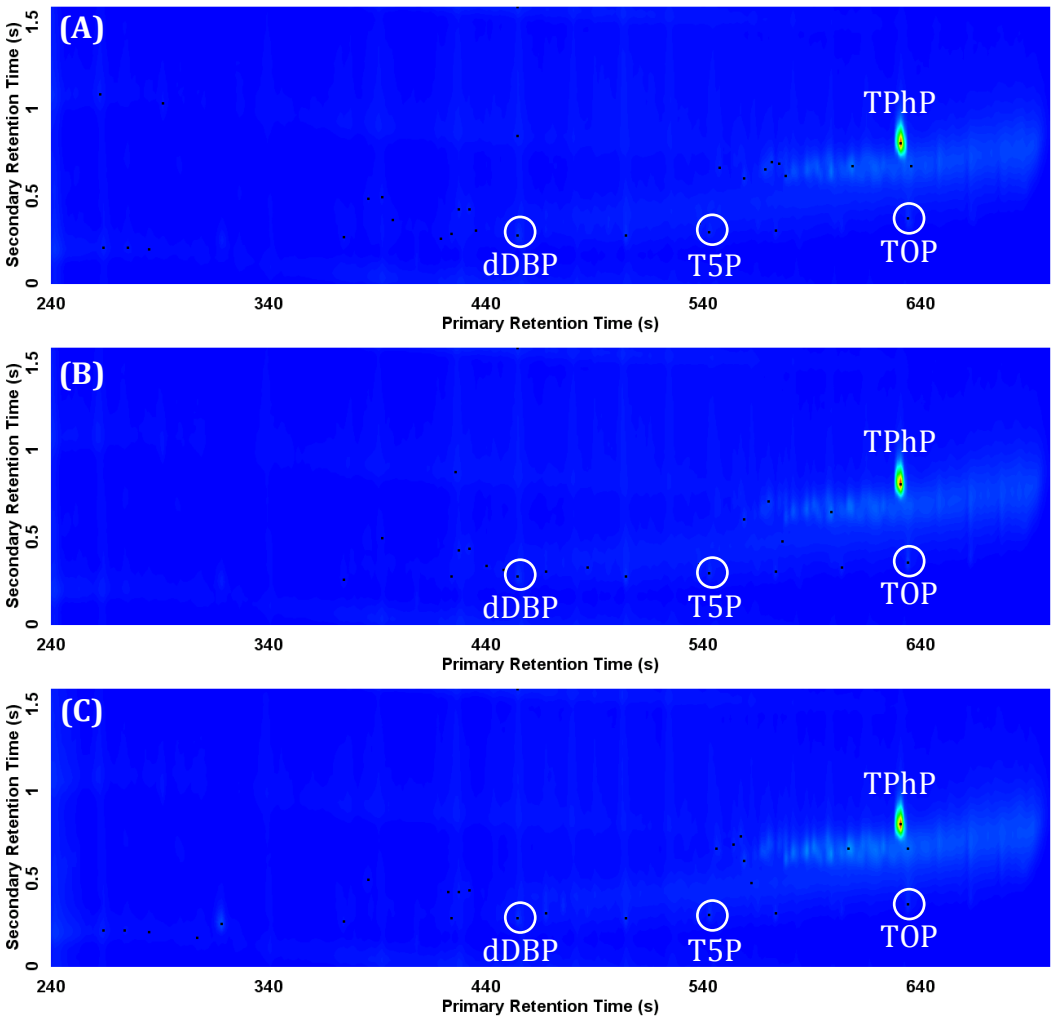

Figure A-3. GC×GC-NPD chromatograms of desalted crude oil samples (diluted 50× in isooctane) collected from unit A on: (A) April 30, (B) May 3, and (C) May 6, 2014 (dDBP = derivatized dibutyl phosphate; T5P = tripentyl phosphate; TOP = trioctyl phosphate). Triphenyl phosphate (TPhP) added as an internal standard at 0.5 μg mL^{-1}. ^{2}D offset of 0.8 s applied to plotted chromatograms.

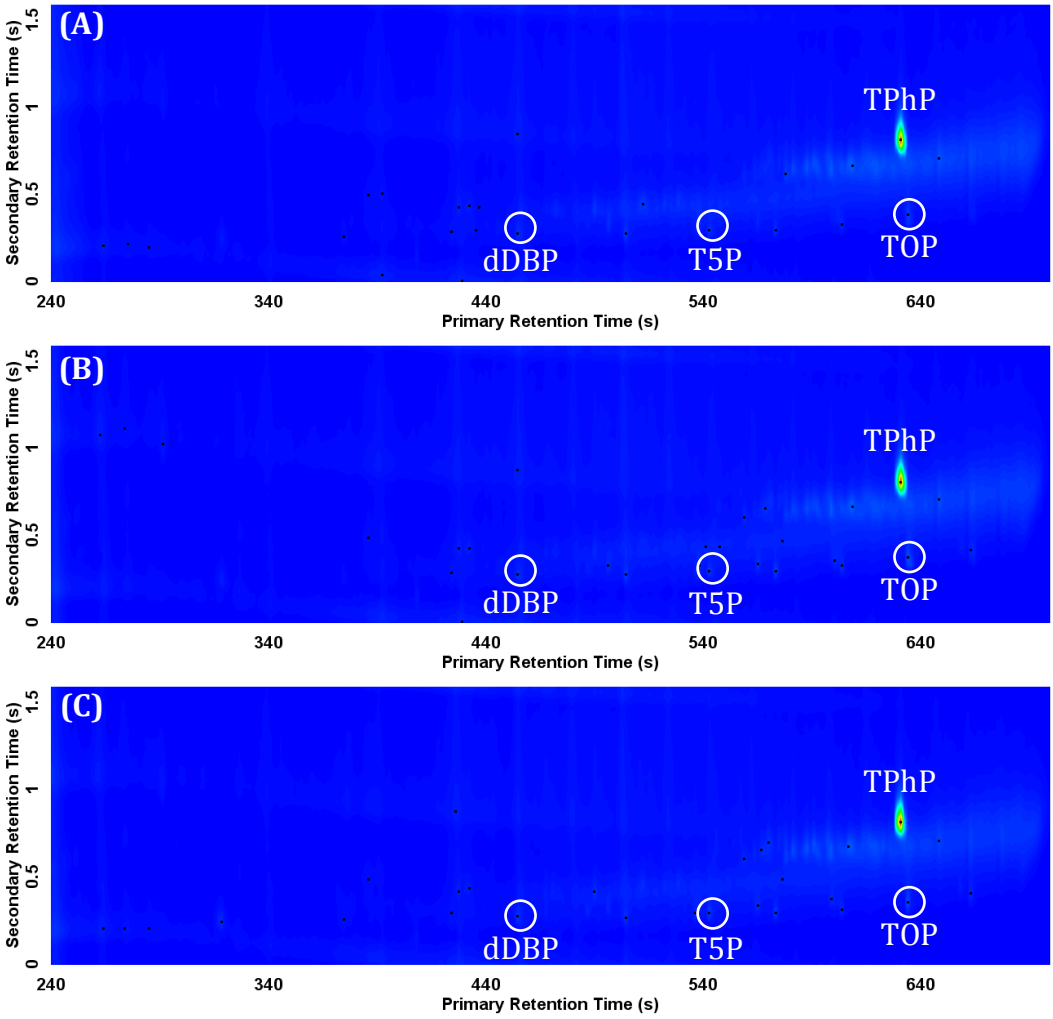

Figure A-4. GC×GC-NPD chromatograms of desalted crude oil samples (diluted 50× in isooctane) collected from unit B on: (A) April 30, (B) May 3, and (C) May 6, 2014 (dDBP = derivatized dibutyl phosphate; T5P = tripentyl phosphate; TOP = trioctyl phosphate). Triphenyl phosphate (TPhP) added as an internal standard at 0.5 µg mL^{-1}. ^{2}D offset of 0. 8 s applied to plotted chromatograms.

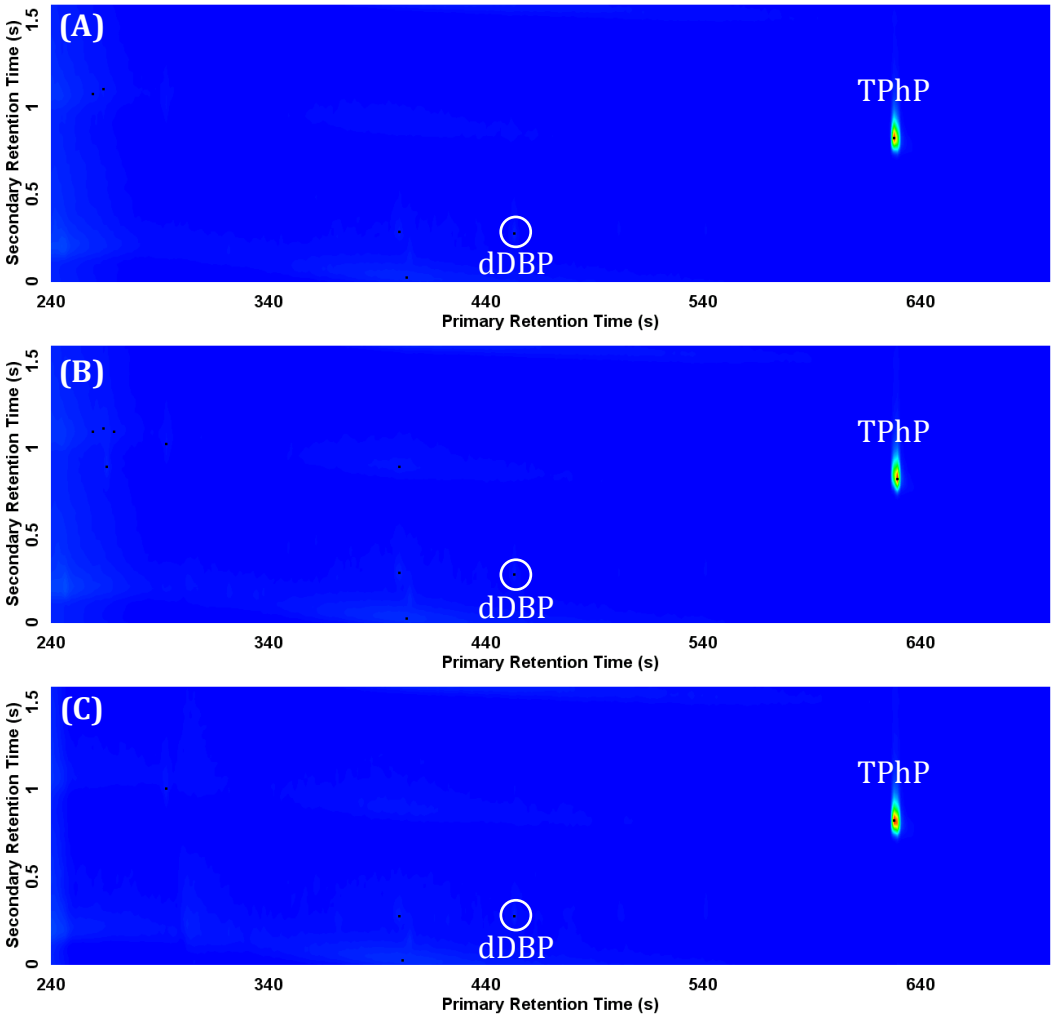

Figure A-5. GC×GC-NPD chromatograms of distillate 1 samples (diluted 10× in isooctane) collected from unit A on: (A) April 30, (B) May 3, and (C) May 6, 2014 (dDBP = derivatized dibutyl phosphate). Triphenyl phosphate (TPhP) added as an internal standard at 0.5 μg mL^{-1}. ^{2}D offset of 0.8 s applied to plotted chromatograms.

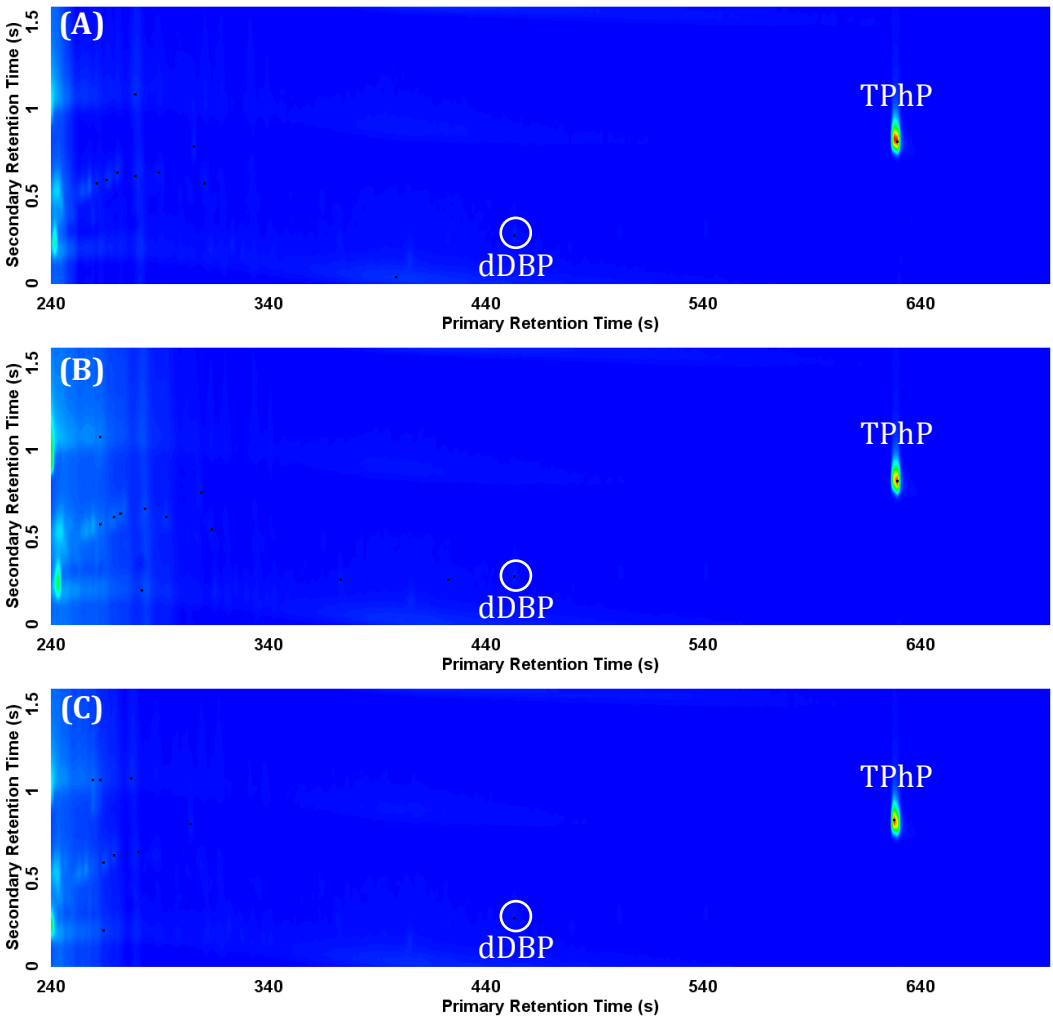

Figure A-6. GC×GC-NPD chromatograms of distillate 1 samples (diluted 10× in isooctane) collected from unit B on: (A) April 30, (B) May 3, and (C) May 6, 2014 (dDBP = derivatized dibutyl phosphate). Triphenyl phosphate (TPhP) added as an internal standard at 0.5 μg mL^{-1}. ^{2}D offset of 0.8 s applied to plotted chromatograms.

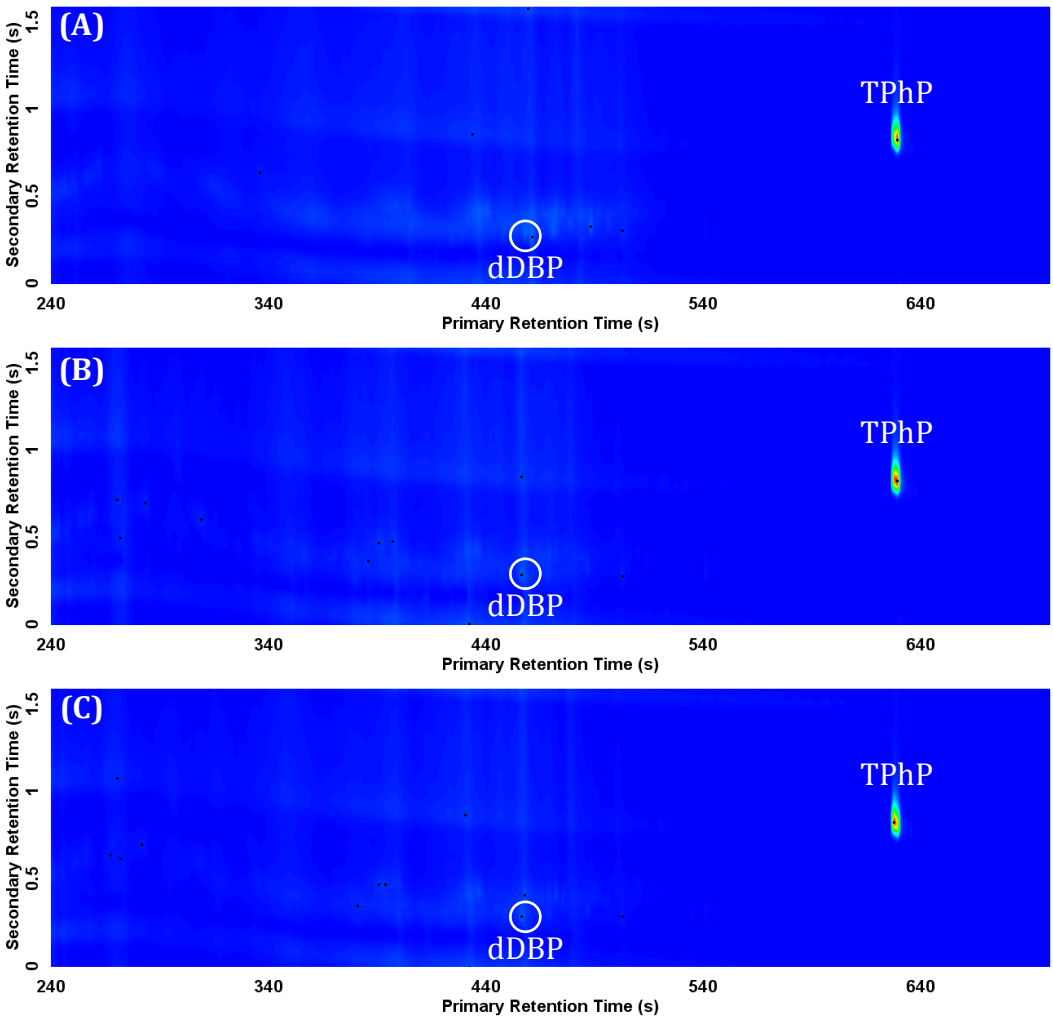

Figure A-7. GC×GC-NPD chromatograms of distillate 2 samples (diluted 50× in isooctane) collected from unit A on: (A) April 30, (B) May 3, and (C) May 6, 2014 (dDBP = derivatized dibutyl phosphate). Triphenyl phosphate (TPhP) added as an internal standard at 0.5 μg mL^{-1}. ^{2}D offset of 0.8 s applied to plotted chromatograms.

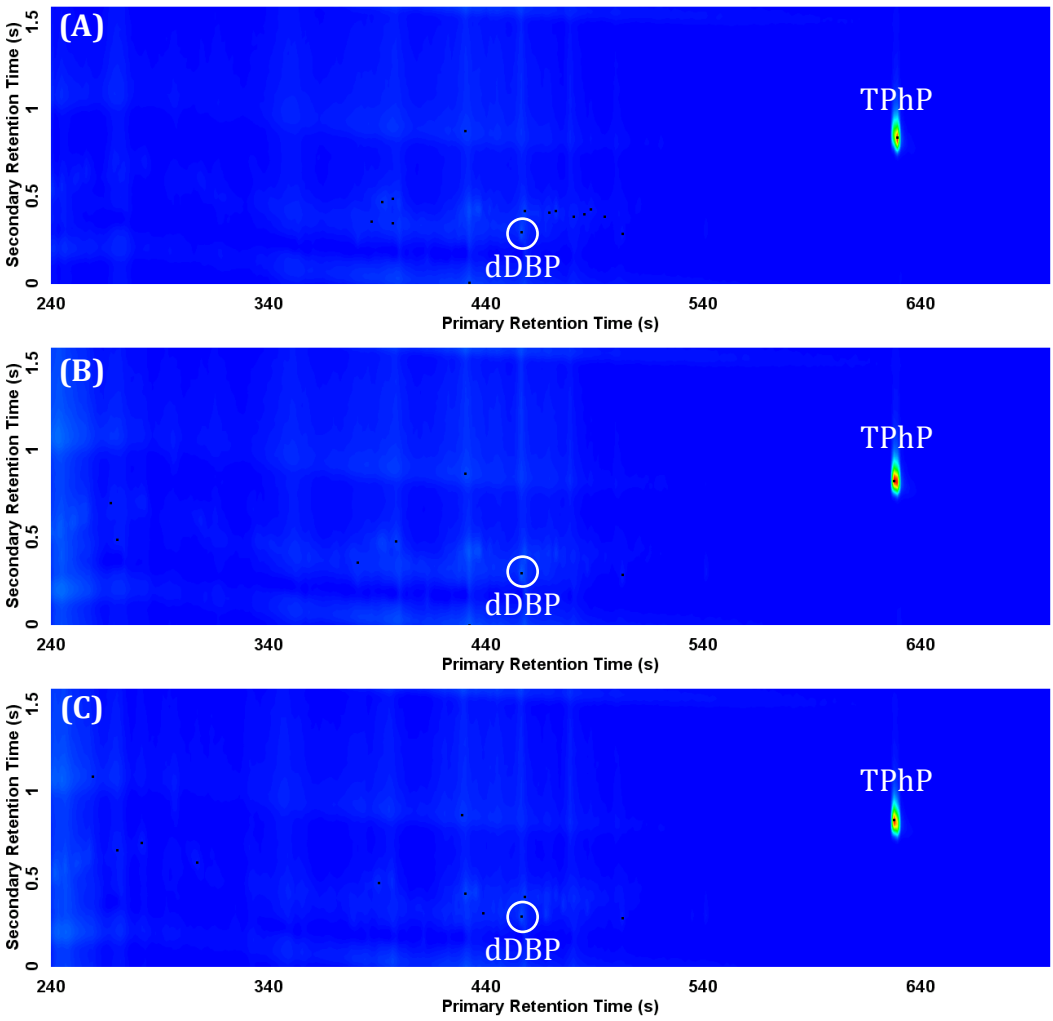

Figure A-8. GC×GC-NPD chromatograms of distillate 2 samples (diluted 50× in isooctane) collected from unit B on: (A) April 30, (B) May 3, and (C) May 6, 2014 (dDBP = derivatized dibutyl phosphate). Triphenyl phosphate (TPhP) added as an internal standard at 0.5 μg mL^{-1}. ^{2}D offset of 0.8 s applied to plotted chromatograms.

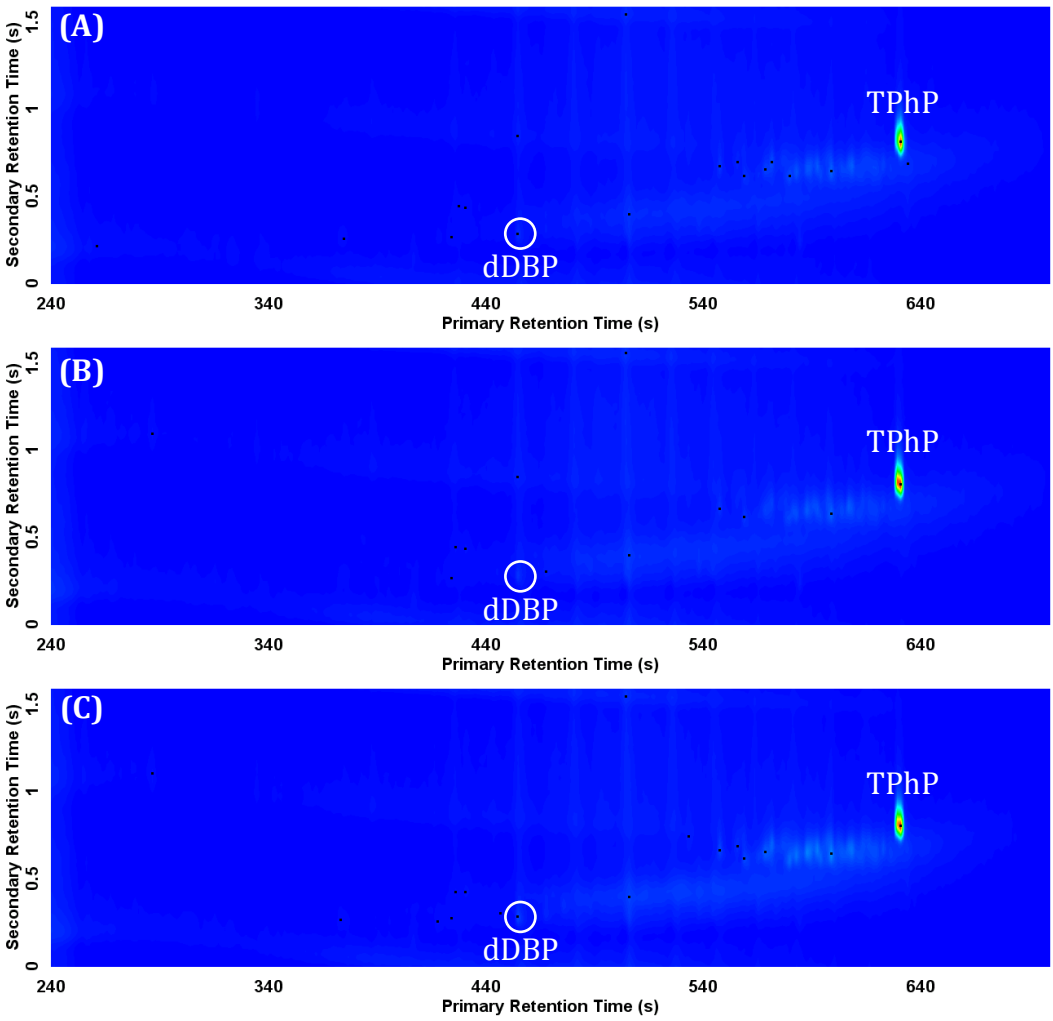

Figure A-9. GC×GC-NPD chromatograms of distillate 3 samples (diluted 100× in isooctane) collected from unit A on: (A) April 30, (B) May 3, and (C) May 6, 2014 (dDBP = derivatized dibutyl phosphate). Triphenyl phosphate (TPhP) added as an internal standard at 0.5 μg mL^{-1}. ^{2}D offset of 0.8 s applied to plotted chromatograms.

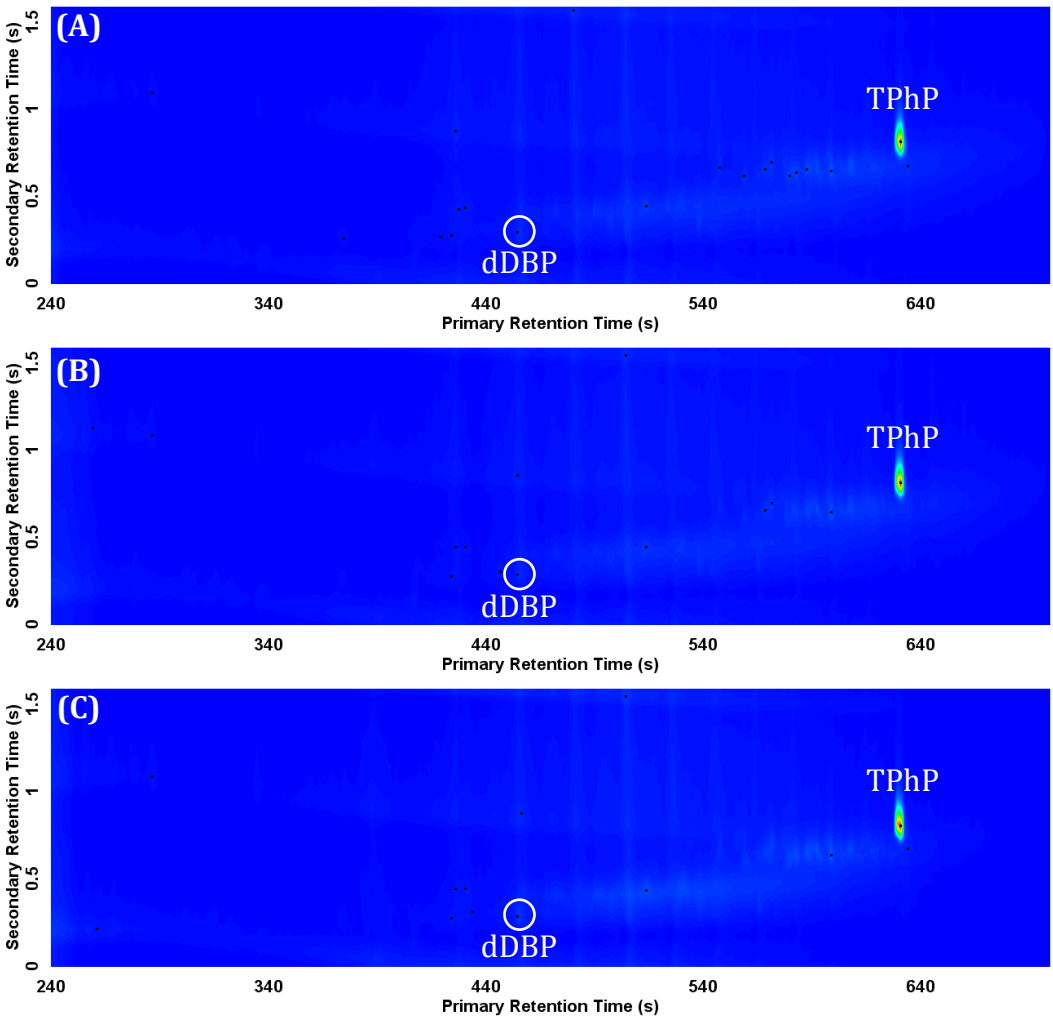

Figure A-10. GC×GC-NPD chromatograms of distillate 3 samples (diluted 100× in isooctane) collected from unit B on: (A) April 30, (B) May 3, and (C) May 6, 2014 (dDBP = derivatized dibutyl phosphate). Triphenyl phosphate (TPhP) added as an internal standard at 0.5 μg mL^{-1}. ^{2}D offset of 0.8 s applied to plotted chromatograms.